HYDRODYNAMIC STABILITY OF MULTIPHASE REACTORS

J. B. Joshi,* N. S. Deshpande,[1] M. Dinkar,[2] and D. V. Phanikumar[3]

Department of Chemical Technology, University of Bombay, Matunga, Mumbai-400 019, India

* Corresponding author.

Present addresses: [1] Hindustan Lever Research Center, Chakala, Andheri (East), Mumbai 400; [2] Principal Research Scientist, Honeywell Technology Center, 3660 Technology Center, Minneapolis, MN 55418, U.S.A.; and [3] GE India Technology Center, Innovation Building, International Technology Park, Whitefield Rd., Banglore-560066 India.

ADVANCES IN CHEMICAL ENGINEERING, VOL. 26 0065-2377/01 $35.00

Gas–liquid bubble columns, solid–liquid fluidized beds, gas–solid fluidized beds, gas–liquid–solid fluidized beds, and transport reactors are very widely used multiphase reactors. These reactors operate in either of the two characteristic regimes: particulate or homogeneous, and aggregative or heterogeneous. The rates of heat, mass, momentum transfer, and mixing are quite different in these two regimes. Therefore, it is important to know the range of operating and design parameters over which the two regimes prevail and the conditions under which the transition occurs. This subject has been extensively investigated during the past 50 years and numerous fundamental, semiempirical, and empirical approaches have been reported for the prediction of transition. All these studies have been analyzed in this monograph. Further, unified and generalized criteria have been developed. In view of these, the past published results have been discussed. Stability maps have been presented. For several multiphase reactors, comprehensive comparison has been presented between the predicted and the experimental conditions of transitions. The characteristic differences among the various multiphase systems have been brought out. Suggestions have been made for future work.

I. Introduction

In multiphase reactors, the dispersed phase moves in one of two characteristic regimes, depending upon the nature of dispersion. The two regimes are homogeneous and heterogeneous. These regimes are commonly known as particulate and aggregative, respectively.

In bubble columns, the gas phase exists as the dispersed phase in the continuous liquid phase. The homogeneous regime is characterized by almost uniformly sized bubbles. Further, the concentration of bubbles is uniform, particularly in the transverse direction. Therefore, bulk liquid circulation is practically absent. If the gas is sparged uniformly at the column bottom, it remains uniformly distributed all over the column. All the bubbles rise virtually vertically with minor transverse and axial oscillations. For all

bubble sizes, there is practically no coalescence or redispersion. Hence, size of the bubbles in homogeneous regime is almost entirely dictated by the type and design of the sparger and the physical properties of the system.

In contrast, the heterogeneous regime is characterized by nonuniform bubble concentration, especially in the transverse direction, and the existence of gross liquid circulation. There exists a wide bubble size distribution in the main bulk region, and the average bubble size in the bulk region is governed by coalescence and redispersion phenomena, which in turn are controlled by the energy dissipation rate in the bulk. The intensity of turbulence is also much higher. Such highly turbulent recirculation results into substantially high values of eddy diffusivities for mass, heat, and momentum. As a result, the rates of heat and mass transfer and mixing are quite different in homogeneous and heterogeneous regimes. Therefore, it is important to know the range of physical properties and operating parameters over which the two regimes prevail. As the transition from the homogeneous to the heterogeneous regime starts, there is an onset of liquid circulation that is upward in the central region and downward near the column wall. So more bubbles enter the central region, as it is the path of lower resistance. As a result, a transverse holdup profile begins to build up, which in turn intensifies the liquid circulation. Therefore, the beginning of transition regime is very important, and further development is self-propagating. Joshi (1981, 1983) and Shnip *et al.* (1992) have discussed the pertinent details of these two regimes in bubble columns.

In solid–liquid fluidized beds the particle phase is the dispersed phase and the bed usually operates in the particulate (homogeneous) regime. However, for heavy particles (large size and density or high terminal settling velocity), heterogeneity sets in.

In gas–solid fluidized beds, the particle phase is the dispersed phase up to a certain critical superficial gas velocity. Above this, the excess gas is considered to move in the form of bubbles, and the bubble phase forms the dispersed phase. The critical superficial gas velocity usually equals the minimum fluidization velocity. However, in the case of fine powders or at high pressure, the bed expands homogeneously even above the incipient fluidization velocity without the formation of bubbles. The bubbles are formed at much higher velocity where the void fraction of the emulsion phase is greater than that at the incipient fluidization. It may be pointed out at this stage that the dispersed bubble phase (which is formed either at the incipient fluidization velocity or at a higher velocity) can also remain in the homogeneous regime up to a certain superficial gas velocity, and the formation of bubbles need not be considered as equivalent to the beginning of the heterogeneous regime.

The term ''three-phase fluidization'' refers to that operation in which an upward cocurrent flow of liquid and gas fluidizes the solid particles. The

gas flows as bubbles. For such operations, knowledge of the expansion properties of the bed as well as holdups of the individual phases is important in determining the size and efficiency of the equipment. In three-phase fluidized beds, the particles and the bubbles form the dispersed phases. However, the behavior of bubbles plays a dominant role in deciding the regime of operation and the regime transition can be viewed as similar to that in bubble columns. There is a small difference in that the bubble size (and velocity) depends upon the particle size, density, and solid loading (Pandit and Joshi, 1984, 1986; Khare and Joshi, 1990). The three-phase reactors pose yet another interesting problem. When the three-phase dispersion is obtained by the introduction of gas phase in a solid–liquid fluidized bed, the bed either contracts or expands. This observation is now very well documented and carefully analyzed by many investigators, including Turner (1964), Stewart and Davidson (1964), Ostergaard (1965), Darton and Harrison (1975), Epstein and Nicks (1976), Epstein (1976), and El-Temtamy and Epstein (1979). In a solid–liquid fluidized bed, the particle settling velocity is less than the terminal settling velocity because of hindered settling. When the gas is introduced in a particulate fluidized bed, the gas bubbles extract energy from the liquid phase. As a result, the drag on each particle is reduced the particle settling velocity increases and bed contraction occurs. When gas is introduced in an aggregative fluidized bed, the gas supplies energy to the liquid phase. This energy is reflected in higher turbulence intensity in the liquid phase. Because of this, the particle settling velocity gets further hindered and bed expansion occurs. This initial behavior of contraction/expansion has been shown to depend upon the regime transition (Joshi, 1983). The behavior needs further reexamination in view of recent developments in the understanding of multiphase phenomena.

In the past, some criteria have been developed using both empirical and relatively fundamental approaches. The latter approach can be classified into two categories. In the first category, the multiphase system is assumed to have no bounds. Therefore, this approach does not consider the existence of either the sparger or the column wall. Such beds may be termed as unbounded beds. In the second approach, the existence of the sparger plate and column wall is considered; such beds may be termed bounded beds.

In both these cases, the method of linear stability has been used for obtaining the transition criterion. The state variables such as the local holdup and the phase velocities are given small perturbations. In the homogeneous regime these small disturbances die out with time, indicating that the beds are stable to small fluctuations. If the regime of operation is heterogeneous, then the small perturbations that are superimposed in the homogeneous regime grow exponentially with time, and nonuniformity sets in. This makes the bed heterogeneous, indicating that the beds are unstable.

The terms unstable bed and heterogeneous regime are therefore used synonymously.

Jackson (1963a, 1963b, 1964) was one of the pioneers in formulating the set of Navier–Stokes equations to describe the fluid dynamics of fluidized beds (both bounded and unbounded beds). Jackson and co-workers (Anderson and Jackson, 1967a, 1967b, 1968, 1969; Jackson, 1985; Medlin *et al.,* 1974; Medlin and Jackson, 1975; Agarwal *et al.,* 1980) have also developed the stability criterion. Homsy and co-workers (El-Kaissy and Homsy, 1976; Homsy and El-Kaissy, 1980; Didwania and Homsy, 1981a, 1981b; Green and Homsy, 1987a, 1987b; Ham *et al.,* 1990) performed a comprehensive analysis of unbounded beds and presented their dynamic behavior. They have also reported a systematic set of experimental data for the dynamic behavior. Rietema (1973) and Musters and Rietema (1977) have also presented unbounded bed analysis for gas–solid fluidized beds. Batchelor (1988) systematically derived the particle phase force balance and attributed physical significance to all the terms in the force balance equation. In addition to these theoretical approaches, Wallis (1969), Verloop and Heertjes (1970), and Gibilaro, Foscolo, and co-workers (Foscolo and Gibilaro, 1984; Gibilaro *et al.,* 1984, 1986, 1987a, 1987b, 1989, 1990) have presented very interesting criteria on the basis of heuristic arguments.

All the just-mentioned analyses focus more or less on fluidized beds and under unbounded conditions. The analysis of all these investigators concentrated on whether a periodic disturbance in the axial direction grows with respect to time, leading to instability, or decays with time, indicating a stable system. The treatment is strictly for axial direction and the axial nonuniformities are the source of transition. Analyses such as these have the limitation that the real fluidized bed is not of infinite extent, and that some account must be taken of the boundaries at the upper and lower surface of a bed, the finite depth, and also the walls that bound the beds laterally. Further, the one-dimensional unbounded description does not generally explain all the experimental observations at transition. Shnip *et al.* (1992) have used the theory of linear stability for the analysis of bounded beds.

The present work aims at the following: (i) To derive the stability criterion for gas–liquid, solid–liquid, gas–solid, and gas–liquid–solid unbounded dispersions. (ii) To understand the physical significance of all the terms in the stability criterion. (iii) To present the relative merits of all the previous approaches. (iv) To make an attempt to give physical significance to the unbounded and bounded bed analyses. (v) To analyze all the published experimental information on the stability of gas–liquid, solid–liquid, gas–solid, and gas–liquid–solid systems. (vi) To bring out the relative utility of the unbounded and bounded bed analyses. (vii) To present a generalized

procedure for checking the stability of multiphase systems. (viii) To present stability maps for all types of multiphase reactors from which the stable regions can easily be identified.

II. Generalized Criterion for Unbounded Dispersions

The transition from homogeneous to heterogeneous regime in case of bubble columns was qualitatively described in the introduction. At a certain critical superficial gas velocity, a small disturbance in the hold-up profile sets in liquid circulation, which in turn magnifies the hold-up disturbance. In this way, the disturbance grows, and finally an approximately parabolic gas hold-up profile and intense liquid circulation develop, which are the characteristics of the heterogeneous regime.

Now, consider the case of a solid–liquid fluidized bed operating in the particulate regime. If the liquid flow rate is increased, the bed still remains in the particulate regime up to a certain liquid flow rate. After this, alternate bands of high and low density start appearing in the bed. If the liquid flow rate is increased still further, the bed starts operating in the aggregative or heterogeneous regime characterized by nonuniform hold-up profiles.

In the following section, a criterion has been developed on the basis of linear stability theory. This approach has been described by Jackson (1963a). It will consist of the following steps: (i) The starting point is the equations for continuity and motion for solid–liquid dispersion under turbulent conditions. These equations will be derived in detail, using the time averaging of instantaneous equations and introducing usual turbulent modeling. (ii) The equations of motion of both the phases will be combined to eliminate the pressure term. This step is very important and useful. (iii) Perturbations will be introduced and equations of continuity and motion will be written in terms of perturbation variables. (iv) The resulting equations are linearized. (v) The velocity perturbations will be eliminated using the equations of continuity, and a final linearized equation will be obtained in terms of perturbation in fractional hold-up. (vi) Under the homogeneous regime, any perturbation to the flat hold-up profile decays with respect to time. In contrast, if the small perturbations grow with time, transition to the heterogeneous regime occurs. In the linear stability analysis, perturbations are given in form of a periodic function and the solution to the perturbation equation is obtained for neutral stability. (vii) Initially, the solid–liquid dispersion will be assumed to have no bounds (unbounded case). In other words, the existence of the sparger or the column wall will

not be considered. Later on, the analysis will be extended to a case where the existence of the sparger and column wall is considered (bounded case in Section VI). (viii) The following analysis is for solid–liquid fluidized beds. However, the same analysis applies to other multiphase systems N such as gas–solid fluidized beds and gas–liquid bubble columns.

A. Solid–Liquid Fluidized Beds

Let us begin with the unbounded case. The following additional assumptions are made:

1. The concept of interpenetrating continua (continuum approach) has been used. It involves treating the multiphase dispersion as a continuum in which the variables are related to local averages over regions that are large enough compared with the dispersed particles (bubbles or solid particles) and small enough compared with the length scales over which the variables can be assumed to remain constant.
2. The continuous phase (liquid) is incompressible. This implies that the density is not a function of both time and space. However, the dispersion is compressible because the local hold-up is not a constant. The compressibility is accounted for by the spatial variation of the fractional solid holdup, ε_S.
3. Particles are perfectly spherical and monosized (no size distribution).
4. The flow is assumed to be turbulent. Whenever there is a gradient in solid or liquid holdup, the transport of liquid and solid phases has been assumed to occur by dispersion. Therefore, these terms appear in the equations of continuity.
5. The theory of linear stability has been used. Jackson (1963a) has pioneered this method for the analysis of multiphase dispersions. The pertinent details have been given by Shnip *et al.* (1992).

Using these assumptions, the fundamental transport equations for solid–liquid fluidized beds are given next.

1. The Governing Equations

The equation of continuity for solid phase in a one-dimensional coordinate system can be written as

$$\frac{\partial \varepsilon_S}{\partial t} + \frac{\partial}{\partial z}(\varepsilon_S v_z) = 0. \tag{1}$$

Following the procedure of Reynolds averaging, the instantaneous quantities are written in terms of time-averaged and fluctuating quantities as

$$\varepsilon_S = \bar{\varepsilon}_S + \varepsilon'_S, \quad v_z = \bar{v}_z + v'_z, \tag{2}$$

where the overbars indicate the time-averaged quantities and the primes indicate the fluctuating quantities. Substituting Eq. (2) in Eq. (1) and noting that time average of fluctuating quantities is zero, we get

$$\frac{\partial \bar{\varepsilon}_S}{\partial t} + \frac{\partial}{\partial z}(\bar{\varepsilon}_S \bar{v}_z) = -\frac{\partial}{\partial z}(\overline{\varepsilon'_S v'_z}). \tag{3}$$

The third term of Eq. (3) contains $\overline{\varepsilon'_S v'_z}$, which is generally modeled in terms of turbulent dispersion in a manner analogous to the well-known gradient hypothesis of Boussinesq, as proportional to the gradient of hold-up in the z direction, the constant of proportionality being referred to as the turbulent dispersion coefficient:

$$\overline{\varepsilon'_S v'_z} = -D_S \frac{\partial \bar{\varepsilon}_S}{\partial z}. \tag{4}$$

Substitution of Eq. (4) in (3) gives the equation of continuity as (after removing overbars for convenience)

$$\frac{\partial \varepsilon_S}{\partial t} + \frac{\partial}{\partial z}(\varepsilon_S v_s) - \frac{\partial}{\partial z}\left(D_S \frac{\partial \varepsilon_S}{\partial z}\right) = 0. \tag{5}$$

The equation of continuity for the liquid phase can be derived in a similar manner and is given by

$$\frac{\partial \varepsilon_L}{\partial t} + \frac{\partial}{\partial z}(\varepsilon_L u_z) - \frac{\partial}{\partial z}\left(D_L \frac{\partial \varepsilon_L}{\partial z}\right) = 0. \tag{6}$$

Equations (5) and (6) were derived for solid–liquid dispersions. These can be easily adapted to any other multiphase system such as gas–solid and gas–liquid systems. The one-dimensional equation of motion for solid phase in terms of instantaneous quantities is given by

$$\rho_S \left[\frac{\partial}{\partial t}(\varepsilon_S v_z) + \frac{\partial}{\partial z}(\varepsilon_S v_z v_z)\right] = -\varepsilon_S \frac{\partial p}{\partial z} + \varepsilon_S \rho_S g - \varepsilon_L f_z - \nabla.\tau_S, \tag{7}$$

where f_z is the interaction force. It is a function of the slip velocity between the two phases and the relative acceleration of the two phases. It consists of drag force and the virtual mass force. The drag force per unit volume is given by

$$f_{zd} = C'_D \varepsilon_S (v_z - u_z) \tag{8a}$$

where $C'_D = (\varepsilon_S - \varepsilon_L)g/(\bar{v}_z - \bar{u}_z)$. It may be noted that C'_D is not conventional dimensionless drag coefficient. It has dimensions of kg/m^3s or $N \cdot s/m^4$. The virtual mass force is given by

$$f_{zv} = \varepsilon_S C_v \rho_L \frac{D}{Dt}(u_z - v_z), \tag{8b}$$

where the term Du_z/D_t is based on the continuous phase velocity and Dv_z/D_t is based on the dispersed phase velocity. Therefore, the total interaction force is

$$f_z = C'_D \varepsilon_S (v_z - u_z) + \varepsilon_S C_v \rho_L \frac{D}{Dt}(v_z - u_z). \tag{9}$$

It is known that C_v is either considered as a constant (Cook and Harlow, 1986; Drew *et al.,* 1979) or as a function of voidage (Ham *et al.,* 1990). In the following analysis it will be assumed to be constant.

Using Reynolds' averaging procedure for Eq. (7), and neglecting the laminar stresses, we get:

$$\begin{aligned}
&\rho_S \left[\frac{\partial}{\partial t}(\bar{\varepsilon}_S \bar{v}_z + \overline{\varepsilon'_S v'_z}) + \frac{\partial}{\partial z}(\bar{\varepsilon}_S \bar{v}_z \bar{v}_z + \bar{\varepsilon}_S \overline{v'_z v'_z} + \bar{v}_z \overline{\varepsilon'_S v'_z} + \bar{v}_z \overline{\varepsilon'_S v'_z}) \right] \\
&= -\left(\bar{\varepsilon}_S \frac{\partial \bar{p}}{\partial z} + \overline{\varepsilon'_S \frac{\partial p'}{\partial z}} \right) + \bar{\varepsilon}_S \rho_S g - C'_D \bar{\varepsilon}_L \bar{\varepsilon}_S (\bar{v}_z - \bar{u}_z) - C'_D \overline{\varepsilon'_L \varepsilon'_S} (\bar{v}_z - \bar{u}_z) \\
&\quad - C'_D (1 - 2\bar{\varepsilon}_L)(\overline{\varepsilon'_S v'_z} + \overline{\varepsilon'_L u'_z}) - C_v \rho_L \bar{\varepsilon}_L \bar{\varepsilon}_S \frac{D}{Dt}(\bar{v}_z - \bar{u}_z) \\
&\quad - C_v \rho_L \overline{\varepsilon'_L \varepsilon'_S} \frac{D}{Dt}(\bar{v}_z - \bar{u}_z) - C_v \rho_L (1 - 2\bar{\varepsilon}_L) \left[\overline{\varepsilon'_S v'_z} \frac{\partial \bar{v}_z}{\partial z} - \overline{\varepsilon'_L u'_z} \frac{\partial \bar{u}_z}{\partial z} \right].
\end{aligned} \tag{10}$$

In writing the preceding equation, we have neglected all the triple and quadruple products of the fluctuating quantities. Also, the following double products are assumed to be zero:

$$\overline{\varepsilon'_S \frac{\partial v'_z}{\partial t}} = \overline{\varepsilon'_S \frac{\partial v'_z}{\partial z}} = \overline{v'_z \frac{\partial v'_z}{\partial z}} = 0. \tag{11a}$$

Further,

$$\overline{v'_z v'_z} = -2\nu_t \frac{\partial \bar{v}_z}{\partial z}, \overline{\varepsilon'_S v'_z} = -D_S \frac{\partial \bar{\varepsilon}_S}{\partial z}, \overline{\varepsilon'_L u'_z} = -D_L \frac{\partial \bar{\varepsilon}_L}{\partial z}, \tag{11b}$$

where ν_t represents the turbulent kinematic viscosity. D_S and D_L are the solid-and liquid-phase dispersion coefficients.

$$\begin{aligned}\overline{\varepsilon_L' \varepsilon_S'}(\bar{v}_z - \bar{u}_z) &= -\varepsilon_L' l \frac{\partial \bar{\varepsilon}_S}{\partial z}(\bar{v}_z - \bar{u}_z) \\ &= -\varepsilon_L' l \frac{\partial \bar{\varepsilon}_S}{\partial z}(\bar{v}_z - \bar{u}_z) \\ &= -\xi D_S \frac{\partial \bar{\varepsilon}_S}{\partial z}.\end{aligned} \tag{12}$$

It has been assumed that $\varepsilon_L' l(\bar{v}_z - \bar{u}_z) = l v_S \varepsilon_L' = -\xi D_s$, i.e., some proportion of the dispersion coefficient.

The pressure coupling term has the same magnitude but the opposite sign in the continuous and the dispersed phase momentum equations, which implies a transfer of momentum between the phases. The correlation between the fluctuating hold-up and fluctuating pressure can be modeled as follows (Appendix A):

$$\frac{1}{\rho_S}\overline{\varepsilon_S' \frac{\partial p'}{\partial z}} = +D_S \frac{\partial \bar{\varepsilon}_S}{\partial z}\frac{\partial \bar{v}_z}{\partial z} + \bar{v}_z \frac{\partial}{\partial z}\left(D_S \frac{\partial \bar{\varepsilon}_S}{\partial z}\right). \tag{13}$$

Substitution of Eq. (11)–(13) in Eq. (10), using the continuity equation (5) for simplification, assuming D_S and D_L to be independent of z, and removing the overbars for convenience, we get

$$\begin{aligned}&\varepsilon_S \rho_S \left(\frac{\partial v_z}{\partial t} + v_z \frac{\partial v_z}{\partial z}\right) \\ &\quad = -\varepsilon_S \frac{\partial p}{\partial z} + \varepsilon_S \rho_S g - C_D' \varepsilon_L \varepsilon_S (v_z - u_z) - C_v \rho_L \varepsilon_L \varepsilon_S \frac{D}{Dt}(v_z - u_z) \\ &\qquad + 2\rho_S \nu_t \frac{\partial \varepsilon_S}{\partial z}\frac{\partial v_z}{\partial z} + 2\varepsilon_S \rho_S \frac{\partial}{\partial z}\left(\nu_t \frac{\partial v_z}{\partial z}\right) + \rho_S D_S \frac{\partial \varepsilon_S}{\partial z}\frac{\partial v_z}{\partial z} + C_D' \xi D_S \frac{\partial \varepsilon_S}{\partial z} \\ &\qquad + C_D'(1 - 2\varepsilon_L)\left(D_S \frac{\partial \varepsilon_S}{\partial z} + D_L \frac{\partial \varepsilon_L}{\partial z}\right) + C_v \rho_L \xi D_S \frac{\partial \varepsilon_S}{Dz}\left(\frac{Dv_z}{Dt} - \frac{Du_z}{Dt}\right) \\ &\qquad + C_v \rho_L (1 - 2\varepsilon_L)\left[D_S \frac{\partial \varepsilon_S}{\partial z}\frac{\partial v_z}{\partial z}\frac{\partial v_z}{\partial z} - D_L \frac{\partial \varepsilon_L}{\partial z}\frac{\partial u_z}{\partial z}\right] + \rho_S \left(D_S \frac{\partial \varepsilon_S}{\partial z}\right).\end{aligned} \tag{14}$$

If we assume the equality of turbulent kinematic viscosities of the two phases, the z component of equation of motion for the liquid phase can

be written as

$$
\begin{aligned}
&\varepsilon_{\mathrm{L}}\rho_{\mathrm{L}}\left(\frac{\partial u_z}{\partial t}+u_z\frac{\partial u_z}{\partial z}\right)\\
&\quad=-\varepsilon_{\mathrm{L}}\frac{\partial p}{\partial z}+\varepsilon_{\mathrm{L}}\rho_{\mathrm{L}}g+C'_{\mathrm{D}}\varepsilon_{\mathrm{L}}\varepsilon_{\mathrm{S}}(v_z-u_z)+C_{\mathrm{v}}\rho_{\mathrm{L}}\varepsilon_{\mathrm{L}}\varepsilon_{\mathrm{S}}\frac{D}{Dt}(v_z-u_z)\\
&\qquad+2\rho_{\mathrm{L}}\nu_{\mathrm{t}}\frac{\partial\varepsilon_{\mathrm{L}}}{\partial z}\frac{\partial u_z}{\partial z}+2\varepsilon_{\mathrm{L}}\rho_{\mathrm{L}}\frac{\partial}{\partial z}\left(\nu_{\mathrm{t}}\frac{\partial u_z}{\partial z}\right)+\rho_{\mathrm{L}}D_{\mathrm{L}}\frac{\partial\varepsilon_{\mathrm{L}}}{\partial z}\frac{\partial u_z}{\partial z}-C'_{\mathrm{D}}\xi D_{\mathrm{S}}\frac{\partial\varepsilon_{\mathrm{S}}}{\partial z}\\
&\qquad-C'_{\mathrm{D}}(1-2\varepsilon_{\mathrm{L}})\left(D_{\mathrm{S}}\frac{\partial\varepsilon_{\mathrm{S}}}{\partial z}+D_{\mathrm{L}}\frac{\partial\varepsilon_{\mathrm{L}}}{\partial z}\right)-C_{\mathrm{v}}\rho_{\mathrm{L}}\xi D_{\mathrm{S}}\frac{\partial\varepsilon_{\mathrm{S}}}{\partial z}\left(\frac{Dv_z}{Dt}-\frac{Du_z}{Dt}\right)\\
&\qquad-C_{\mathrm{v}}\rho_{\mathrm{L}}(1-2\varepsilon_{\mathrm{L}})\left[D_{\mathrm{S}}\frac{\partial\varepsilon_{\mathrm{S}}}{\partial z}\frac{\partial v_z}{\partial z}-D_{\mathrm{L}}\frac{\partial\varepsilon_{\mathrm{L}}}{\partial z}\frac{\partial u_z}{\partial z}\right]+\rho_{\mathrm{L}}\frac{\partial}{\partial t}\left(D_{\mathrm{L}}\frac{\partial\varepsilon_{\mathrm{L}}}{\partial z}\right).
\end{aligned}
\tag{15}
$$

The equations of motion of the two phases can be combined by eliminating the pressure gradient, $\partial p/\partial z$. This is achieved by multiplying Eq. (15) by $(1-\varepsilon_{\mathrm{L}})/\varepsilon_{\mathrm{L}}$ and subtracting the resulting equation from Eq. (14). The resulting equation is

$$
\begin{aligned}
&(1-\varepsilon_{\mathrm{L}})[\rho_{\mathrm{S}}+\rho_{\mathrm{L}}C_{\mathrm{v}}]\left[\frac{\partial v_z}{\partial t}+\mathrm{v}_z\frac{\partial v_z}{\partial z}\right]-(1-\varepsilon_{\mathrm{L}})\rho_{\mathrm{L}}[1+C_{\mathrm{v}}]\left[\frac{\partial u_z}{\partial t}+u_z\frac{\partial u_z}{\partial z}\right]\\
&\quad=(1-\varepsilon_{\mathrm{L}})(\rho_{\mathrm{S}}-\rho_{\mathrm{L}})g-\beta(v_z-u_z)+2\rho_{\mathrm{S}}\nu_{\mathrm{t}}\frac{\partial\varepsilon_{\mathrm{S}}}{\partial z}\left(\frac{\partial v_z}{\partial z}\right)\\
&\qquad-2((1-\varepsilon_{\mathrm{L}})/\varepsilon_{\mathrm{L}})\rho_{\mathrm{L}}\nu_{\mathrm{t}}\frac{\partial\varepsilon_{\mathrm{L}}}{\partial z}\left(\frac{\partial u_z}{\partial z}\right)\\
&\qquad+2(1-\varepsilon_{\mathrm{L}})\rho_{\mathrm{S}}\frac{\partial}{\partial z}\left(\nu_{\mathrm{t}}\frac{\partial v_z}{\partial z}\right)-2(1-\varepsilon_{\mathrm{L}})\rho_{\mathrm{L}}\frac{\partial}{\partial z}\left(\nu_{\mathrm{t}}\frac{\partial u_z}{\partial z}\right)\\
&\qquad+\left(\rho_{\mathrm{S}}D_{\mathrm{S}}\frac{\partial\varepsilon_{\mathrm{S}}}{\partial z}\frac{\partial v_z}{\partial z}-[(1-\varepsilon_{\mathrm{L}})/\varepsilon_{\mathrm{L}}]\rho_{\mathrm{L}}D_{\mathrm{L}}\frac{\partial\varepsilon_{\mathrm{L}}}{\partial z}\frac{\partial u_z}{\partial z}\right)\\
&\qquad+[1+(1-\varepsilon_{\mathrm{L}})/\varepsilon_{\mathrm{L}}]C'_{\mathrm{D}}\xi D_{\mathrm{S}}\frac{\partial\varepsilon_{\mathrm{S}}}{\partial z}+C'_{\mathrm{D}}[(1-2\varepsilon_{\mathrm{L}})/\varepsilon_{\mathrm{L}}]\left(D_{\mathrm{S}}\frac{\partial\varepsilon_{\mathrm{S}}}{\partial z}+D_{\mathrm{L}}\frac{\partial\varepsilon_{\mathrm{L}}}{\partial z}\right)\\
&\qquad+[1+(1-\varepsilon_{\mathrm{L}})/\varepsilon_{\mathrm{L}}]C_{\mathrm{v}}\rho_{\mathrm{L}}\xi D_{\mathrm{S}}\left(\frac{Dv_z}{Dt}-\frac{Du_z}{Dt}\right)
\end{aligned}
\tag{16}
$$

$$+ C_v\rho_L[(1-2\varepsilon_L)/\varepsilon_L]\left[D_S\frac{\partial\varepsilon_S}{\partial z}\frac{\partial v_z}{\partial z} - D_L\frac{\partial\varepsilon_L}{\partial z}\frac{\partial u_z}{\partial z}\right] + \rho_S\frac{\partial}{\partial t}\left(D_S\frac{\partial\varepsilon_S}{\partial z}\right)$$

$$-[(1-\varepsilon_L)/\varepsilon_L]\rho_L\frac{\partial}{\partial t}\left(D_L\frac{\partial\varepsilon_L}{\partial z}\right),$$

where

$$\beta = C'_D\varepsilon_S = \frac{(\rho_S-\rho_L)g(1-\varepsilon_L)}{(\bar{v}_z-\bar{u}_z)}.$$

2. Solution under Steady-State Conditions

Under conditions of the homogeneous regime, the steady-state conditions for solid–liquid dispersion are given as follows.

At time $t = 0$:

$$v_z = v_0 = 0 \tag{17a}$$

$$u_z = u_0 = \text{constant} \tag{17b}$$

$$\varepsilon_L = \varepsilon_{L0} = \text{constant}. \tag{17c}$$

Substitution of Eqs. (17a), (17b), and (17c) in Eqs. (1), (2), and (16) gives the corresponding equations at steady state. The continuity equations are trivially satisfied and Eq. (16) gives

$$\beta_0 = -\frac{(\rho_S-\rho_L)g(1-\varepsilon_{L0})}{u_0}, \tag{18}$$

where β_0 is the steady-state drag coefficient evaluated at the steady state, $\varepsilon_L = \varepsilon_{L0}$. It may be pointed out that β_0 is dimensional having units of $kg/m^3\cdot s$.

3. Linearization

According to the theory of linear stability analysis, infinitesimally small perturbations are superimposed on the variables in the steady state and their transient behavior is studied. At this stage the difference between turbulent fluctuations and perturbations may be noted. Turbulence is the characteristic feature of the multiphase flow under consideration; the mean and fluctuating quantities were given by Eq. (2). The fluctuating components result in eddy diffusivity of momentum, mass, and Reynolds stresses. The turbulent fluctuations do not alter the mean value. In contrast, the perturbations are superimposed on steady-state average values and another steady

state is obtained. Therefore, in our procedure, we first time-smooth to erase turbulent fluctuations and then examine the larger scale instabilities in averaged variables. The time and length scale of perturbations is usually much higher than those for turbulent fluctuations. Using Eq. (17) we get the variables in their perturbed state as

$$\varepsilon_{\mathrm{L}} = \varepsilon_{\mathrm{L0}} + \varepsilon_{\mathrm{L1}} \tag{19a}$$

$$u_z = u_0 + u_1 \tag{19b}$$

$$v_z = v_1 . \tag{19c}$$

The drag coefficient term (β) is linearized with respect to the steady-state value β_0 as

$$\beta = \beta_0 + \beta_0' \varepsilon_{\mathrm{L1}} . \tag{19d}$$

We now introduce perturbations in the equations of continuity (5) and (6). We get

$$\frac{\partial v_1}{\partial z} = \frac{1}{(1 - \varepsilon_{\mathrm{L0}})} \left[\frac{\partial \varepsilon_{\mathrm{L1}}}{\partial t} - D_{\mathrm{S}} \frac{\partial^2 \varepsilon_{\mathrm{L1}}}{\partial z^2} \right]. \tag{20a}$$

The continuity equation for the liquid phase can be written in a similar fashion:

$$\frac{\partial u_1}{\partial z} = - \frac{1}{\varepsilon_{\mathrm{L0}}} \left[\frac{\partial \varepsilon_{\mathrm{L1}}}{\partial t} + \mathrm{u}_0 \frac{\partial \varepsilon_{\mathrm{L1}}}{\partial z} - D_{\mathrm{L}} \frac{\partial^2 \varepsilon_{\mathrm{L1}}}{\partial z^2} \right]. \tag{20b}$$

Similarly, we introduce the perturbations into the equation of motion (16) and neglect the nonlinear terms arising out of it. We also note two more points. First, $-C_{\mathrm{D}}' \xi D_{\mathrm{s}} \, \partial \varepsilon_{\mathrm{s}} / \partial z = C_{\mathrm{D}}' \overline{\varepsilon_{\mathrm{L}}' \varepsilon_{\mathrm{S}}'} (\bar{v}_z - \bar{u}_z)$ is also nonlinear, and we neglect it. Further, $\varepsilon_{\mathrm{S}} + \varepsilon_{\mathrm{L}} = 1$ and $\partial \varepsilon_{\mathrm{S}} / \partial z = - \partial \varepsilon_{\mathrm{L}} / \partial z$. Simplification of Eq. (16) gives

$$\begin{aligned} (1 - \varepsilon_{\mathrm{L0}})[\rho_{\mathrm{S}} + \rho_{\mathrm{L}} C_{\mathrm{v}}] \left(\frac{\partial v_1}{\partial t} \right) - (1 - \varepsilon_{\mathrm{L0}}) \rho_{\mathrm{L}} [1 + C_{\mathrm{v}}] \left[\frac{\partial u_1}{\partial t} + u_0 \frac{\partial u_1}{\partial z} \right] \\ = (\rho_{\mathrm{S}} - \rho_{\mathrm{L}})(-\varepsilon_{\mathrm{L1}}) g - \beta_0 (v_1 - u_1) - \beta_0' (\varepsilon_{\mathrm{L1}})(v_0 - u_0) \\ + (1 - \varepsilon_{\mathrm{L0}}) \rho_{\mathrm{S}} \nu_{\mathrm{t}} \left[\frac{\partial}{\partial z} \left(2 \frac{\partial v_1}{\partial z} \right) \right] - (1 - \varepsilon_{\mathrm{L0}}) \rho_{\mathrm{L}} \nu_{\mathrm{t}} \left[\frac{\partial}{\partial z} \left(2 \frac{\partial u_1}{\partial z} \right) \right] \\ - \rho_{\mathrm{S}} \frac{\partial}{\partial t} \left(D_{\mathrm{S}} \frac{\partial \varepsilon_{\mathrm{L1}}}{\partial z} \right) - \rho_{\mathrm{L}} \frac{(1 - \varepsilon_{\mathrm{L0}})}{\partial_{\mathrm{L0}}} \frac{\partial}{\partial t} \left(D_{\mathrm{L}} \frac{\partial \varepsilon_{\mathrm{L1}}}{\partial z} \right). \end{aligned} \tag{20c}$$

Now we take the divergence of Eq. (20c) and simplify the resulting equation using Eqs. (20a) and (20b) to get

$$A\frac{\partial^2\varepsilon_{L1}}{\partial t^2} + B\frac{\partial^2\varepsilon_{L1}}{\partial t\partial z} + C\frac{\partial^2\varepsilon_{L1}}{\partial z^2} + Z\nabla^2\varepsilon_{L1} + E\frac{\partial^3\varepsilon_{L1}}{\partial t\partial z^2} + F\frac{\partial\varepsilon_{L1}}{\partial t} + G\frac{\partial\varepsilon_{L1}}{\partial z} + H\nabla^4\varepsilon_{L1} + I\frac{\partial^4\varepsilon_{L1}}{\partial z^4} = 0. \tag{21}$$

Equation (21) is similar to the general expression obtained by Anderson and Jackson (1968) and Liu (1982), where *A, B, C, Z, E, F, G, H,* and *I* are constants given as follows:

$$A = 1 + \frac{\rho_L}{\rho_S}\left[\frac{(1+C_v)}{\varepsilon_{L0}} - 1\right] \tag{22a}$$

$$B = 2\frac{1-\varepsilon_{L0}}{\varepsilon_{L0}}\frac{\rho_L}{\rho_S}(1+C_v)u_0 \tag{22b}$$

$$C = \frac{1-\varepsilon_{L0}}{\varepsilon_{L0}}\frac{\rho_L}{\rho_S}(1+C_v)u_0^2 \tag{22c}$$

$$Z = -\frac{\beta_0}{\rho_S}\left(\frac{D_S}{(1-\varepsilon_{L0})} + \frac{D_L}{\varepsilon_{L0}}\right) \tag{22d}$$

$$E = -2\left[1 + \frac{(1-\varepsilon_{L0})\rho_L}{\varepsilon_{L0}\rho_S}\right]\nu_t - \frac{\rho_L C_v}{\rho_S}\left(\frac{D_S\varepsilon_{L0} + (1-\varepsilon_{L0})D_L}{\varepsilon_{L0}}\right) \tag{22e}$$

$$F = \frac{\beta_0}{\rho_S}\left[\frac{1}{\varepsilon_{L0}} + \frac{1}{(1-\varepsilon_{L0})}\right] \tag{22f}$$

$$G = \frac{\beta_0 u_0}{\varepsilon_{L0}\rho_S} - \frac{\beta_0' u_0}{\rho_S} + \frac{(\rho_S - \rho_L)}{\rho_S}g \tag{22g}$$

$$H = \frac{2\nu_t}{\varepsilon_{L0}\rho_S}[D_S\rho_S\varepsilon_{L0} + (1-\varepsilon_{L0})\rho_L D_L] \tag{22h}$$

$$I = -\frac{2\rho_L u_0(1-\varepsilon_{L0})}{\varepsilon_{L0}\rho_S}[(1+C_v)D_L + \nu_t]. \tag{22i}$$

We seek a solution to the foregoing partial differential equation to be of the form

$$\varepsilon_{L1} = \varepsilon_{L0}e^{ikz}e^{st}, \tag{23}$$

where k is the wave number in the z direction and s is the growth rate constant in time. If the real part of s is positive, then there is positive growth. This indicates that the disturbance or the perturbation will grow in time. For neutral stability the real part of s will be zero and for stability the real part of s is negative. Substituting Eq. (23) in Eq. (21), we get a quadratic equation in s. Equating then the real and the imaginary parts of the quadratic equation, we get the final stability criterion as

$$\frac{[A(G/F) - B/2]^2}{A(Z - C) + B^2/4} < 1. \tag{24}$$

Equation (24) gives the stability criterion for the solid–liquid fluidized beds. Equation (24) can be rewritten as

$$f_1 = 1 - \frac{[A(G/F) - B/2]^2}{A(Z - C) + B^2/4}. \tag{25}$$

The solid–liquid fluidized bed is stable when f_1 is positive, unstable when f_1 is negative, and neutrally stable when $f_1 = 0$.

It may be noted that the viscous terms given by constants *E, H,* and *I* appear with second-order derivative terms and these have a stabilizing effect for large wave number disturbances. Liu (1982) has recast Eq. (21) in a form interpretable in terms of wave hierarchies. He has shown that the terms involving *A, B, C, F, Z,* and *G* appear in the expressions for lower order kinematic wave velocity and higher order elastic wave velocity, and that the stability criterion depends on the relative magnitudes of kinematic wave velocity and the elastic wave velocity. He has shown that for a humplike initial disturbance, the exponential growth is made milder by the viscous modification through the viscous term (E) by a factor $1/(\nu_e t)^{1/2}$. The importance of viscous correction depends on the wavelengths relative to the effective viscous length scale $(\nu_e(A/F))^{1/2}$, where A and F are given by Eqs. (22a) and (22f), respectively. This length scale will be still larger if we use eddy viscosity instead of molecular viscosity. The terms such as H and I do not appear in Liu's analysis, but these are the terms with higher order similar to *E,* and the stability criterion is still decided by the relative magnitudes of kinematic and elastic wave velocity.

B. Gas–Solid Fluidized Beds

The preceding mathematical analysis also holds for gas–solid fluidized beds. In this case, the gas phase is the continuous phase and the solid phase is the dispersed phase. The criterion given by Eq. (24) holds where the values of the constants are given in Table I. It may be noted that the terms

TABLE I
PARAMETERS APPEARING IN THE GENERALIZED STABILITY CRITERION (UNBOUNDED ANALYSIS) FOR VARIOUS MULTIPHASE SYSTEMS

Solid–liquid fluidized beds

$$A = 1 + \frac{\rho_L}{\rho_S}\left[\frac{(1 + C_V)}{\varepsilon_L} - 1\right]$$

$$B = 2\frac{(1 - \varepsilon_L)}{\varepsilon_L}\frac{\rho_L}{\rho_S}(1 + C_V)\frac{u_{sup}}{\varepsilon_L}$$

$$C = \frac{(1 - \varepsilon_L)}{\varepsilon_L}\frac{\rho_L}{\rho_S}(1 + C_V)\left(\frac{u_{sup}}{\varepsilon_L}\right)^2$$

$$Z = -\frac{\beta_0}{\rho_S}\left(\frac{D_S}{(1 - \varepsilon_L)} + \frac{D_L}{\varepsilon_L}\right)$$

$$F = \frac{\beta_0}{\rho_S}\left[\frac{1}{\varepsilon_L} + \frac{1}{(1 - \varepsilon_L)}\right]$$

$$G = \frac{\beta_0}{\rho_S}\frac{u_0}{\varepsilon_L} - \frac{\beta_0' u_0}{\rho_S} + \frac{(\rho_S - \rho_L)}{\rho_S}g$$

$$\beta_0 = \frac{(\rho_S - \rho_L)(1 - \varepsilon_L)\,g}{v_s}$$

$$v_S = v_0 - u_0 = -u_0$$
$$= -V_{S\infty}\varepsilon_L^{m-1}$$

Gas–solid fluidized beds

$$A = 1 + \frac{\rho_G}{\rho_S}\left[\frac{(1 + C_v)}{\varepsilon_G} - 1\right]$$

$$B = 2\frac{(1 - \varepsilon_G)}{\varepsilon_G}\frac{\rho_G}{\rho_S}(1 + C_v)\frac{u_{sup}}{\varepsilon_G}$$

$$C = \frac{(1 - \varepsilon_G)}{\varepsilon_G}\frac{\rho_G}{\rho_S}(1 + C_v)\left(\frac{u_{sup}}{\varepsilon_G}\right)^2$$

$$Z = -\frac{\beta_0}{\rho_S}\left(\frac{D_S}{(1 - \varepsilon_G)} + \frac{D_L}{\varepsilon_G}\right)$$

$$F = \frac{\beta_0}{\rho_S}\left[\frac{1}{\varepsilon_G} + \frac{1}{(1 - \varepsilon_G)}\right]$$

$$G = \frac{\beta_0}{\rho_S}\frac{u_0}{\varepsilon_G} - \frac{\beta_0' u_0}{\rho_S} + \frac{(\rho_S - \rho_G)}{\rho_S}g$$

$$\beta_0 = \frac{(\rho_S - \rho_G)(1 - \varepsilon_G)\,g}{v_s}$$

$$v_S = v_0 - u_0 = -u_0$$
$$= -V_{S\infty}\varepsilon_G^{m-1}$$

TABLE I (*continued*)

Gas–liquid systems

1. Liquid phase velocity = 0

$$A = \frac{\rho_G}{\rho_L} + \frac{(1 + C_v)}{\varepsilon_L} - 1$$

$$B = 2\left[\frac{\rho_G}{\rho_L} + C_v\right]\frac{v_{sup}}{(1 - \varepsilon_L)}$$

$$C = \left[\frac{\rho_G}{\rho_L} + C_v\right]\left(\frac{v_{sup}}{(1 - \varepsilon_L)}\right)^2$$

$$Z = -\frac{\beta_0}{\rho_L}\left[\frac{D_L}{\varepsilon_L} + \frac{D_G}{(1 - \varepsilon_L)}\right]$$

$$F = \frac{\beta_0}{\rho_L}\left[\frac{1}{\varepsilon_L} + \frac{1}{(1 - \varepsilon_L)}\right]$$

$$G = \frac{\beta_0}{\rho_L}\frac{v_0}{(1 - \varepsilon_L)} + \frac{\beta_0' v_0}{\rho_L} + \frac{(\rho_G - \rho_L)}{\rho_L} g$$

$$\beta_0 = \frac{(\rho_G - \rho_L)(1 - \varepsilon_L)\, g}{v_s}$$

$$v_S = v_0 - u_0 = v_0$$
$$= V_{B\infty}\varepsilon_L^{m-1}$$

2. Liquid phase velocity = u_0 (cocurrent or countercurrent)

$$A = \frac{\rho_G}{\rho_L} + \frac{(1 + C_v)}{\varepsilon_L} - 1$$

$$B = 2\left[\frac{\rho_G}{\rho_L} + C_v\right]\frac{v_{sup}}{(1 - \varepsilon_L)} + 2\frac{(1 - \varepsilon_L)}{\varepsilon_L} C_v \frac{u_{sup}}{\varepsilon_L}$$

$$C = \left[\frac{\rho_G}{\rho_L} + C_v\right]\left(\frac{v_{sup}}{(1 - \varepsilon_L)}\right)^2 + \frac{(1 - \varepsilon_L)}{\varepsilon_L} C_v \left(\frac{u_{sup}}{\varepsilon_L}\right)^2$$

$$Z = -\frac{\beta_0}{\rho_L}\left[\frac{D_L}{\varepsilon_L} + \frac{D_G}{(1 - \varepsilon_L)}\right]$$

$$F = \frac{\beta_0}{\rho_L}\left[\frac{1}{\varepsilon_L} + \frac{1}{(1 - \varepsilon_L)}\right]$$

$$G = \frac{\beta_0}{\rho_L}\left[\frac{v_0}{(1 - \varepsilon_L)} + \frac{u_0}{\varepsilon_L}\right] + \frac{\beta_0'}{\rho_L}(v_0 - u_0) + \frac{(\rho_G - \rho_L)}{\rho_L} g$$

$$\beta_0 = \frac{(\rho_G - \rho_L)(1 - \varepsilon_L)\, g}{(v_0 - u_0)}$$

$\varepsilon_{S0}, \varepsilon_{L0}, u_0, v_0, \beta_0$, etc., in Eq. (22) indicate the initial condition required for the perturbation analysis. Now, after obtaining the constants, the subscript 0 (which indicates initial condition) has been deleted. The important use of Table I is to discern the operating regime of a given multiphase system. For instance, if for a given gas–solid fluidized bed (ρ_S, ρ_L, ε_S, u_{sup}, d_P) we are interested in finding the operating regime, then the stepwise procedure is as follows: (i) For given ρ_S, ρ_L, ε_S, u_{sup}, d_P, etc., find the values of *A, B, C, F, G, Z* by using Table I. (ii) Find the operating regime using Eq. (24).

C. Gas–Liquid Bubble Columns

The preceding mathematical analysis also holds for gas–liquid bubble columns. In this case, the gas phase is the dispersed phase and the liquid phase is the continuous phase. The criterion given by Eq. (24) holds where the values of the constants are given in Table I. For the procedure of using Table I, refer to Sections V.A.2 and V.B.2.

D. Liquid–Liquid Spray Columns

When the dispersed phase is the light phase, the constants are similar to those for bubble columns. The case of a heavy dispersed phase can also be handled in a similar manner.

E. Typical Behavior of f_1

1. Fluidized Beds

Figures 1 and 2 show typical behavior of f_1 as a function of liquid hold-up and gas hold-up for solid–liquid fluidized beds and gas–solid fluidized beds, respectively. In both these cases, three distinct regions can be observed. In region I, up to some critical value of hold-up (point P), the function is positive. In region II, the function is negative up to point Q, and in region III, the function again becomes positive. Region I represents the particulate regime for solid–liquid and gas–solid fluidized beds, with point P representing the liquid (or gas) hold-up up to which the solid–liquid (or gas–solid) fluidized bed remains in the particulate regime. To the right of the point P, the function f_1 is negative and the region II represents the aggregative regime, up to the point Q. At point Q the function f_1 again

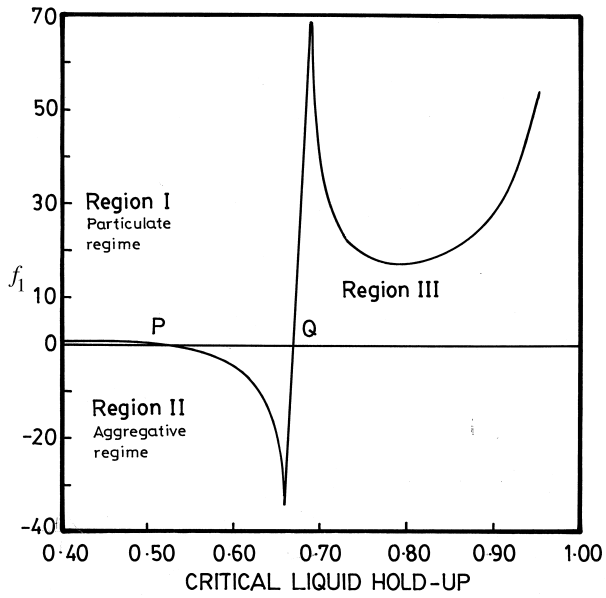

FIG. 1. Typical behavior of f_1: solid–liquid fluidized beds. $d_P = 655.0$ μm, $\alpha = 3.0$; $C_V = f(\varepsilon)$; $\rho_L = 1000$ kg/m^3; $\mu_L = 1.0$ mPas.

becomes positive, and thus region III on the right of the point Q represents a homogeneous regime of a different sort. For solid–liquid and gas–solid fluidized beds, Region III may be considered as a homogeneous regime under dilute conditions, i.e., the solid hold-up is low (say 3–40%), and again there are no axial/radial hold-up variations.

From Figs. 1 and 2, it can be seen that the transition at point Q (between regions II and III) is very sharp as compared to the transition at point P (between regions I and II). This difference in nature can be attributed to the different terms through which the function becomes negative. It can be seen from Eq. (25) that the numerator in the second term on the RHS is always positive, whereas its denominator can be either negative or positive. When the denominator becomes zero, f_1 will become discontinuous. The other way in which the function f_1 can become negative is when the denominator is smaller than the numerator.

In the case of the transition from region I to region II, which is gradual, the function f_1 becomes negative as the numerator exceeds the denominator (which remains positive). This generally happens when the inertial terms B and C are small, term A approaches unity, and thus the transition is decided by the comparison between G/F and $\sqrt{Z}$. It will be shown later

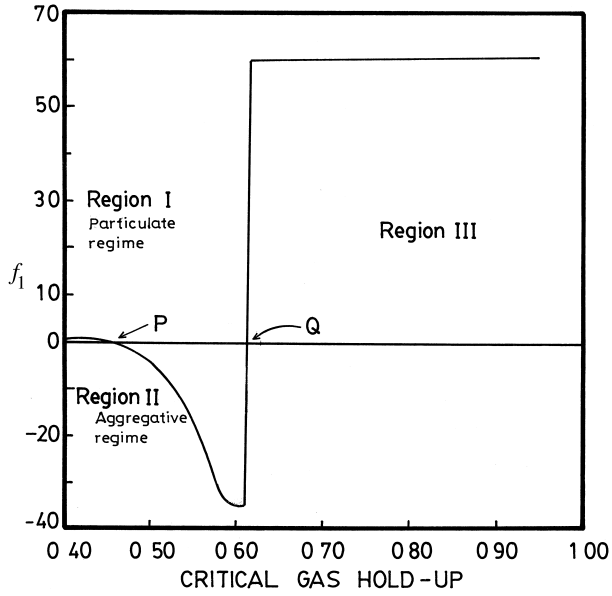

FIG. 2. Typical behavior of f_1: gas–solid fluidized beds. $d_P = 40.0\ \mu$m, $\alpha = 3.0$; $C_V = f(\varepsilon)$; $\rho_G = 1.15$ kg/m^3; $\mu_G = 2 \times 10^{-2}$ mPas.

that G/F represents the voidage propagation velocity and $\sqrt{Z}$ represents the restoring or homogenizing velocity in case of fluidized beds. Thus transition from region I to region II occurs when the inertial terms are negligible, and the transition is decided by the relative magnitudes of the disturbance propagation velocity (G/F) and the restoring velocity ($\sqrt{Z}$). In the case of transition from region III to region II, which is very sharp, the reason is that the denominator changes from negative to positive, and when the denominator approaches zero, the function f_1 approaches $-\infty$. From Eq. (25), it can be seen that the sign of the denominator is governed by relative magnitudes of Z (the dispersion term) and C (the inertial term). Thus, for the transition from region III to region II, the relative magnitude of inertia and dispersion is generally the deciding factor and the gravity and interaction terms have little, if any, bearing on the transition from region III to region II. The sharp transition at point Q means that the function f_1 is more sensitive to small changes in the inertial as well as the stabilizing dispersion term. A small change in the physical properties or in the value of other parameters, such as virtual mass coefficient, dispersion coefficient, or the slip velocity–terminal velocity relation, can cause a considerable change in the value of transition from region III to region II.

2. Bubble Columns

Figure 3 gives the typical behavior of f_1 in the case of bubble columns as a function of liquid phase hold-up. Figure 3 is similar to Figs. 1 and 2 as far as its nature is concerned. However, the stable operating regime of fluidized beds is commonly defined in terms of continuous phase hold-up and that for bubble columns is commonly defined in terms of the dispersed phase (gas) hold-up. Thus, the homogeneous regime at low gas hold-up is represented by region III (and not region I). As the gas hold-up increases (liquid hold-up decreases), the point Q is approached. The point Q represents the critical gas hold-up at which the transition from homogeneous to heterogeneous regime occurs. Region II, to the left of point Q, represents the heterogeneous regime up to point P, at which the function again becomes positive. Region I (to the left of point P) has such a high gas hold-up that the column may be thought as a stable gas–liquid froth (gas hold-up is high and there are no axial or radial gradients in the gas hold-up). Any gas hold-up to the right of point P (region II) may be thought of as the gas hold-up below which the froth is unstable (gas hold-up becomes low, liquid hold-up becomes high, and liquid draining may cause axial gas hold-up gradients).

In the present work, we have analyzed only one transition for all the multiphase systems. For bubble columns, we have considered the transition from region III to region II (point Q). In region I, gas hold-up is typically

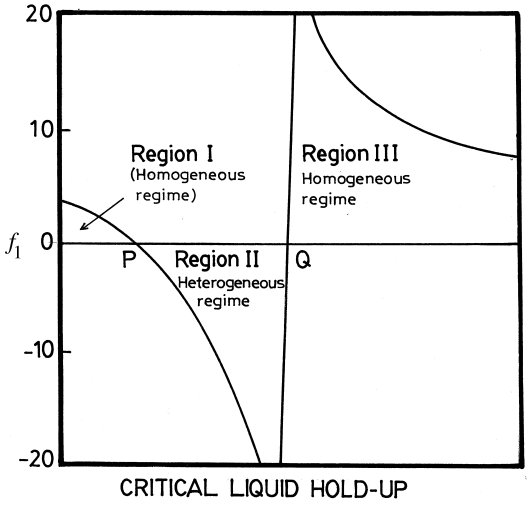

FIG. 3. Typical behavior of f_1: gas–liquid bubble columns. $d_B = 40.0$ μm, $\alpha = 0.5$, $C_V = 1.0$, $\rho_L = 1000$ kg/m^3; $\mu_L = 1.0$ mPas.

greater that 70%, which appears difficult in bubble columns. For fluidized beds, we have considered the transition between region I and region II (point P). Other transitions (point P in case of gas–liquid flows and point Q in the case of gas–solid and solid–liquid systems) will be analyzed in future.

III. Review of Stability Criteria Based on Fundamental Approach

In the previous section, stability criteria were obtained for gas–liquid bubble columns, gas–solid fluidized beds, liquid–solid fluidized beds, and three-phase fluidized beds. Before we begin the review of previous work, let us summarize the parameters that are important for the fluid mechanical description of multiphase systems. The first and foremost is the dispersion coefficient. During the derivation of equations of continuity and motion for multiphase turbulent dispersions, correlation terms such as $\overline{\varepsilon_S' v_z'}$ appeared [Eqs. (3) and (10)]. These terms were modeled according to the Boussinesq hypothesis [Eq. (4)], and thus the dispersion coefficients for the solid phase and liquid phase appear in the final forms of equation of continuity and motion [Eqs. (5), (6), (14), and (15)]. However, for the creeping flow regime, the dispersion term is obviously not important.

The second important term is the virtual mass coefficient (C_v). When the dispersed phase accelerates (or decelerates) with respect to the continuous phase, the surrounding continuous phase has to be accelerated (or decelerated). For such a motion, additional force is needed, which is called ''added or virtual mass force.'' This force was given by the second term in Eq. (8). The constant C_v is called the virtual or added mass coefficient. It is difficult to estimate the value of C_v with the present status of knowledge. Therefore, many recommendations are available in the published literature. In an extreme case of potential flow, the value of C_v is 0.5.

As regards the pressure, at a given location the pressure has been considered to be the same for all the phases. Further, when any area is occupied by different phases, the pressure has been assumed to be shared by the phases proportional to the fractional area occupied by the phases. This approach has been used by several investigators in the past (Kataoka, 1986; Kataoka and Serizawa, 1989; Elgobashi and Abou-Arab, 1983).

As regards to the estimation of force due to buoyancy, there have been two schools of thought. One considers the force equal to $v_p \rho_r g$ where ρ_r is the continuous phase density and v_p is the particle volume (Clift *et al.,* 1987; Clift, 1993; Joshi, 1983; Epstein, 1984). The other school considers the buoyancy force equal to $v_p \rho_D g$ where ρ_D is the average density of dispersion (Foscolo and Gibilaro, 1984; Gibilaro *et al.,* 1987; Astarita, 1993).

The details pertaining to the debate are given in Appendix B. It has been concluded that the buoyancy force is governed by the fluid density.

The drag force depends upon the particle Reynolds number. Different C_D–Re relationships have been used in the past. Further, several investigators have attempted fluid-mechanical description of multiphase systems. It was thought desirable to analyze all these attempts in view of the discussion given earlier. Such an analysis is summarized in Table II. Some additional points are given next.

Jackson and co-workers were probably the first to embark on the theoretical analysis of the regime transition. They were primarily interested in describing a fluidized bed with the help of equations of motion. Stability analysis was carried out as a test to support their model equations. They presented the analysis of unbounded as well as bounded beds. While comparing the model predictions with experimental observations, they needed the values of particle phase viscosity and particle phase pressure. They selected some values and predicted that the gas–solid and solid–liquid fluidized beds are always unstable. This was probably because the stabilizing effect of dispersion was not included in the model. Jackson (1985) assigned the significance of elasticity to particle phase pressure and considered this to be responsible for the bed stability. The method for the estimation of particle phase pressure was, however, not given. The order of magnitude for particle phase pressure was given by

$$p'_S \propto u_{sup}^2, \tag{26}$$

where u_{sup} is the superficial liquid velocity. Dorgelo *et al.* (1985) have reported the following correlation for the particle phase dispersion coefficient in solid–liquid fluidized beds:

$$D_s \propto u_{sup}^2. \tag{27}$$

The similarity between Eqs. (26) and (27) is worth noting. Batchelor (1988) has proposed that the dispersion is the principal cause for the bed stability.

Homsy and co-workers consolidated the theory proposed by Jackson and co-workers. More importantly, they (El-Kaissy and Homsy, 1976; Didwania and Homsy, 1981a, 1981b, 1982; Ham *et al,* 1990) developed an elegant experimental setup and procedure for noting the transition. Their earlier experiments (El-Kaissy and Homsy, 1976; Didwania and Homsy, 1981a) showed transition at the condition of minimum fluidization itself. It was clearly shown later by Ham *et al.* (1990) that this observation was due to the selection of large particles. Further, Ham *et al.* (1990) systematically investigated the effect of particle size, liquid viscosity, and the density ratio on transition. They attributed the stability to the bed elasticity and showed

that the elasticity is the combined effect of Reynolds stress and hydrodynamic dispersion. From the experimental results, they found the values of bed elasticity over a wide range of particle size, liquid viscosity, and density ratio. The resulting values of elasticity were empirically correlated. However, they have not suggested any procedure for the independent measurement of bed elasticity, on the basis of which the transition can be predicted.

Rietema (1973) and Musters and Rietema (1977) presented the stability analysis of gas–solid fluidized beds. They have presented results of ingenious experiments where the effect of bed angle on the stability was investigated. It was convincingly shown that the bed becomes unstable only at a certain angle of tilting. Up to this angle, there is some force that stabilizes the bed and prevents it from becoming heterogeneous. This stability was

TABLE II
SUMMARY OF TWO-PHASE FORMULATIONS USED BY VARIOUS INVESTIGATORS

	JC[a]	HC	MR	BT	BG	LF	PB	SC
Dispersion in the equation of continuity	NC	NC	NC	NC	NC	NC	NC	NC
Dispersion in the equation of motion	NC	NC	C	C[5]	C[5]	C	C	NC
Definition of pressure	ρ_s	ρ_s	—		8	11		16
Pressure sharing among the two phases	NC	NC	NC	C	C	C	C	C
Definition of buoyancy[b]	ρ_f	ρ_f	ρ_f	e_D	e_D	ρ_f	ρ_f	ρ_f
Virtual mass effect	C	C	NC	C	C	C	C	NC
Formulation of particle phase drag	1	3		6	9	12	14	3
Any other feature	2	2	4	7	10	13	15	17

[a] JC, Jackson and co-workers; HC, Homsy and co-workers; MR, Musters and Rietema; BT, Batchelor; BG, Biesheuvel and Gorrisen; LF, Lisseter and Fowler; PB, Pauchon and Banerjee; SC, Shnip and co-workers; C, considered; NC, not considered.

[b] ρ_f means the buoyancy is decided by the fluid density, whereas e_D means the buoyancy is decided by the disperse phase mixture density.

[1] β, drag coefficient, depends only on hold-up and slip velocity.

[2] Particle phase pressure has been assumed to provide the stabilizing mechanism.

[3] $\alpha_3 = \varepsilon_0(1 - \varepsilon_0)(\rho_s - \rho_F)g/v_S$, where α_3 is the drag coefficient and V_s is the slip velocity.

[4] Interparticle cohesion force was considered to provide the stabilizing mechanism.

attributed to the cohesion between the particles, which imparts the property of elasticity to the bed. However, this hypothesis needs reexamination. Further, the analysis was restricted to beds where the particle Reynolds number was in the creeping flow region. The constant used for the evaluation of the drag term is for packed bed conditions and the changes due to fluidization are not included (for example, see Joshi, 1983, and Foscolo and Gibilaro, 1984). Other investigators have also argued in favor of interparticle forces. Tsinontides and Jackson (1993) have argued that stability in gas–solid fluidized beds is due to yield stresses of particle assemblies and the particle–particle contact forces are responsible for stability of fluidized beds. They have used the well-known hysteresis behavior that is observed when the flow rate is first increased (particulate–aggregative transi-

TABLE II (*continued*)

[5] The dispersion in equation of motion (12) appears in the second-order derivative, while Batchelor (1988) has considered mobility to derive the dispersion term, which is a first-order derivative.

[6] Drag coefficient has been obtained under creeping flow conditions.

[7] Particle diffusion considered to stabilize while particle inertia forces promote the amplitude.

[8] Kinetic contribution to the effective pressure is considered.

[9] $C_D = \frac{48}{Re} + O(Re^{-3/2})$.

[10] Uniform bubbly flow is unstable to void fraction disturbances above some critical value of the void fraction (>45%).

[11] Liquid side pressure is considered mainly due to hydrostatic head.

[12] $C_D = \frac{kD_b}{2}\frac{[1 + 17.67(\varepsilon_L^{3/2})^{6/7}]^2}{(18.67\varepsilon_L^{3/2})^2}$.

[13] Wall friction has been considered.

[14] Frictional force was assumed to be constant in the first case, while it was assumed to be a function of void fraction in the second case.

[15] Turbulence has been assumed to provide the stabilizing mechanism through axial dispersion.

[16] $\Delta P = k_V V_G + k_T V_G^2$.

[17] Transition from the homogeneous to the heterogeneous regime occurs as follows:

Semibatch operation:

$$\frac{\frac{gL}{v_{B\infty}^2}}{[k_V + 2\varepsilon_{G0}k_T V_S](1 - \varepsilon_{G0})^{m-1}[1 - (m+1)\varepsilon_{G0}]} < \frac{\pi \sinh(\pi h)}{\cosh(\pi h) - 1}.$$

Continuous operation:

$$\frac{\frac{gL}{v_{B\infty}^2}}{[k_V + 2\varepsilon_{G0}k_T(W_0 + V_S)](W_0 + V_S + \varepsilon_{G0}V_S')} < \pi \coth(\pi h).$$

tion) and then decreased (aggregative–particulate transition). Also, the hysteresis is perhaps an inherent characteristic of transitions. For example, Maruyama *et al.* (1981) have observed similar hysteresis behavior in the case of gas–liquid bubble columns. They have argued that the hysteresis indicates that once the transition to the heterogeneous regime occurs, the heterogeneous regime with ordered liquid circulation is more stable than flow without ordered liquid circulation. In any case, the bubble–bubble contact forces or yield stresses may not be able to explain the observed hysteresis behavior in case of gas–liquid bubble columns.

Clift (1993) has also argued that the hydrodynamic models are not sufficient to explain the stability of fluidized beds and that the interparticle forces that determine the elasticity of the bed are important to explain the stability. He has given expressions of Abdel-Ghani *et al.* (1991) for the mean elasticity modulus of the bed,

$$E^* = \left(\frac{9\pi\Gamma E_s^2 d_P^5}{16(1 - m_P^2)^2} \right)^{1/3}, \tag{28}$$

where E_s is the elasticity modulus of the material of the bed, Γ is the interfacial energy, and m_p is the Poisson ratio of the material of the bed. For particles that contact at asperities with radius of curvature r_c, the mean elasticity modulus is given by

$$E^* = \frac{f(\varepsilon)}{d_P} \left(\frac{9\pi\Gamma E_s^2 r_c^5}{4(1 - m_P^2)^2} \right)^{1/3}. \tag{29}$$

However, the measured values of elasticity modulus are several orders of magnitude lower than the values predicted by these equations. Perhaps the bed elasticity may have a role to play for fine cohesive particles at high solid hold-ups. In that case, this can be included in future in the equation of motion for the particle phase as an extra force arising out of particle–particle interaction, without affecting the fundamental approach of linear stability analysis.

Batchelor (1988), for the first time, bridged the gap between stability and instability in fluidized beds in a more cogent manner. The elusive stabilizing term was given the significance of dispersion. In fact, the previous theories had to resort to some fictitious terms that stabilize the bed. For example, Jackson and co-workers attributed it to the particle phase pressure, Homsy and co-workers to the collisional pressure, Musters and Rietema (1977) to the cohesion forces of the particle network, and Foscolo and Gibilaro (1984) to the residual force acting on the particles when a pressure disturbance propagates. It is likely that particle–particle interactions are important under certain conditions, such as fine particles and/or

high solid hold-ups. However, such interactions may not be important when the solid hold-up is small ($< 30\%$). Further, in gas–liquid dispersion, such interactions are unlikely to play any significant role in governing the transition.

Batchelor (1988) developed a force balance equation for the solid phase in fluidized beds using the ensemble average method. With the help of the resulting equation and the theory of linear stability the following criterion was obtained by Ham *et al.* (1990):

$$N_{\mathrm{m}} = \frac{[A(G/F) - B/2]^2}{A(Z - C) + B^2/4} < 1. \tag{30}$$

The values of *A, B, C, G,* and *F* for various multiphase equipment are given by Table I. Z is defined as

$$Z = \frac{K_0}{u_0^2} + \frac{\nu_0(\rho_{\mathrm{S}} - \rho_{\mathrm{f}})D_{\mathrm{S}}}{\rho_{\mathrm{S}}\mathrm{Fr}}, \tag{31}$$

where

$$\mathrm{Fr} = \mathrm{u}_0^2/gd_{\mathrm{P}}.$$

The first term on the LHS of Eq. (31) represents the Reynolds stress associated with particle fluctuations, and ν_0 is the mobility. Thus, the contribution to Z may be considered to be made up of two parts: one arising from the mean square velocity fluctuations, and the other due to dispersion.

Batchelor (1988) has derived the particle phase governing equation directly without any need for writing a liquid phase momentum equation. This enabled elimination of the pressure term. The dispersion term was not included in the equation of continuity. However, it was included in the equation of motion. A revisit to the derivation of governing equations is expected to be useful in future development.

Ham *et al.* (1990) used Eqs. (30) and (31) and estimated the values of the solid phase dispersion coefficient using the experimental results on transition in solid–liquid fluidized beds. However, the estimated values of D_{s} deviate from the experimental values of D_{s} obtained by Dorgelo *et al.* (1985). It may be noted that the RTD based experimental D_{s} values includes gross nonidealities in addition to the turbulent dispersion.

Pauchon and Banerjee (1988), in their analysis of bubbly flows, have shown that the kinematic wave velocity based on a constant interfacial friction is weakly stable. They have also obtained a functional dependence of the interfacial friction factor on the void fraction by assuming the kinetic wave velocity equal to the characteristic velocity (kinetic waves are neutrally stable). They have assumed that turbulence provides the stabilizing mechanism through axial dispersion of the void fraction.

Biesheuvel and Gorrisen (1990) have derived one-dimensional conservation equations for void fraction disturbances in a uniform bubbly fluid. They have studied the features of the propagation of void fraction disturbances and investigated the stability of uniform bubbly flows. They observed that the voidage fraction waves are unstable for void fractions above some critical value (>45%). Their method of approach was similar to that of Batchelor (1988) in many respects.

Lisseter and Fowler (1992) have derived a simple set of equations for bubbly flow through a vertical tube. They have shown that under steady flow conditions, the void fraction will relax from its inlet value to an asymptotic value within only a short distance from the inlet. They have obtained a relationship between the inlet void fraction and the imposed pressure drop and derived a simple expression for the equilibrium void fraction. They have also considered the wall friction in their analysis of bubbly flows.

Shnip *et al.* (1992) have developed criteria for predicting the transition from the homogeneous to the heterogeneous regime in two-dimensional bubble columns, using the theory of linear stability. They analyzed both for semibatch and continuous modes of operation. They found good agreement between the predicted and experimental values of the critical gas velocity over a wide range of hole diameters and numbers of holes. They obtained 0.42 as the maximum value of the predicted critical gas hold-up. The transition criterion developed by them was found to be independent of the viscosity.

Sangani and Didwania (1993) have derived averaged equations for large-Reynolds-number, laminar-flow gas–liquid dispersions accounting for slowly varying spatial and temporal fields. In particular, they obtained an exact expression for the dispersed-phase stress tensor to be used in the force balance equation for gas bubbles and illustrated its application by evaluating the stress tensor for a few special cases. It is shown that the dispersed-phase stress tensor gradient with respect to the mean relative motion or the void fraction for the uniformly random bubbly liquids under conditions of large Reynolds number laminar flows is negative and thus has a destabilizing influence on the dynamics of void fraction waves in bubbly liquids.

IV. Review of Stability Criteria Based on Heuristic Approach

Wallis (1969) proposed a very elegant and simple criterion for the transition in fluidized beds. The criterion is based on the concept of elasticity of fluidized beds. It assumes that a fluidized bed resists deformation like any

other elastic material. Also, it possesses an upper limit of elasticity beyond which the bed can no longer sustain the strain and collapses to become heterogeneous. Mathematically, it states that the bed becomes heterogeneous when the propagation velocity of voidage disturbance (also called continuity wave velocity) exceeds the velocity of elastic waves (also called the dynamic wave velocity) in the bed. The theoretical justification behind such a criterion has been given by Whithman (1974). The physical significance of these two velocities is given next.

Slis *et al.* (1959) investigated the voidage propagation velocity. The authors not only provided the theoretical basis but provided an excellent experimental support for u_ϵ. Therefore, this investigation has been used extensively by the subsequent workers in this area. Following is the mathematical derivation of u_ϵ in its simplest form. For more comprehensive derivation, the original work of Slis *et al.* (1959) is recommended.

Consider a gas–solid fluidized bed operating in the homogeneous regime. Let the gas flowrate be reduced suddenly. The adjustment to this new flowrate starts from the bottom of the bed. Visually we can see a line of demarcation that separates the two regions of equilibrium voidage. This sharp front travels up through the bed. The unsteady behavior ends when this sharp front and the falling bed surface confront each other and the voidage becomes completely uniform according to the new flowrate. It is this sharp front velocity that is commonly termed the voidage propagation velocity.

Considering the mass balance on the dispersed phase, if in time Δt the distance traveled by the sharp front is Δh, then

$$\Delta h(\varepsilon_{GB} - \varepsilon_{GA}) = \Delta t \Delta u_{sup}(1 - \varepsilon_{GA}), \tag{32}$$

where Δu_{sup} is the change in the continuous phase superficial velocity. Rearranging Eq. (32), we get

$$\frac{\Delta h}{\Delta t} = \frac{(1 - \varepsilon_{GA})}{(\varepsilon_{GB} - \varepsilon_{GA})} \Delta u_{sup}. \tag{33}$$

In the limiting case of infinitesimally small change in the gas velocity, we get the following relation:

$$u_\varepsilon = (1 - \varepsilon_G) \frac{du_{sup}}{d\varepsilon}. \tag{34}$$

We have the equation

$$u_{sup} = V_{s\infty} \varepsilon_G^m, \tag{35}$$

where $V_{s\infty}$ is the terminal settling velocity and ε_G is the voidage.

Substituting Eq. (35) in (34) gives

$$u_\varepsilon = V_{s\infty} m(1 - \varepsilon_G).\varepsilon_G^{m-1}. \tag{36}$$

It has been mentioned earlier that the voidage propagation velocity is the same as the sharp front velocity. Thus, the equation for u_ε is the same in gas–solid fluidized beds and liquid–solid fluidized beds. However, for bubble columns, the sharp front velocity is given by the following equation:

$$u_\varepsilon = V_{B\infty}\varepsilon_L^{m-1} - m\varepsilon_G V_{B\infty}\varepsilon_L^{m-1}. \tag{37}$$

While presenting a comprehensive analysis of two-phase flow, Wallis (1969) has discussed the problem of transition. He has given a very systematic derivation for the voidage propagation velocity and takes the form of Eq. (36) for the case of small variations about the steady state.

Wallis (1969) also derived an equation for the elastic wave velocity:

$$u_e = (\partial p/d\rho)^{0.5}. \tag{38}$$

The value of u_e was evaluated from equation of motion and for the case of solid–liquid fluidized beds, and under some simplifying conditions it is given by

$$u_e = \left[\frac{v_S^2}{\varepsilon_L/\rho_L + \varepsilon_S/\rho_S}\right]^{1/2}\left[\frac{\varepsilon_S}{\rho_S} + \frac{\varepsilon_L}{\rho_L}\right]^{-1/2}. \tag{39}$$

Wallis (1969) compared the values of u_ε and u_e for solid–liquid fluidized beds and gas–solid fluidized beds and concluded that all the beds are unstable.

Verloop and Heertjes (1970) used Eq. (36) for the voidage propagation velocity. The elastic wave velocity was calculated on the basis that the fluidized bed was considered to be an elastic substance:

$$u_e = (E_S/\rho)^{1/2}, \tag{40}$$

where

$$E_S = (\Delta F/\Delta X)(4/\pi d). \tag{41}$$

ΔF is the increase in drag force when the distance between two particles is decreased by ΔX. The following relationship of Rowe (1984) was assumed:

$$\frac{F_D}{F_{D\infty}} = \frac{0.68}{\delta_r}. \tag{42}$$

F_D and F_∞ are the values of drag force on a particle in a fluidized bed and on a particle in an infinite medium, respectively. δ_r is the dimensionless distance (x/d_p) between the particles. The following equations were derived for the elastic wave velocity:

$$u_e = [128 g d_P (V_{mf}/v_S)^a]^{1/2}, \tag{43}$$

where $a = 1$ when $Re_P < 2$

$a = 1.4$ when $2 < Re_P < 500$.

This analysis suffers from the following limitations:

1. Equation (42) indicates that the drag force depends upon the interparticle distance. In fact, for a fluidized particle, the drag force equals the net force due to gravity and buoyancy,

$$F_D = v_P(\rho_S - \rho_L)g, \tag{44}$$

and the value of F_D is independent of voidage. It may be noted that the drag coefficient increases with an increase in the solid hold-up. However, the slip velocity decreases with an increase in the solid hold-up. However, the overall effect of drag coefficient and slip velocity is that the value of F_D remains constant irrespective of value of ε_s.

2. The structure of fluidized bed is highly idealized.

For deriving equation for elastic wave velocity, Foscolo and Gibilaro (1984) designed an ingenious thought experiment. A fluidized bed was considered to be supported by a frictionless piston that also acted as a gas distributor. In the steady state, the piston was maintained in position by means of an external pressure, *p,* acting on its bottom face. A small increase Δp in this pressure caused an upward movement of the piston and the compression of the bottom portion of the bed. A net force ΔF acts on each of the N_S particles in the bottom layer in contact with the distributor. The consequent upward displacement reduces the local voidage in such a way that each particle in the next layer experiences the same net force, which in turn is transmitted to the layer above. In the way, the pressure wave was considered to travel longitudinally through the bed. The relations obtained were

$$\Delta F = A_S \Delta p / N_S, \tag{45}$$

where N_S is the number of particles,

$$N_S = \frac{4\varepsilon_S A_S}{\pi d_P^2}. \tag{46}$$

Substitution of Eqs. (45) and (46) in (38) gives

$$u_c = \left[\frac{4\varepsilon_S}{\pi d_P^2}\right]^{0.5}\left[\frac{dF}{d\bar{\rho}}\right]^{0.5} = \left[\frac{4\varepsilon_S}{\pi d_P^2}\right]^{0.5}\left[\frac{dF/d\varepsilon_C}{d\bar{\rho}/d\varepsilon_C}\right]^{0.5}, \tag{47}$$

where $\bar{\rho}$ is the average density of the bed and ε_C is the fractional hold-up of continuous phase,

$$\bar{\rho} = \varepsilon_C \rho_C + \varepsilon_D \rho_D . \tag{48a}$$

For a gas–solid fluidized bed,

$$\bar{\rho} = \varepsilon_G \rho_G + \varepsilon_S \rho_S . \tag{48b}$$

For a solid–liquid fluidized bed,

$$\bar{\rho} = \varepsilon_L \rho_L + \varepsilon_S \rho_S . \tag{48c}$$

Foscolo and Gibilaro (1984) assumed the continuous phase density (ρ_C) to be negligible. Though this is true for gas–solid fluidized beds, $\varepsilon_C \rho_C$ should be considered in liquid–solid fluidized beds and particularly in gas–liquid bubble columns.

The net force (F) was considered to be the difference between the drag force (F_D) and the effective weight (W_e). F_D was derived on the basis of particle bed model. For instance, for the case of a solid–liquid fluidized bed,

$$F = F_D - W_e = F_{D\infty} \left(\frac{u_{sup}}{V_{S\infty}} \right)^{4.8/m} \varepsilon_G^{-3.8} - \frac{\pi d_P^3}{6} (\rho_S - \rho_G) g \varepsilon_G . \tag{49}$$

While estimating $dF/d\varepsilon$, the value of the superficial velocity was assumed constant. Substitution of Eqs. (48) and (49) in (47) results in the following equation for the elastic wave velocity:

$$u_e = [3.2 g d_P (1 - \varepsilon_G)(\rho_S - \rho_G)/\rho_S]^{1/2} . \tag{50}$$

In the preceding thought experiment and derivation where there are two regions of ε, some explanation is needed for the physical significance of F and $dF/d\varepsilon_C$. In fact, if The Richardson-Zaki correlation is substituted in Eq. (49), F works out to be zero. This point becomes particularly relevant because, in the derivation of elastic wave velocity, Verloop and Heertjes (1970) have used the drag force directly [Eq. (41)], whereas Foscolo and Gibilaro (1984) have used the difference between the drag force and the effective weight of particles [Eq. (49)].

Foscolo and Gibilaro (1984) have claimed excellent agreement between the model predictions and the experimental observations. However, Tsinontides and Jackson (1993) have expressed some reservations regarding such an agreement.

A. Relationship between Fundamental Approach and Heuristic Approach

1. Solid–Liquid and Gas–Solid Fluidized Beds

In all the criteria developed using the heuristic approach (discussed earlier in this section) a comparison is made between the dynamic (elastic)

wave velocity (u_e) and the continuity wave (voidage propagation) velocity (u_ε). The transition is said to occur when u_ε exceeds u_e. It will be worth while if this criterion is derived from the fundamental approach. Further, it will be good to know the range of parameters over which the heuristic criterion can be safely used.

Let us start with the criterion developed using the fundamental approach [Eq. (24)]:

$$\frac{[A(G/F) - B/2]^2}{A(Z - C) + B^2/4} < 1.$$

Simplifying,

$$A(G/F)^2 - B(G/F) + C < Z. \tag{51}$$

The values of *A, B, C, F, G, and Z* for gas–solid fluidized beds, solid–liquid fluidized beds, gas–liquid bubble columns, and three-phase fluidized beds are given in Table I. Let us consider these parameters for gas–solid fluidized beds (refer to Table I). Since ρ_G/ρ_S can be considered negligible,

$$A = 1, \qquad B = 0, \qquad C = 0. \tag{52}$$

Substitution of Eq. (52) in (51) gives the stability criterion

$$G/F < \sqrt{Z}, \tag{53}$$

where

$$\frac{G}{F} = mV_{S\infty}\varepsilon_S\varepsilon_G^{m-1} \tag{54}$$

which is the same as Eq. (36) and represents the voidage propagation velocity.

$$Z = \frac{\varepsilon_S(\rho_S - \rho_G)g}{\rho_S\nu_S}\left[\frac{D_S}{\varepsilon_S} + \frac{D_G}{\varepsilon_G}\right]. \tag{55}$$

Further, as a first approximation, if we neglect gas phase dispersion as compared with solid phase dispersion, Eq. (55) takes the following form:

$$Z = \frac{(\rho_S - \rho_G)}{\rho_S\nu_S} D_S g = \frac{-\beta_0}{\rho_S}\left(\frac{D_S}{\varepsilon_S}\right). \tag{56a}$$

There is little information regarding the form of D_G. A possible alternative is to assume that $D_G = D_S$. If we had taken $D_G = D_S$, the expression for Z would be

$$Z = \frac{-\beta_0}{\rho_S}\left(\frac{D_S}{\varepsilon_S\varepsilon_G}\right). \tag{56b}$$

The assumption of equality of dispersion coefficients of both the phases implies that the root mean square velocity and length scale of turbulence of the gas phase is the same as that of the solid (dispersed) phase. We have taken the length scale of the solid phase to be equal to twice the particle diameter. It is not clear whether the same length scale can be assumed for the gas phase, as the gas phase eddies can be smaller than the particle diameter. Also, the root mean square velocities of both the phases may not be equal. Furthermore, because of the slip velocity, sufficient time may not be available for the local gas phase eddies to be in equilibrium with the dispersed phase eddies.

Thus, both of these assumptions are restrictive, and in the absence of additional information, one of these assumptions needs to be made. For the case of gas–solid fluidized beds and solid–liquid fluidized beds, if we assume $D_G = D_L = 0$, we get a criterion [Eq. (61)] that is almost same as the criterion of Gibilaro and Foscolo (1984), given in Eq. (50). Therefore, this assumption was made.

The solid phase dispersion coefficient can be written as the product of the length and velocity scale of turbulence:

$$D_S = u'_z l. \tag{57}$$

Handley *et al.* (1966) measured the solid-phase rms velocity in solid–liquid fluidized beds. These values can be correlated on the basis of energy balance developed by Joshi and Lali (1984):

$$u'_z = 1.5\varepsilon_S v_S \tag{58a}$$

$$l = 2d_P. \tag{58b}$$

Therefore,

$$D_S = 3\varepsilon_S v_S d_P. \tag{59}$$

The proportionality constant of 3 may be considered as preliminary estimate. Substitution of Eq. (59) in (56) gives

$$Z = 3d_P\varepsilon_S(\rho_S - \rho_G)g/\rho_S. \tag{60}$$

Substitution of Eq. (54) and (60) in (53) gives the following condition for the transition:

$$\sqrt{3d_P\varepsilon_S(\rho_S - \rho_G)g/\rho_S} > m\varepsilon_S V_{S\infty}\varepsilon_G^{m-1}. \tag{61}$$

It can be readily seen by comparison with Eq. (50) that the left-hand side of Eq. (61) is the elastic wave or dynamic wave velocity of Gibilaro Foscolo and co-workers.

Thus, Eq. (61) forms the basis of comparison of dynamic wave velocity

with continuity wave velocity. This is a very useful result. At this state, the following additional points may be noted.

1. The stabilizing property of the dynamic or elastic wave velocity is due to the dispersion in the solid phase. The higher the dispersion coefficient, the greater the ability of the bed to remain homogeneous. In earlier work, this property was not clearly recognized (Section III). Jackson attributed the stability to particle phase pressure; Homsy and co-workers attributed it to collisional pressure, whereas Musters and Rietema (1977) attributed it to the elastic property of the bed. In all these cases, it is difficult to measure the respective properties. Batchelor (1988) was the first to recognize the ability of dispersion to keep the bed homogeneous.

2. Equation (61) is the transition criterion provided the conditions given by equation (52) are satisfied. From Table I it can be seen that these conditions are satisfied only in the case of gas–solid fluidized beds and in some cases of solid–liquid fluidized beds where $\rho_S \gg \rho_L$. Therefore, for other multiphase dispersions [such as gas–liquid (bubble columns) and solid–liquid fluidized beds (where ρ_L is not negligible)] the comparison of dynamic wave velocity with continuity wave velocity is not valid for deciding the bed stability. Further, the above analysis holds for transition from region I to II (point P in Fig. 1) and not for III to II (point Q). Therefore, the criterion does not hold for bubble columns and dilute dispersions.

3. Equation (36) gives the voidage propagation velocity (sharp front or continuity wave velocity) for gas–solid and solid–liquid fluidized beds. However, for the other multiphase dispersions, the procedure given by Eqs. (32) to (37) should be used. Thus, for gas–liquid dispersions, the sharp front velocity is given by Eq. (37).

4. The stability criterion given by Eq. (61) can be simplified even further. Rearranging equation and considering $\rho_S \gg \rho_G$,

$$\frac{V_{S\infty}}{\sqrt{gd_P}} < \frac{1}{m\varepsilon_G^{m-1}} \sqrt{\frac{3}{\varepsilon_S}}. \tag{62}$$

The left-hand side is Froude number.

For gas–solid fluidized beds, in many cases, the aggregative fluidization occurs at the condition of incipient fluidization. Substituting $\varepsilon_S = 0.6$, $\varepsilon_G = 0.4$, $m = 2.4$, the right-hand side works out to be 3.3. This is again an interesting result. As early as 1948, Wilhelm and Kwauk were probably the first to provide some insight in the transition criterion. Wilhelm and Kwauk concluded that beds with small Froude numbers do not bubble easily. It may be pointed out that Eq. (62) was derived for gas–solid fluidized beds with a simplyfying assumption. The bubbling condition may coincide

with transition in gas–solid fluidized beds; however, it may not coincide with transition in solid–liquid fluidized beds. In fact, the experiments of Anderson and Jackson (1968) and Homsy and co-workers have revealed clearly that the liquid fluidized beds are not linearly stable and that voidage waves exist in them as well. Thus, the lack of presence of bubbles in solid–liquid fluidized beds may not be equivalent to stability.

2. Gas–Liquid Bubble Columns

Lockett and Kirkpatrick (1975) have presented an interesting analysis for the prediction of critical gas hold-up (ε_{GC}). In the absence of liquid flow, $V_G/\varepsilon_G = V_S$. Therefore,

$$V_G = \varepsilon_G(1 - \varepsilon_G)^{m-1}V_{B\infty}. \tag{63a}$$

A plot of ε_G vs V_G passes through a maximum and gives a value of maximum gas throughput which may be achieved. The maximum permissible gas hold-up can be obtained by setting $dV_G/d\varepsilon_G = 0$. The result is

$$\varepsilon_{GC} = \frac{1}{m}. \tag{63b}$$

Ideally, it should be possible to reach the maximum and still remain in the bubbly flow regime. Thereafter, any further increase in the gas flow rate results in a continuity limitation on the gas. Flooding occurs, resulting in the formation of large bubbles and transition. Thus, ε_{GC} may be considered as the transition gas hold-up.

In the preceding analysis, the velocity–hold-up relationship was expressed in terms of the Richardson–Zaki equation. Alternatively, the relationship can be derived from the Ergun (1952) equation. This latter approach was used by Molerus (1993).

In the homogeneous regime, the hindered velocity of the dispersed phase is known to be due to an increase in the drag coefficient. Thus,

$$C_{D\infty}\frac{\pi d_B^2}{4}\frac{\rho_L V_{B\infty}^2}{2} = \frac{\pi}{6}d_B^3(\rho_L - \rho_G)g \tag{64a}$$

$$C_D\frac{\pi d_B^2}{4}\frac{\rho_L v_S^2}{2} = \frac{\pi}{6}d_B^3(\rho_L - \rho_G)g, \tag{64b}$$

where $C_{D\infty}$ is the drag coefficient under the terminal rise conditions, C_D is the drag coefficient in the presence of other particles (or bubbles), and v_S is the hindered velocity. For solid–liquid fluidized beds, C_D is given by

$$C_D = \frac{4}{3}\frac{(\rho_S - \rho_L)d_P g}{\rho_L v_S^2}. \tag{65}$$

Molerus established the following correlation for C_D on the basis of bed expansion characteristics:

$$C_D = \frac{24}{Re_P}\left[1 + K_1\left(\frac{r_o}{\delta} + 0.5\frac{r_o^2}{\delta^2}\right)\right] + \frac{4}{\sqrt{Re_P}}\left[1 + K_2\left(\frac{r_o}{\delta}\right)^{1.5}\right] + 0.4 + K_3\frac{r_o}{\delta}\frac{1}{Re_P^n}. \tag{66}$$

Here,

$$\frac{r_o}{\delta} = \frac{1}{\zeta/\varepsilon_L^{1/3} - 1} \qquad \text{and} \qquad Re_P = \frac{u_{sup} d_P \rho_L}{\varepsilon_L \mu_L} \tag{67}$$

$$\zeta = 0.9,\ K_1 = 0.341,\ K_2 = 0.07,\ K_3 = 0.907,\ n = 0.1, \tag{68}$$

and

$$C_D Re_P^2 = \frac{4}{3}\left(\frac{\rho_S - \rho_L}{\rho_L}\right)\frac{d_P^3 g}{\nu_L^2}. \tag{69}$$

It may be noted from Eq (66) that the value of C_D for a single particle in an infinite, medium is given by 24/Re and 0.4 in the creeping and turbulent flow conditions, respectively. Molerus (1993) assumed that Eqs. (65)–(69) also hold for gas–liquid systems, though marked differences are known to exist. He defined the dimensionless parameters

$$\hat{d}_B^3 = \left(\frac{\rho_L - \rho_G}{\rho_L}\right)\frac{d_B^3 g}{\nu_L^2} \tag{70}$$

$$Re_B = \frac{v_S d_B \rho_L}{\mu_L} \tag{71}$$

$$\sigma_o^3 = \frac{\rho_L}{\rho_L - \rho_G}\frac{v_S^3}{\nu_L g} \tag{72}$$

$$\gamma^3 = \frac{\rho_L}{\rho_L - \rho_G}\frac{v_{sup}^3}{\nu_L g}, \tag{73}$$

where $\hat{d}_B$ defines the dimensionless bubble diameter, σ_0 the dimensionless relative velocity, and γ is the dimensionless gas throughput. A typical plot of ε_G vs σ_0 with $\hat{d}_B$ and γ as parameters is shown in Fig. 4. The solid lines are lines of dimensionless bubble size d_B = constant. Numbers indicate the bubble sizes d_B (mm) for air in water. These lines end at the abscissa for dimensionless single bubble rise velocity ($\varepsilon_G = 0$). The dotted lines are

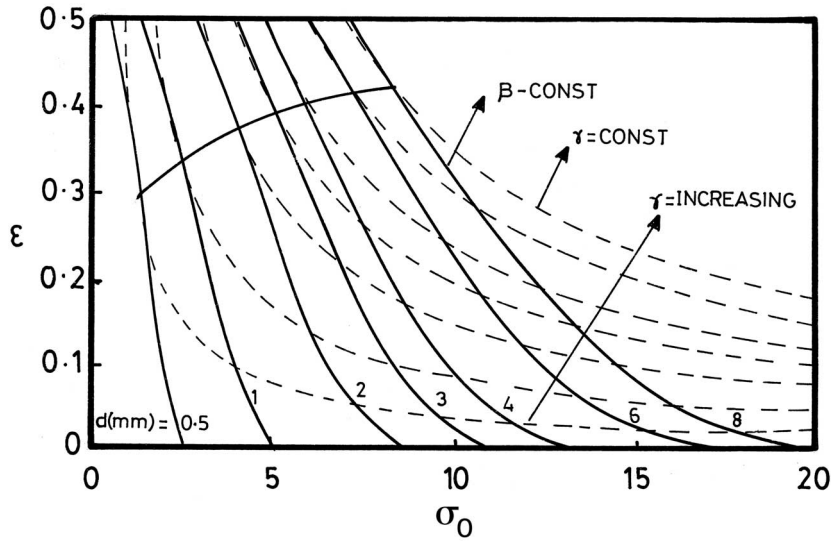

FIG. 4. Transition plot from Molerus (1993).

lines of constant gas throughput. The direction of increasing gas throughput is shown by an arrow. It can be seen from the figure that each line of γ = constant shows tangential contact with a particular line $\hat{d}_B$ = constant. This behavior means that for a given bubble size, a maximum gas throughput exists that cannot be exceeded with homogeneous bubble flow. If gas throughput is increased beyond the limit of homogeneous bubble flow, Molerus suggested the following two different means of transition:

1. Froth formation can occur if coalescence of small bubbles is completely suppressed.
2. Liquid circulation will begin for accommodating the higher gas throughput.

Ranade and Joshi (1987) have developed a criterion for small bubbles. The small bubbles rise upward without any oscillations. The liquid carried upward in the bubble wakes is released at the top liquid surface, which then flows downward in the bubble-free region. The downward liquid flow hinders the bubble rise. It was proposed that the transition will occur when the bubble rise velocity equals the downward liquid velocity. Under this condition, the bubble rise velocity with respect to the column wall is zero and the gas phase accumulates in the column, leading to transition.

If ζ is the fractional wake volume, the liquid phase mass balance gives

$$\zeta\varepsilon_G V_{B\infty} = (1 - \varepsilon_G - \zeta\varepsilon_G)\, U_D. \tag{74}$$

The bracketed term corresponds to the bubble-free region where the liquid down flow occurs. U_D is the downward liquid velocity. At transition, equating U_D and $V_{B\infty}$, we get

$$\zeta\varepsilon_{GC} = (1 - \varepsilon_{GC} - \zeta\varepsilon_{GC}). \tag{75}$$

Selecting ζ equal to 11/15 (Kumar and Kuloor, 1972), the value of critical gas hold-up at transition works out to be 0.42. This value, estimated for small bubbles, is in agreement with the experimental findings of Oels *et al.* (1978) and Koetsier *et al.* (1976).

The difference between the analysis of Lockett and Kirkpatrick (1975), Molerus (1993), and Ranade and Joshi (1987) may be noted. In the former case [Lockett and Kirkpatrick (1975) and Molerus (1993)], flooding occurs because the bubble slip velocity gets reduced with an increase in the gas hold-up and at ε_{GC} flooding occurs. In the latter case (Ranade and Joshi, 1987), flooding occurs because of the downflow of liquid (which was carried upward through wakes). However, both the analyses give the upper limit that is observed by small bubbles (due to sparger design, low surface tension, high gas density or non-coalescing system). For relatively large bubbles, transition may occur below the flooding point because of either coalescence (formation of large bubbles) or intrinsic hydrodynamic instability (explained in the next subsection).

For relatively large bubbles (>2 mm) and coalescing liquids, the value of ε_{GC} may be obtained by the following consideration. The large bubbles rise with oscillations due to periodic shedding of vortices behind the bubbles. Since the size of a vortex is of the order of $d_P/2$, it may be assumed that the scale of oscillations is approximately $d_P/2$. Using this value for the bubble clearance and the cubic lattice structure, the value of critical gas hold-up works out to be 0.16. This is in good agreement with the experimental values of 0.15 to 0.2 reported by Deckwer *et al.* (1977), Whalley and Davidson (1974), and Kelkar (1983). It may be pointed out that Taitel *et al.* (1980) have observed enhanced coalescence when ε_{SC} exceeds 0.18. This value supports the preceding heuristic arguments.

The stability criterion can considerably be simplified for the case of gas–liquid dispersion. The constants in Eq. (24), for the case of semibatch operation ($u = 0$), are defined in Table I. Since the ratio ρ_G/ρ_L is negligible, the constants are simplified and are given by

$$A = \frac{(1 + C_v)}{\varepsilon_L} - 1 \tag{76a}$$

$$B = 2C_v v_S \tag{76b}$$

$$C = C_v v_S^2 \tag{76c}$$

$$Z = \alpha d_B \varepsilon_G g, \tag{76d}$$

where α is the proportionality constant for dispersion.

As discussed earlier, transition in bubble columns occurs in most cases because the denominator in Eq. (24) becomes zero, i.e.,

$$A(Z - C) + B^2/4 = 0. \tag{77}$$

Equations (76) and (77) give the following simplified criterion:

$$\frac{V_{B\infty}}{\sqrt{d_B g}} = \sqrt{\frac{\alpha(\varepsilon_G + C_v)}{C_v(1 + C_v)}} \frac{1}{\varepsilon_L^{m-1}}. \tag{78}$$

Again, the left hand side is the Froude number. For $C_v = 0.5$, $m = 1$ $\alpha = 1.2$, $V_{B\infty} = 200$ mm/s, and $d_B = 3$ mm, Eq. (78) gives

$$\varepsilon_{GC} = 0.34. \tag{79}$$

Thus, different combination of parameters C_V, α and m can lead to some maximum transition gas hold-up. This is again an interesting result. Equation (76) then provides a fundamental basis for many empirical criteria in the literature that simply give a maximum value of gas hold-up up to which the homogeneous regime can prevail. For example, Bach and Pilhofer (1978) gave the transition gas hold-up as 0.25, Mersmann (1978) gave $\varepsilon_{GC} = 0.2$, Taitel *et al.* (1980) gave $\varepsilon_{GC} = 0.18$, and Schugerl *et al.* (1977) gave $\epsilon_{GC} = 0.42$.

V. Model Predictions and Experimental Observations

A. Estimation of Model Parameters

Various model parameters involved in the derivation of the stability criterion need to be specified in order to use the stability criterion for quantitative predictions. Model parameters essential for this purpose include the slip velocity, the virtual mass coefficient, and the dispersion coefficient. The procedure for estimation of these parameters is given for gas–solid (and solid–liquid) fluidized beds and bubble columns.

1. Fluidized beds

a. Estimation of Slip Velocity. In the case of fluidized beds, the slip velocity is given by ($V_{sup} = 0$)

$$v_s = \frac{u_{sup}}{\varepsilon_c}, \tag{80}$$

where u_{sup} is the superficial fluid velocity. It is given by an equation similar to the Richardson–Zaki equation:

$$u_{sup} = V_{S\infty}\varepsilon_c^m. \tag{81}$$

The terminal settling velocity was predicted using the following procedure.

The Galileo number at given particle diameter d_p was calculated as

$$\mathrm{Ga} = \frac{d_P^3 \rho_c(\rho_s - \rho_c)g}{\mu_c^2}. \tag{82}$$

The Reynolds number (based on the terminal settling velocity) was estimated from the Galileo number using the correlations given by Lali *et al.* (1989). The terminal settling velocity was then calculated from the Reynolds number and the physical properties. The Richardson–Zaki index m was estimated using the correlations given by Richardson (1971).

b. Estimation of the Dispersion Coefficient. An important parameter in the stability criterion is the dispersion coefficient. Correlations for the dispersion coefficient are mostly obtained by the one-dimensional model. The estimated value of the dispersion coefficient for solid–liquid and gas–solid fluidized beds was obtained from Eq. (59) given earlier:

$$D_S = 3d_P\varepsilon_S v_S. \tag{59}$$

Equation (59) was used to estimate the dispersion coefficient with a proportionality constant of 3. However, the effect of extreme values of the proportionality constant of dispersion was also studied. The dispersion coefficient for the continuous phase was taken as zero for the model predictions.

c. Estimation of Virtual Mass Coefficient. The virtual mass coefficient C_V represents the acceleration reaction of the dispersed phase on the continuous phase. Virtual mass plays an important role in case of gas–solid fluidized beds and solid–liquid fluidized beds when $\rho_S \gg \rho_L$.

Jackson (1985) used a constant value of 0.5 as the virtual mass coefficient, which is for an isolated sphere in an infinite medium. Homsy *et al.* (1980)

assumed the virtual mass coefficient to be a function of the continuous phase hold-up, given by

$$C_v = \frac{3 - 2\varepsilon_C}{2\varepsilon_C}, \tag{83}$$

which, in the limiting case of $\varepsilon_C = 1$, gives $C_v = 0.5$.

Equation (83) was used to estimate C_v for model predictions. The effect of C_v values of zero and 0.5 was also studied.

2. *Bubble Columns*

In bubble columns, the estimation of parameters is more difficult than in the case of either gas-solid or solid–liquid fluidized beds. Major uncertainties in the case of bubble columns are due to the essential differences between solid particles and gas bubbles. The solid particles are rigid, and hence the solid–liquid (or gas–solid) interface is nondeformable, whereas the bubbles cannot be considered as rigid and the gas–liquid interface is deformable. Further, the effect of surface active agents is much more pronounced in the case of gas–liquid interfaces. This leads to uncertainties in the prediction of all the major parameters such as terminal bubble rise velocity, the relation between bubble diameter and terminal bubble rise velocity, and the relation between hindered rise velocity and terminal rise velocity. The estimation procedure for these parameters is reviewed next.

a. Estimation of Terminal Rise Velocity of Bubbles. Clift *et al.* (1978) have critically reviewed the literature on terminal rise velocity of bubbles. One of the major factors influencing the terminal bubble rise velocity is the bubble shape, which can deviate from spherical to ellipsoidal or spherical cap because of the deformable interface. The presence of surface active agents also influences bubble shape. The bubble shape determines the drag force and, in turn, the terminal bubble rise velocity, since the terminal rise velocity of bubbles is decided by the balance among gravity, buoyancy, and drag. Another factor that affects the bubble rise velocity is the manner in which the bubble rises. The bubbles with diameter less than 1 mm travel in a straight line, whereas the bubbles with diameter greater than 1 mm oscillate horizontally while traveling upwards or follow a steady motion up a helix with a vertical axis. Depending on the manner of bubble travel (true vertical or zigzag), the distance covered by bubbles changes, thus affecting the terminal bubble rise velocity. The expressions for terminal rise velocities of bubbles in pure and contaminated liquids are given below.

(i) *Terminal Bubble Rise Velocity in Pure Liquids.* For spherical bubbles with Re $\ll 1$ (creeping flow), two extreme cases are possible depending on the nature of the gas–liquid interface. If the bubble is assumed to be similar to a rigid solid particle, the bubble rise velocity is given by Stokes relationship,

$$V_{B\infty} = \frac{(\rho_L - \rho_G) g d_B^2}{18 \mu_L}. \tag{84}$$

However, if the bubble interface is assumed deformable and completely free from contaminants, the bubble rise velocity is given by the Hadamard–Rybczynski equation. When the viscosity ratio (μ_G/μ_L) is zero, the terminal bubble rise velocity is given by

$$V_{B\infty} = \frac{(\rho_L - \rho_G) g d_B^2}{12 \mu_L}. \tag{85}$$

For ellipsoidal gas bubbles, Mendelsen (1967) has given the following correlation for terminal bubble rise velocity:

$$V_{B\infty} = \left(\frac{2\sigma}{\rho_L d_B} + \frac{g d_B}{2} \right)^{1/2}. \tag{86}$$

Here, ρ_G has been assumed to be much less than ρ_L.

For spherical cap bubbles, Davies and Taylor (1950) have given the relationship

$$V_{B\infty} = 0.711 (d_B g)^{1/2}. \tag{87}$$

(ii) *Terminal Bubble Rise Velocity in Contaminated Liquids.* For contaminated liquids, Clift *et al.* (1978) have given a generalized correlation in terms of dimensionless groups, which cover all bubble shapes. Based on this correlation, the relationship between bubble diameter and terminal rise velocity of bubble for an air-water system is given in Fig. 5.

In the same Fig. 5, two more curves based on experimental data of Gaudin (1977) are given for air–water systems. From this figure, one of the key problems in estimation of terminal bubble rise velocity becomes apparent. For a widely used system such as air–water, if a bubble diameter of 2 mm is taken, the rise velocity can have any value between 150 mm/s and 300 mm/s. Conversely, if we take the terminal rise velocity of bubbles to be 200 mm/s, bubble diameter can be anywhere between 1 and 10 mm, depending upon the degree of contamination, which is difficult to quantify and can change over a period of time. In the present work, we have used correlations of Clift *et al.* (1978) for the predictions. We also have used the

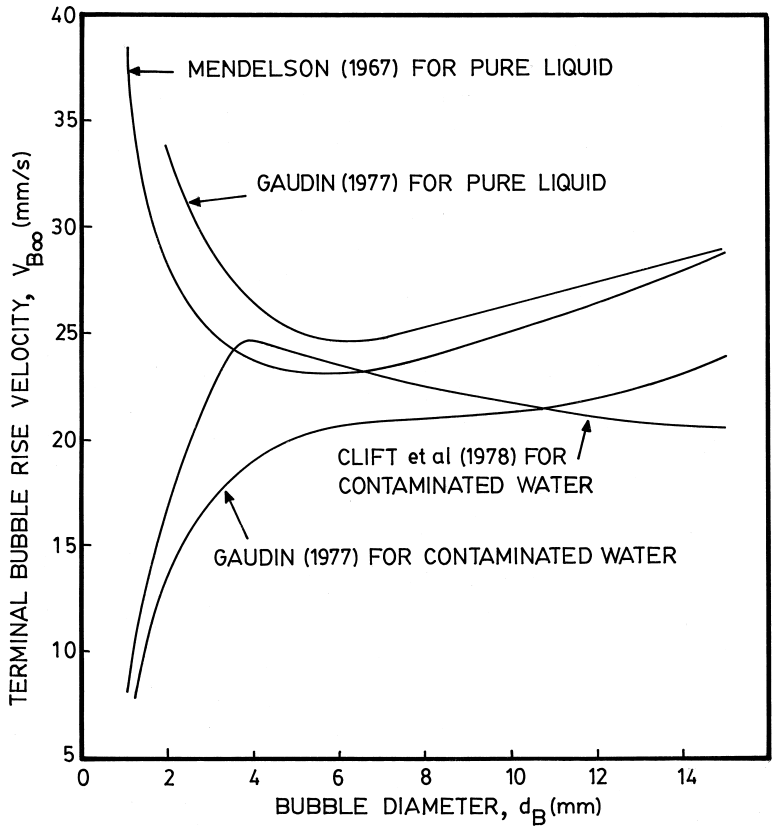

FIG. 5. Various relations between bubble diameter and terminal rise velocity: air–water system.

predictions based on the data of Gaudin (1977) to demonstrate the effect of the relationship between the bubble diameter and the terminal rise velocity of bubbles.

b. Estimation of the Slip Velocity for Gas–liquid Bubble Columns. The slip velocity can be given as

$$v_S = V_{B\infty}(1 - \varepsilon_G)^{m-1}. \tag{88}$$

For the case of a semibatch bubble column (no liquid flow), the drift flux model takes the form

$$J = v_S\varepsilon_G(1 - \varepsilon_G) = V_{B\infty}\varepsilon_G(1 - \varepsilon_G)^m. \tag{89}$$

Various investigators have suggested different values of m:

1. Davidson and Harrison (1966), $m = 0$
2. Turner (1966), $m = 1$
3. Wallis (1969), $m = 0$ for large bubbles and $m = 2$ for small bubbles
4. Zuber and Hench (1962), $m = 1.5$ for large bubbles and $m = 3$ for small bubbles
5. Richardson and Zaki (1954), $m = 2.39$
6. Pal and Masliyah (1989), $m = 2.39$

Some investigators have given different forms of correlation. For instance,

7. Marucci (1965), $v_S = V_{B\infty}(1 - \varepsilon_G)/(1 - \varepsilon_G^{5/3})$
8. Lockett and Kirkpatrick (1975), $v_S = V_{B\infty}(1 - \varepsilon_G)^{1.39}(1 + 2.55\varepsilon_G^3)$
9. Zhou and Egiebor (1993), $v_S = V_{B\infty}(1 - 1.06\varepsilon_G)$ when $\epsilon_G < 0.3$

The wide variation in the value of m may be attributed to the following reasons:

1. The different investigators have covered different regimes of operation. Any value of m less than 1.0 indicates the possibility of heterogeneous regime and Eqs. (87) and (88) are not applicable for such a regime.
2. The range of bubble size covered by different investigators is markedly different.
3. The most important reason for the wide variation in m seems to be due to the presence of surface active agents. These agents have two roles to play: (a) to retain the bubble size that is formed at the sparger, and (b) to reduce the interface mobility. In an extreme case, the interface becomes rigid enough so that the bubbles behave like solid particles in the same range of Reynolds number.
4. When $\varepsilon_G < 0.2$ the value of J becomes insensitive to the value of m.
5. For a given gas–liquid system, the value of m perhaps does not remain constant over a wide range of ε_G. The variation in m depends upon the coalescing nature of the bubbles.

From the foregoing discussion, it is clear that the value of m depends upon the properties of the gas–liquid system under consideration. In the present work, the transition will be examined at four levels of m, namely, $m = 1$, $m = 1.4$, $m = 1.9$, and $m = 2.4$.

c. Estimation of the Dispersion Coefficient. An equation similar to Eq. (59) was assumed to hold for gas–liquid bubble columns. For bubble columns, Eq. (59) is slightly modified as follows:

$$D_L = 3d_B\varepsilon_G v_S. \tag{90}$$

The gas phase dispersion coefficient was assumed to be zero.

d. Prediction of the Virtual Mass Coefficient. In the case of bubble columns, the virtual mass coefficient was estimated in a manner similar to the method used in case of fluidized beds. Equation (83) was used for the estimation of virtual mass coefficient in case of bubble columns. Two other values of C_v were also examined.

B. Stability Maps

1. Gas–Solid and Solid–Liquid Fluidized Beds

In order to study the effects of the fluid properties and particle sizes using the stability criterion developed in Section II, the following numerical calculations were undertaken. For a given set of physical properties of the system, two critical particle diameters were determined by employing the stability criterion derived earlier. The lower limit of the critical particle diameter, d_{PL}, is the largest particle diameter up to which the particulate or homogeneous regime prevails. All the particle diameters less than the lower critical particle diameter are stable (i.e., they will exhibit particulate fluidization) even up to a hold-up of 95%. The upper limit of the critical particle diameter, d_{PU}, is defined as the smallest diameter above which the heterogeneous regime prevails. All particle diameters greater than the upper limit will exhibit aggregative fluidization right at incipient fluidization conditions, i.e., at a hold-up value of 40%. Particle diameters between the two limits ($d_{PL} < d_P < d_{PU}$) will exhibit transition from particulate to aggregative fluidization at progressively lower values of hold-up.

The values of d_{PL} and d_{PU} were determined using

$$f(d_P) = 1 - N_m, \tag{91}$$

where N_m is the parameter defined by Eq. (28) and the constants *A, B, C, Z, G, and F* for solid–liquid fluidized beds and gas–solid fluidized beds are summarized in Table I. Since these constants depend on the hold-up under steady-state conditions, the function f_1 was evaluated for the entire range of ε_L, from packed bed condition (40% voidage) to 95% voidage, starting with an extremely small value of particle diameter, say 0.5 mm. The particle diameter was progressively increased and the function f_1 was again evaluated for the entire hold-up range. The critical diameter d_{PL} is that diameter for which the function f_1 first becomes negative.

The lower and upper limits mark the limits of the homogeneous and

heterogeneous regimes. All diameters of the particle below the lower limit will be stable, and therefore the area under the lower limit shows the stable area. Similarly, diameters above the upper limit will become unstable even at incipient fluidization, and therefore the area above this limit is called the unstable region and will always exhibit aggregative behavior. Typical transition plots for solid–liquid and gas–solid fluidized beds are shown in Fig. 6a and 6b, respectively.

Physical properties of the fluid such as density, viscosity, and particle density and the model parameters such as dispersion coefficient and virtual mass coefficient have a substantial effect on the critical diameter. These effects are discussed systematically in the following paragraphs.

a. Effect of Fluid Viscosity. In the final stability criterion, viscosity of the fluid does not appear explicitly. However, it appears implicitly through the particle settling velocity and the Richardson–Zaki index. As the viscosity of the fluid increases, the terminal settling velocity of the particle decreases, and this leads to a reduction in the voidage propagation velocity, making the system more stable. This fact is shown in Fig. 7 for solid–liquid fluidized beds and in Fig. 8 for gas-solid fluidized beds. The stable area represented by the area under the lower critical diameter limit increases with an increase in the viscosity. Similarly, Figs. 9 and 10 show the effect of fluid viscosity on the upper critical diameter for liquid and gas fluidized beds, respectively.

Figure 11a shows the effect of density difference on the particle Reynolds number, based on the terminal settling velocity, for solid–liquid fluidized beds. Reynolds number was evaluated at the lower critical particle diameter. In this plot, the stability limit is represented by taking the Reynolds number as ordinate, instead of the lower critical particle diameter itself. When represented in this manner, the plot exhibits a remarkable feature that the stability curve, plotted by taking density difference as abscissa, remains almost same even when there is a hundredfold change in the liquid viscosity. Figure 11b shows similar plot for gas-solid fluidized beds. Figures 12a and 12b show the effect of density difference on particle Reynolds number evaluated at the upper limit of the critical diameter. In all these figures (11a–12b), the similar unified curves, independent of liquid viscosity can be observed. An attempt was made to write the stability criterion in a suitable dimensionless form. This would clarify the reasons for the unified curves in Figs. 11a, 11b, 12a, and 12b. However, such an exercise was found to be difficult cause (i) the relationship between m and Re_p is empirical, and further, m is an exponent on ε_C, and (ii) the relationships between the viscosity and $V_{S\infty}$ and also d_P and $V_{S\infty}$ are empirical. Figure 11c is a generalized plot of particle Reynolds number vs density difference for solid–liquid

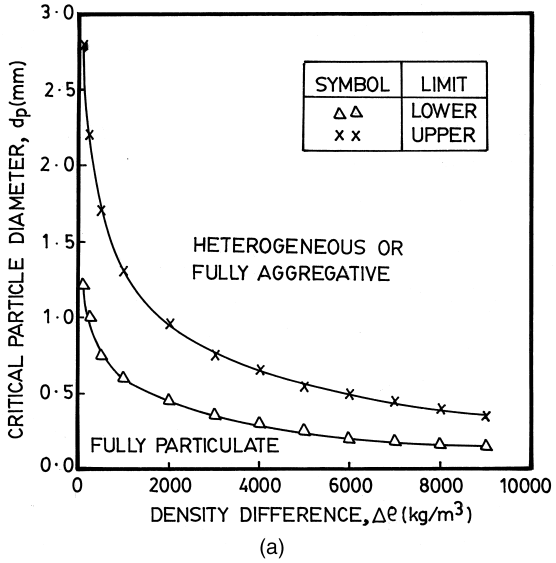

FIG. 6. Typical stability maps. (a) Solid–liquid fluidized beds [$\alpha = 3.0$, $C_V = f(\varepsilon)$, $\mu_L = 1$ mPas, $\rho_L = 1000$ kg/m^3]; (b) gas–solid fluidized beds [$\alpha = 3.0$, $C_V = f(\varepsilon)$, $\mu_G = 0.02$ mPas, $\rho_G = 1$ kg/m^3].

fluidized beds, plotted for transitions occurring at intermediate values of hold-up. Figure 12c shows a similar plot for gas–solid fluidized beds.

b. Effect of Fluid Density. Fluid density has an important role to play in deciding the transition in both solid–liquid and gas–solid fluidized beds, as shown in Fig. 13 and 14, respectively. An increase in the fluid density makes the bed more stable, as indicated by an increase in the stable area under the lower critical diameter limit. This can be explained as follows: The simplified stability criterion was given by Eq. (61). It states that for stability the following condition should be satisfied:

$$\sqrt{3d_P\varepsilon_S(\rho_S - \rho_G)g/\rho_S} > m\varepsilon_S V_{S\infty}\varepsilon_G^{m-1}.$$

With an increase in fluid density, the Reynolds number increases and the Richardson–Zaki index (m) decreases. This results in a decrease in the voidage propagation velocity (RHS) and brings in more stability to the system.

There is yet another reason. Let us consider the two extreme cases of creeping and turbulent flows. In the former case, we know from Stokes' equation that $V_{S\infty}$ varies linearly with $(\rho_S - \rho_G)$. Therefore, with an increase in the fluid velocity, the RHS (voidage propogation velocity) decreases

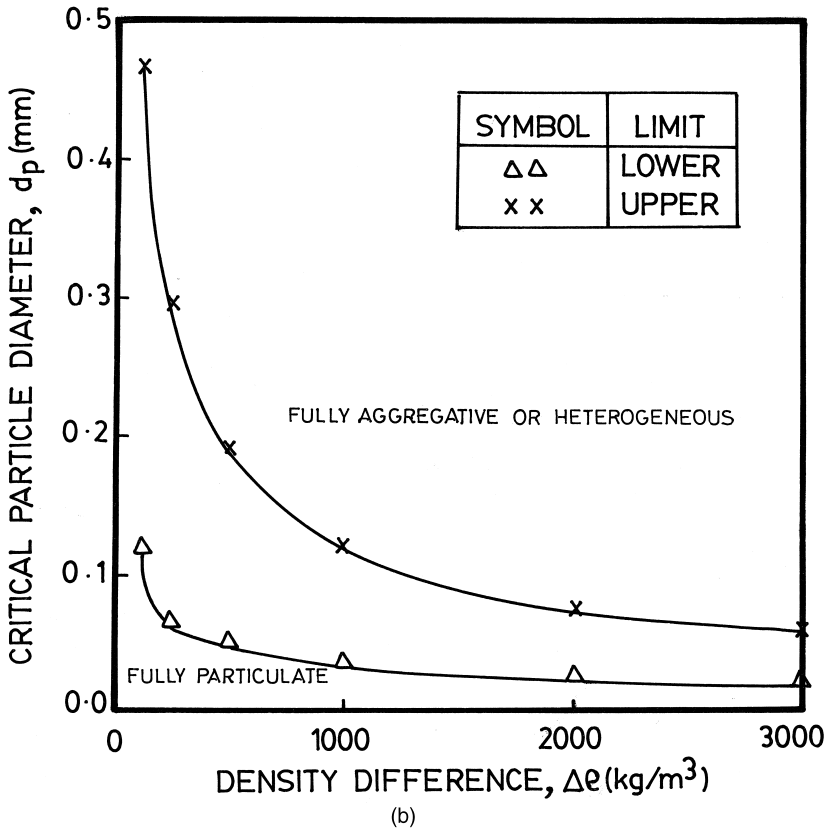

(b)

FIG. 6. (*continued*)

faster than the LHS (elastic wave velocity). This brings more stability to the system.

For the case of turbulent flow, the preceding equation can be modified as

$$\sqrt{3d_P\varepsilon_S(\rho_S-\rho_G)g/\rho_L}\cdot\sqrt{\rho_G/\rho_S} > m\varepsilon_S V_{S\infty}\varepsilon_G^{m-1}. \tag{92}$$

The first part of LHS is $V_{S\infty}$. Therefore,

$$\sqrt{\rho_G/\rho_S} > m\varepsilon_S\varepsilon_G^{m-1}. \tag{93}$$

From this equation, it is clear that, with an increase in fluid velocity, the LHS increases and imparts more stability to the system.

c. Effect of Particle Density. An increase in the particle density leads to earlier transitions as shown in Figs. 6a and 6b. The critical diameter of a

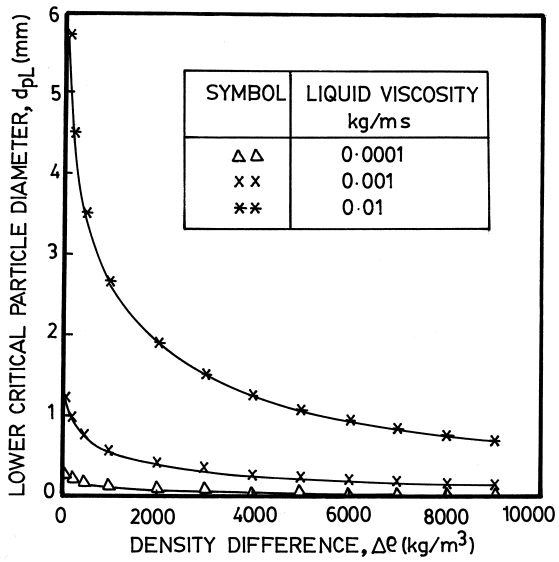

FIG. 7. Effect of liquid viscosity on lower critical particle diameter solid–liquid fluidized beds [$\alpha = 3.0$, $C_V = f(\varepsilon)$, $\rho_L = 1000$ kg/m^3].

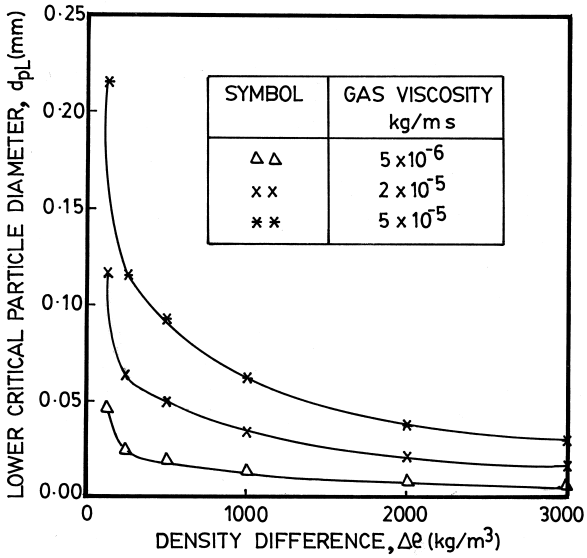

FIG. 8. Effect of gas viscosity on lower critical particle diameter: gas–solid fluidized beds [$\alpha = 3.0$, $C_V = f(\varepsilon)$, $\rho_G = 1$ kg/m^3].

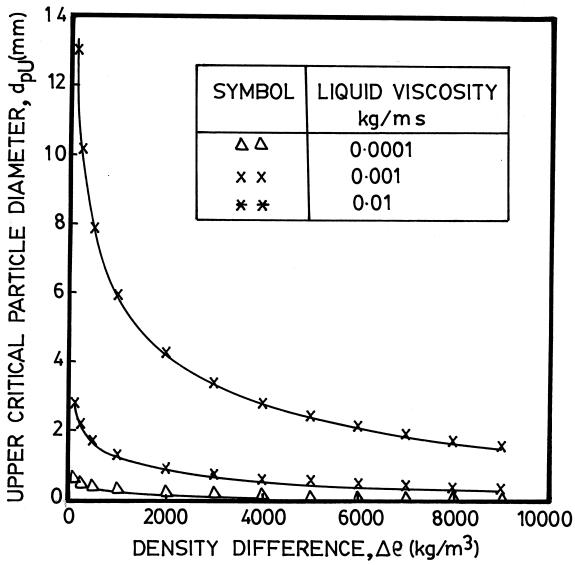

FIG. 9. Effect of liquid viscosity on upper critical particle diameter: solid–liquid fluidized beds [$\alpha = 3.0$, $C_V = f(\varepsilon)$, $\rho_L = 1000$ kg/m^3].

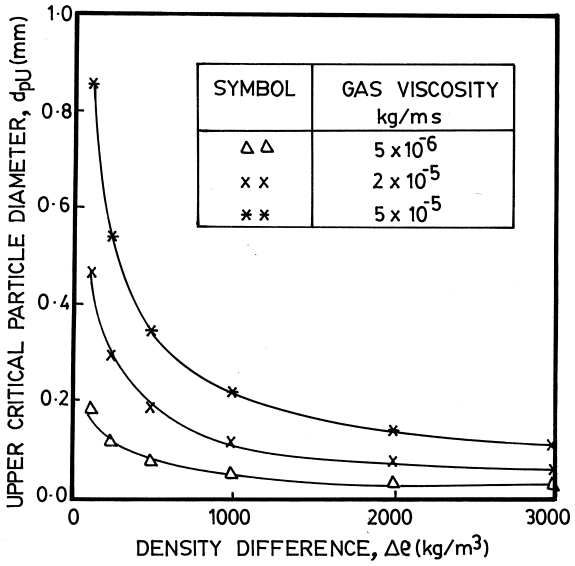

FIG. 10. Effect of gas viscosity on upper critical diameter: gas–solid fluidized beds [$\alpha = 3.0$, $C_V = f(\varepsilon)$, $\rho_G = 1$ kg/m^3].

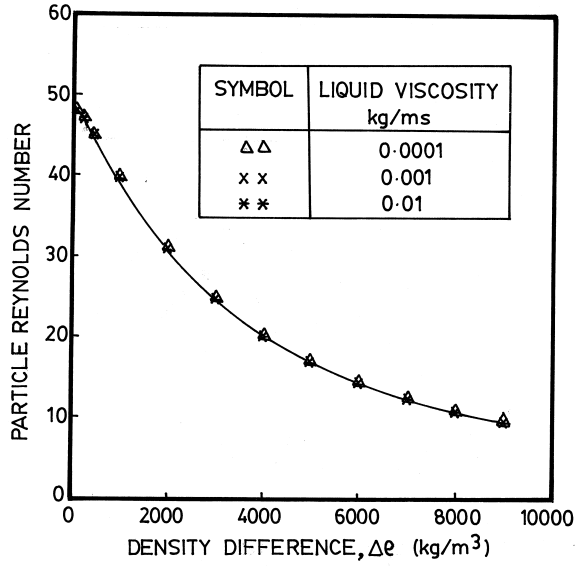

(a)

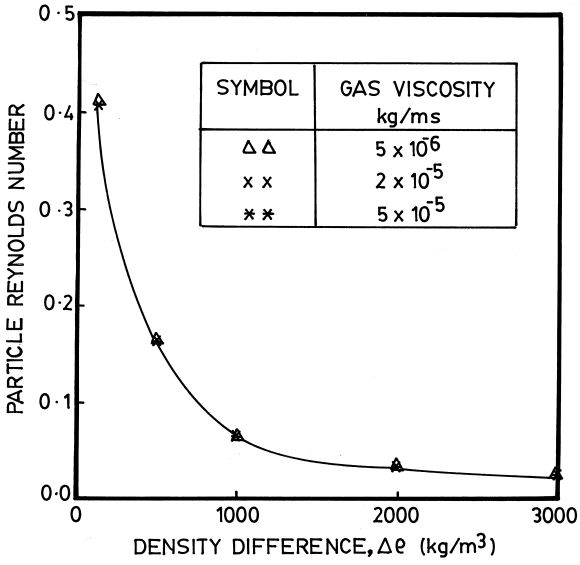

(b)

FIG. 11. Effect of density difference at various liquid viscosities on particle Reynolds number evaluation at lower critical particle diameter. (a) Solid–liquid fluidized beds [α = 3.0, $C_v = f(\varepsilon)$, ρ_L = 1000 kg/m^3]. (b) Gas–solid fluidized beds [α = 3.0, $C_V = f(\varepsilon)$, ρ_G = 1 kg/m^3]. (c) Unified stability map of particle Reynolds number vs density difference for different values of transition hold-up: solid–liquid fluidized beds [α = 3.0, $C_V = f(\varepsilon)$, μ_L = 1 mPas, ρ_L = 1000 kg/m^3].

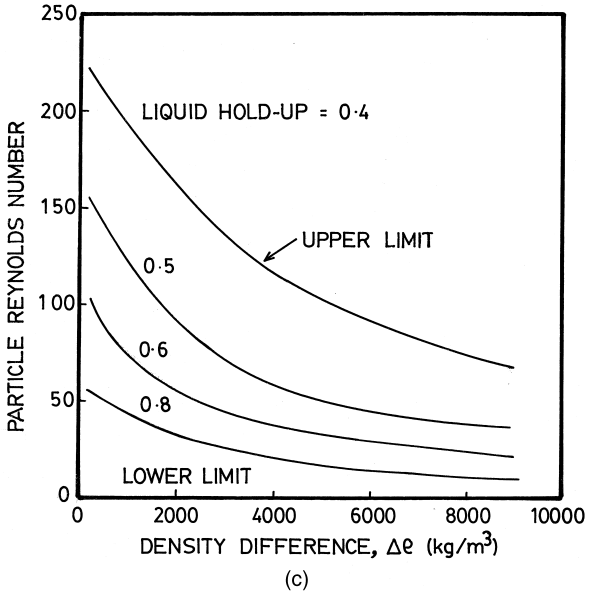

FIG. 11. (*continued*)

lighter particle is much more than that of a heavier particle. As the particle density approaches that of the liquid, the critical diameter increases almost exponentially.

d. Effect of Particle Diameter. For obtaining the dependence of particle diameter on transition, Fig. 15 was constructed for a particular solid–liquid system and noting the liquid hold-up at which the transition from homogeneous to heterogeneous regime occurs. As seen from Fig. 15, the transition occurs earlier as the particle diameter is increased. Figure 16 shows critical hold-ups for solid particles in gas–solid fluidized beds.

e. Effect of Dispersion Coefficient. As pointed out earlier, the hydrodynamic dispersion is the main stabilizing parameter in the model. For estimating the effect quantitatively, the value of dispersion coefficient was varied over a wide range. For this purpose, the proportionality constant in Eq. (59) was varied. Figures 17 and 18 show the effect of dispersion coefficient on the lower limit of critical particle diameter for solid–liquid and gas–solid fluidized beds, respectively. The values of critical particle diameters were found to be very sensitive to the dispersion coefficient. An increase in the dispersion coefficient is seen to increase the stable region of fluidiza-

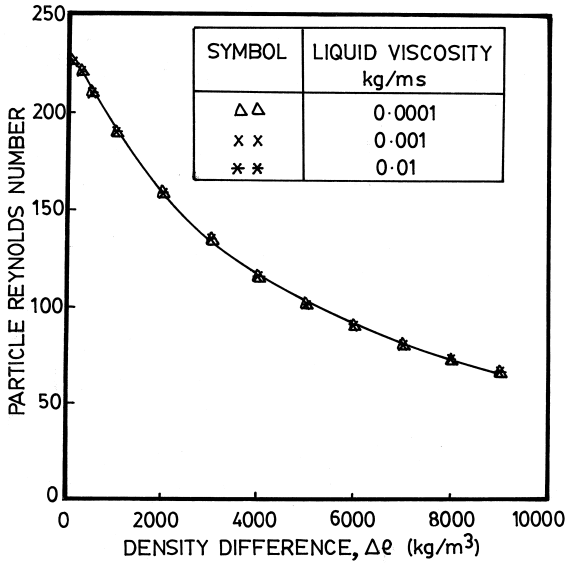

(a)

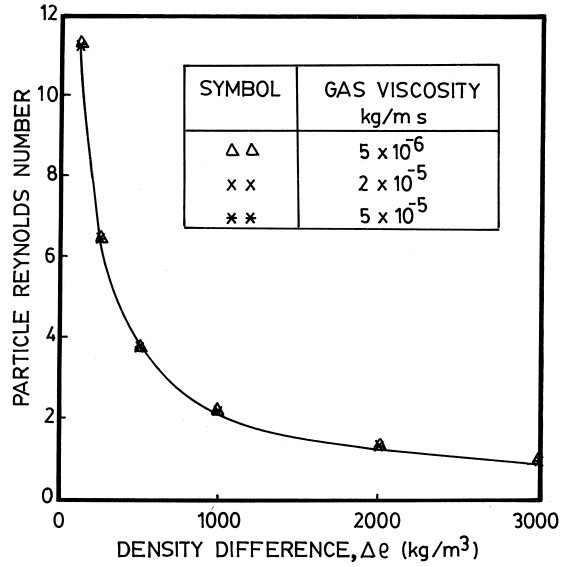

(b)

FIG. 12. Effect of density difference at various liquid viscosities on particle Reynolds number evaluated at upper critical diameter: (a) Solid–liquid fluidized beds [$\alpha = 3.0$, $C_V = f(\varepsilon)$, $\rho_L = 1000$ kg/m^3]. (b) Gas–solid fluidized beds [$\alpha = 3.0$, $C_V = f(\varepsilon)$, $\rho_G = 1$ kg/m^3]. (c) Unified stability map of particle Reynolds number vs density difference for different values of transition hold-up: gas–solid fluidized beds [$\alpha = 3.0$, $C_V = f(\varepsilon)$, $\mu_G = 0.02$ mPas, $\rho_G = 1$ kg/m^3].

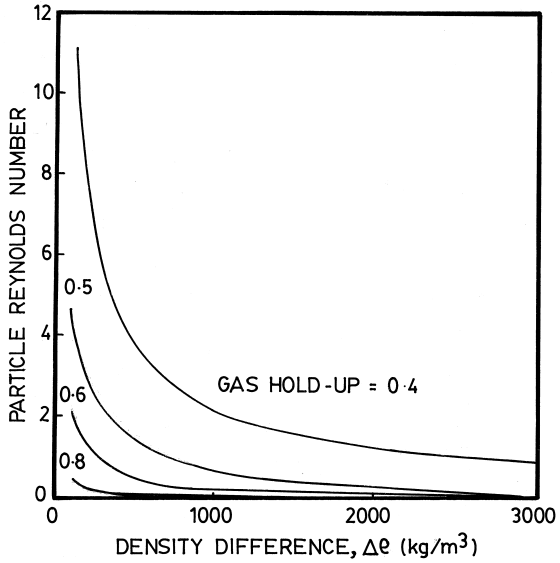

(c)

FIG. 12. (*continued*)

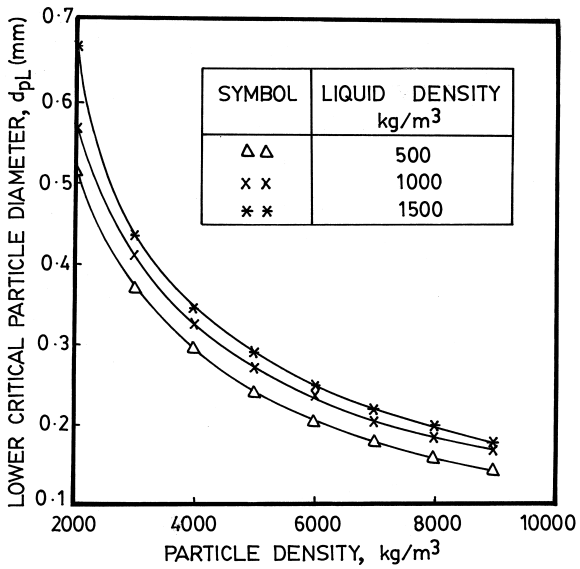

FIG. 13. Effect of liquid density on lower particle critical diameter: solid–liquid fluidized beds [$\alpha = 3.0$, $C_V = f(\varepsilon)$, $\mu_L = 1$ mPas].

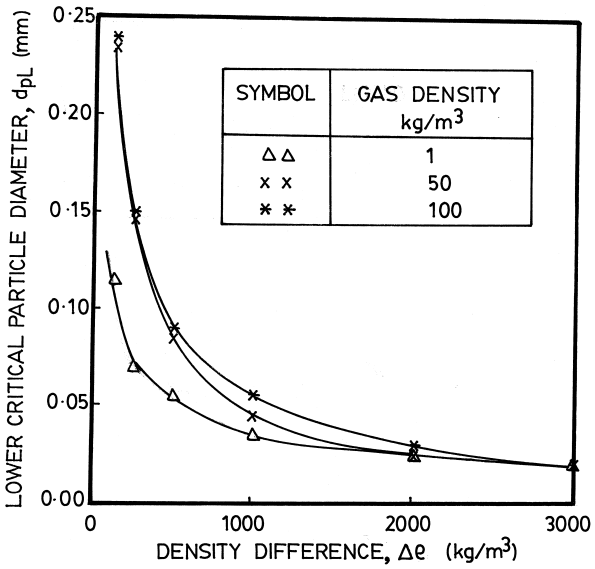

FIG. 14. Effect of gas density on lower particle critical diameter: gas–solid fluidized beds [α = 3.0, $C_V = f(\varepsilon)$, μ_G = 0.02 mPas].

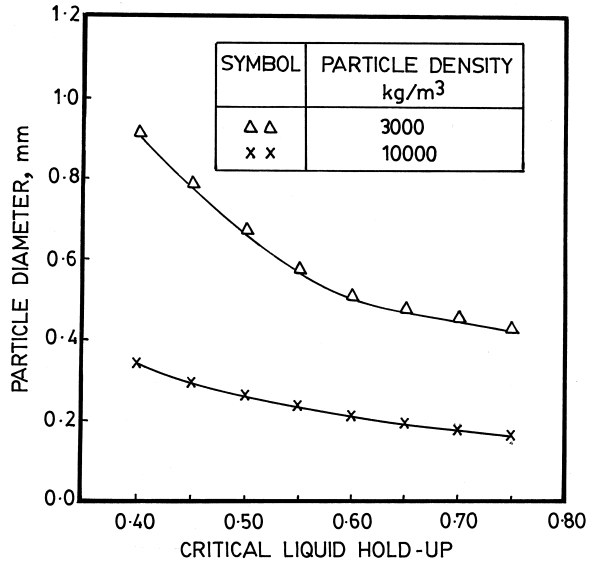

FIG. 15. Effect of particle diameter on critical liquid hold-up at different particle densities: solid–liquid fluidized beds [α = 3.0, $C_V = f(\varepsilon)$, μ_L = 1 mPas, ρ_L = 1000 kg/m^3].

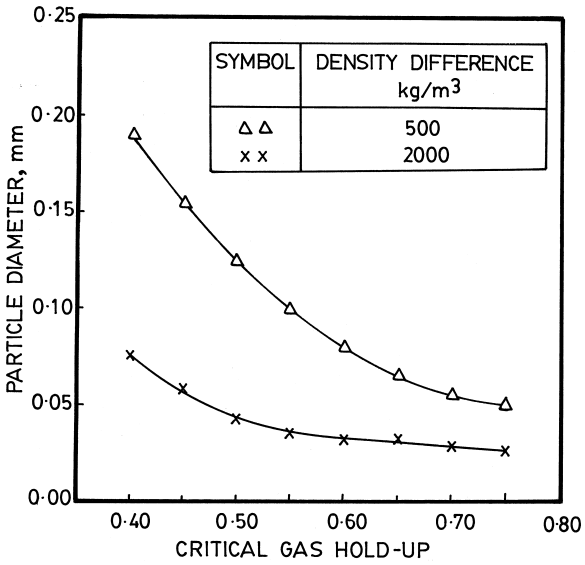

FIG. 16. Effect of particle diameter on critical gas hold-up at different density differences: gas–solid fluidized beds [$\alpha = 3.0$, $C_V = f(\varepsilon)$, $\mu_G = 0.02$ mPas, $\rho_G = 1$ kg/m^3].

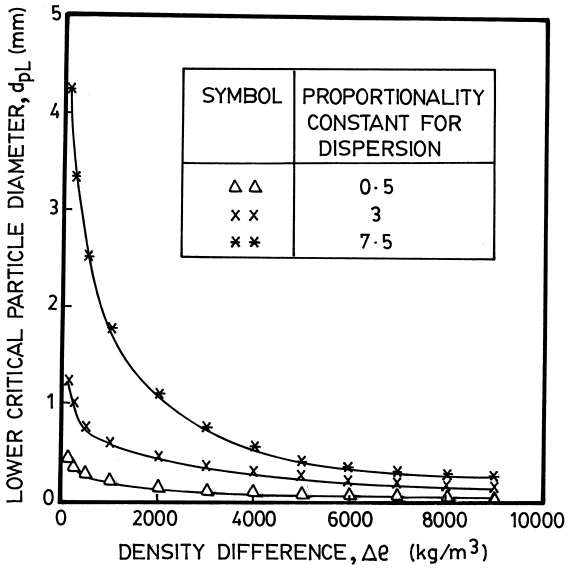

FIG. 17. Effect of proportionality constant for dispersion on lower critical diameter: solid–liquid fluidized beds [$C_V = f(\varepsilon)$, $\mu_L = 1$ mPas, $\rho_L = 1000$ kg/m^3].

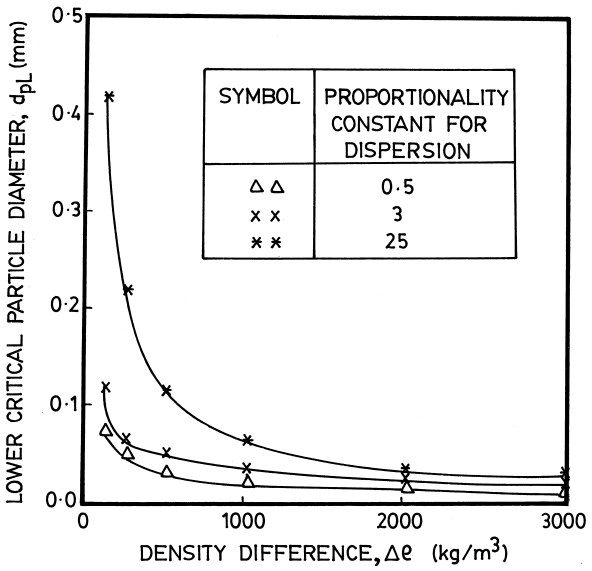

FIG. 18. Effect of proportionality constant for dispersion of lower particle critical diameter gas–solid fluidized beds [$C_V = f(\varepsilon)$, $\mu_G = 0.02$ mPas, $\rho_G = 1$ kg/m^3].

tion. This is true for the upper limit of critical diameter as well, as shown in Fig. 19 and 20, for solid–liquid and gas–solid fluidized beds, respectively.

f. Effect of Virtual Mass Coefficient. For studying the effect of the virtual mass coefficient, the value of C_v was taken as 0.0, 0.5, and as a function of hold-up given by Eq. (83).

In the case of solid–liquid fluidized beds, the effect of virtual mass is to make the bed more unstable as shown in Fig. 21. This can be explained as follows: The effect of virtual mass is to increase the apparent density of the particle. As discussed in this section earlier, an increase in the particle density makes the system more unstable. This observation is consistent with Fig. 21. As the particle density increases, say, $\rho_S = 9000$ kg/m^3 and $\rho_L = 1000$ kg/m^3, the effect of virtual mass is negligible and the curves are seen to merge irrespective of the formulation of virtual mass coefficient.

In the case of gas–solid fluidized beds, the effect of virtual mass coefficient is negligible as shown in Fig. 22. However, as the gas density increases the effect of virtual mass becomes similar to that observed in solid–liquid systems as shown in Fig. 23.

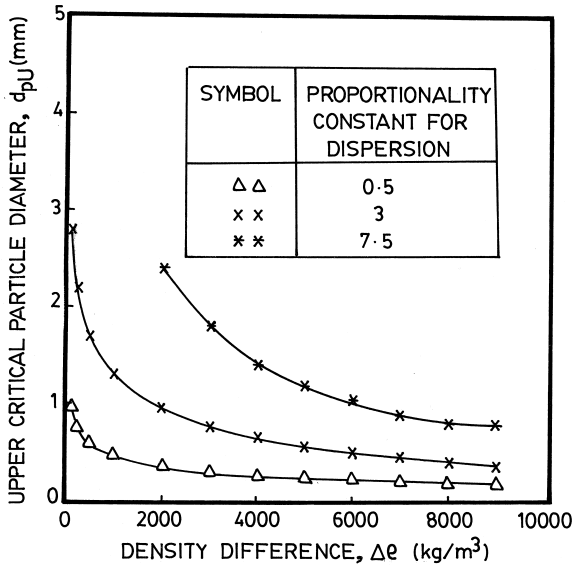

FIG. 19. Effect of proportionality constant for dispersion on upper particle critical diameter solid–liquid fluidized beds [$C_V = f(\varepsilon)$, $\mu_L = 1$ mPas, $\rho_L = 1000$ kg/m^3].

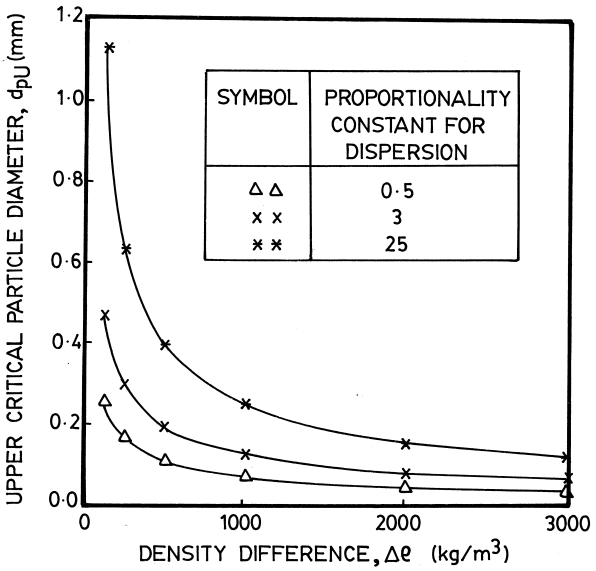

FIG. 20. Effect of proportionality constant for dispersion on upper particle critical diameter: gas–solid fluidized beds [$C_V = f(\varepsilon)$, $\mu_G = 0.02$ mPas, $\rho_G = 1$ kg/m^3].

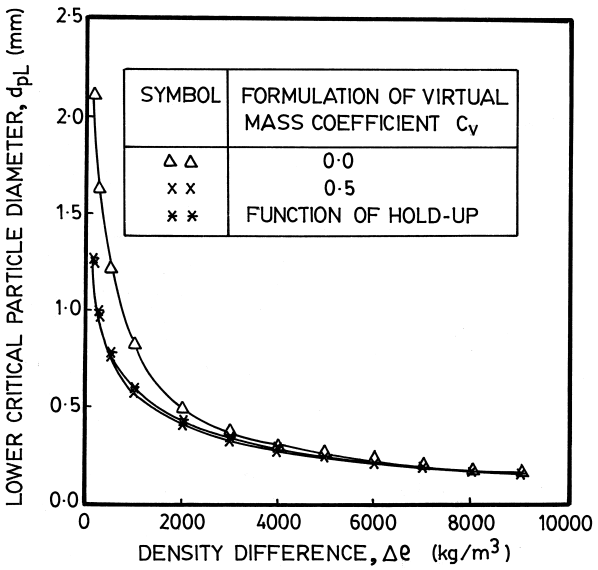

FIG. 21. Effect of formulation of virtual mass coefficient on lower particle critical diameter solid–liquid fluidized beds [α = 3.0, μ_L = 1 mPas, ρ_L = 1000 kg/m^3].

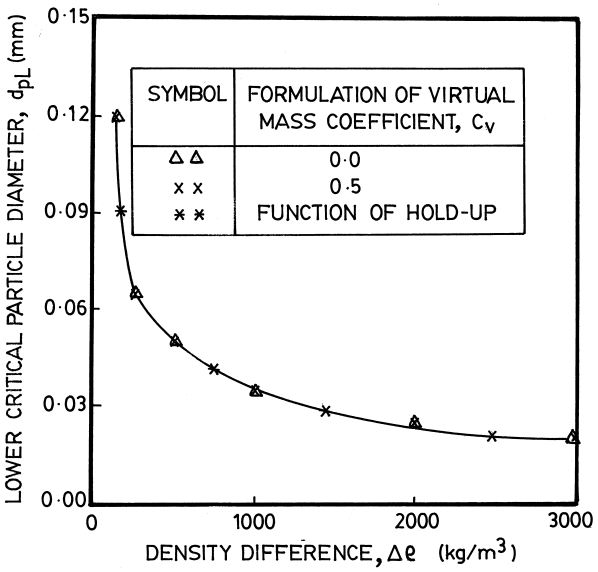

FIG. 22. Effect of formulation of virtual mass coefficient on lower particle critical diameter gas–solid fluidized beds [α = 3.0, μ_G = 0.02 mPas, ρ_G = 1 kg/m^3].

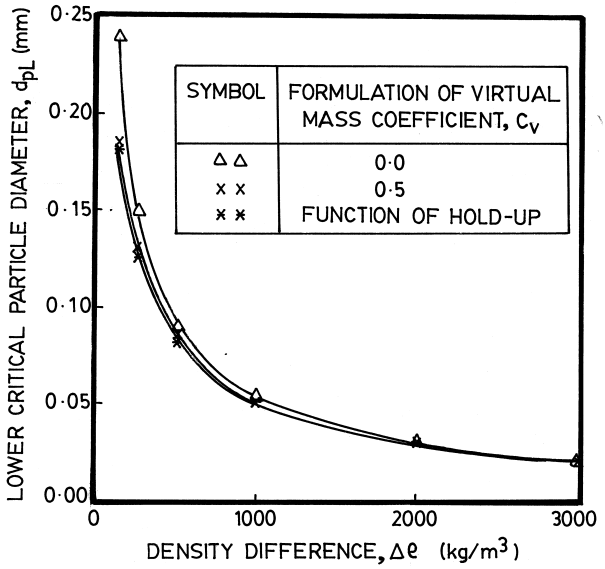

FIG. 23. Effect of formulation of virtual mass coefficient on lower particle critical diameter gas–solid fluidized beds [α = 3.0, μ_G = 0.02 mPas, ρ_G = 1 kg/m^3].

2. *Gas–Liquid Bubble Columns*

Equation (25) was used to obtain the critical transition gas hold-up. Critical gas transition hold-up is plotted against terminal bubble rise velocity in a typical stability map. The effects of various parameters such as virtual mass coefficient, Richardson–Zaki index, and proportionality constant for dispersion are described next.

a. Effect of the Relation of Bubble Diameter to Terminal Rise Velocity. Figure 24 shows the effect of various d_B–$V_{B\infty}$ relationships on the transitions in gas–liquid bubble columns. It can be seen that the transitions are highly sensitive to this relationship. In contaminated systems, the contaminants tend to accumulate at the gas–liquid interface and reduce the mobility of the interface. Therefore, in contaminated systems, for the same bubble diameter, the rise velocity is more than that in the pure systems.

b. Effect of Virtual Mass Coefficient. Three different prescriptions were used for the virtual mass coefficient. The virtual mass coefficient was taken as 0.5, 1.0, and as a function of ε_L as already given in Eq. (83). Figure 25 shows the effect of virtual mass coefficient on stability of bubble columns, with the proportionality constant for dispersion equal to 0.5 and the value

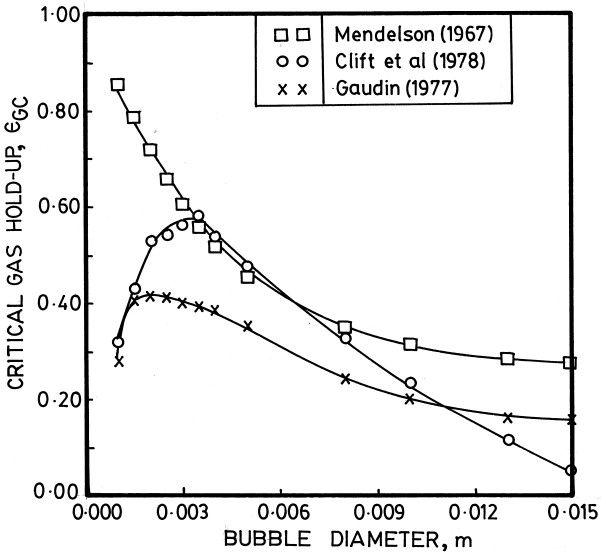

FIG. 24. Effect of bubble diameter–terminal rise velocity on transitions: bubble columns [$\alpha = 0.5$, $C_V = 1.0$, $m = 1.9$].

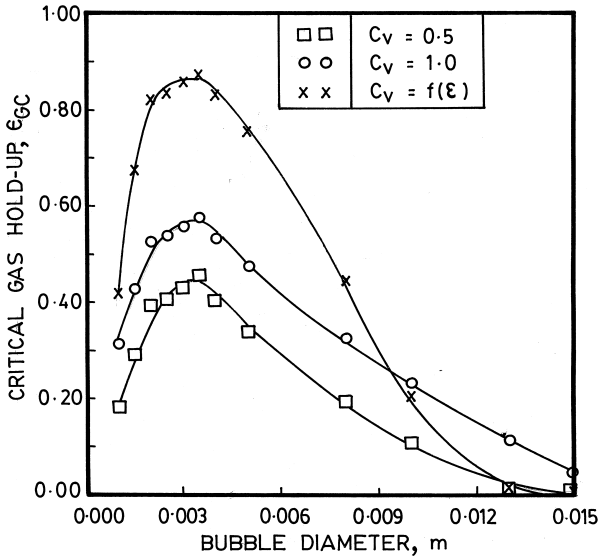

FIG. 25. Effect of virtual mass coefficient on transition gas hold-up: bubble columns [$\alpha = 0.5$, $m = 1.9$, d_B–$v_{B\infty}$ Clift *et al.* relation].

of R–Z index m equal to 1.9. For this combination, it can be seen that the critical transition gas hold-up increases as the C_v increases from 0.5 to 1.0 and to $f(\varepsilon_L)$. The increase in stability with increase in the virtual mass coefficient in case of bubble columns may appear as opposite to the trend observed for solid–liquid and gas–solid fluidized beds. However, as described in Section IIE, the transition points are different for fluidized beds and bubble columns. It can be seen from Fig. 25 that the transition gas hold-up is quite sensitive to the formulation of virtual mass coefficient. Another interesting feature of Fig. 25 is the initial increase in the critical gas hold-up with the increase in bubble diameter upto about 3 mm, where the critical gas hold-up reaches a maximum value with respect to the bubble diameter and then starts decreasing as the bubble diameter increases above 3 mm. The maximum in the critical gas hold-up at a bubble diameter of about 3 mm reflects a similar maximum in the bubble rise velocity at a bubble diameter of 3 mm. The dependence of critical gas hold-up on the relation between d_B and $V_{B\infty}$ can be explained using Eq. (78), which clearly indicates that the critical gas hold-up at transition is proportional to the ratio $V^2_{B\infty}/d_B$.

c. Effect of Dispersion Coefficient. To elucidate the effect of dispersion coefficient on stability, the proportionality constant for dispersion coefficient was varied in the range 0.5–3.0. However, it must be noted that once all the remaining parameters (physical properties and turbulence level) are fixed, the proportionality constant for dispersion will also be fixed, and in reality it cannot be changed as an independent variable. However, because the dependence of the dispersion coefficient on other parameters is unclear, the proportionality constant has been varied independently in the present work. Figure 26 shows the effect of the proportionality constant for the dispersion coefficient on the stability of bubble columns, for the value of C_v equal to 1.0. and m equal to 1.9. It can be seen that, as the proportionality constant increases, the bubble column becomes more unstable. Figure 26 also shows the maximum in the critical gas hold-up at a bubble diameter of about 3 mm.

d. Effect of Richardson–Zaki index (m). Figure 27 shows the effect of the Richardson–Zaki index on the stability of bubble columns, with C_v equal to 1.0 and the proportionality constant for dispersion equal to 0.5. It can be seen that as the value of Richardson–Zaki index increases, the bubble column becomes more unstable (i.e., transition occurs at a lower value of gas hold-up). This is explained as follows: The condition for stability is given by Eqs. (76) and (77). Usually, the contribution of $B^2/4$ is negligible.

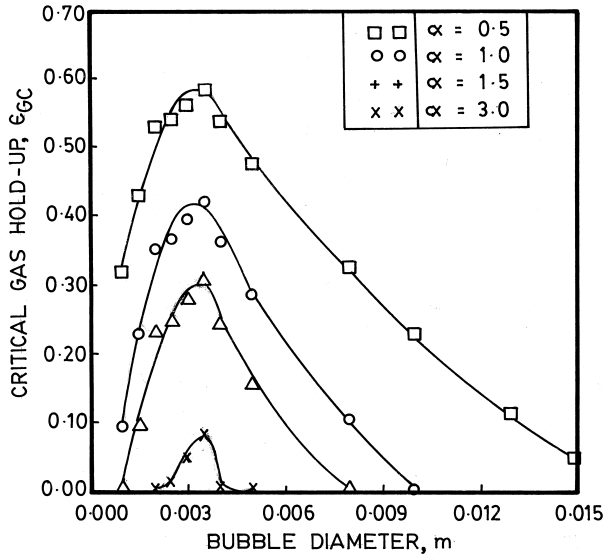

FIG. 26. Effect of proportionality constant for dispersion on transition gas hold-up: bubble column [C_V = 1.0, m = 1.9, d_B–$v_{B\infty}$ Clift *et al.* relation].

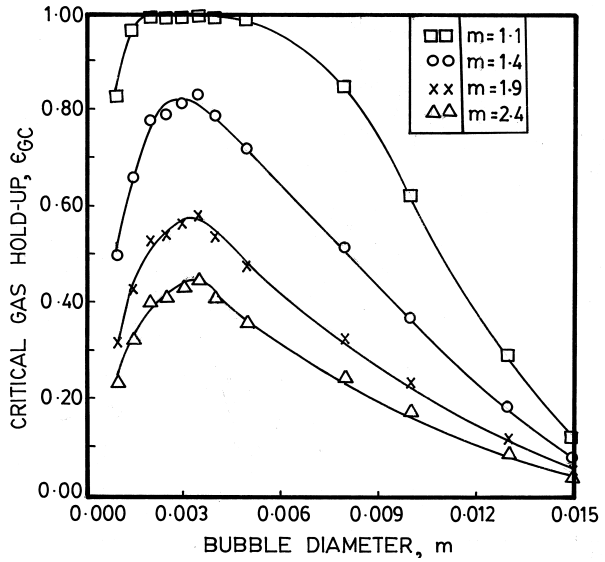

FIG. 27. Effect of Richardson–Zaki index on transition gas hold-up: bubble column [α = 0.5, C_V = 1.0, d_B–$v_{B\infty}$ Clift *et al.* relation].

Under these conditions, Eq. (77) gets simplified to

$$Z - C = 0$$

or

$$\varepsilon_{GC} = \frac{C_v v_S^2}{\alpha d_B g}.$$

With an increase in m, the slip velocity (v_s) decreases. Therefore, the critical gas hold-up also decreases.

C. Comparison of Experimental Results with Unbounded Bed Analysis

1. Fluidized Beds

Tables III and IV summarize the experimental details pertaining to the the solid–liquid fluidized beds and gas–solid fluidized beds, respectively. For the prediction of critical continuous phase hold-ups, the criterion developed in Section II is used. The value of dispersion coefficient was estimated using Eq. (59). The predicted values are given in Tables III and IV. It can be seen that the agreement is excellent when the continuous phase hold-up is less than 60%. Beyond the hold-up of 60%, the agreement is fairly good with average deviation of 7% and maximum deviation of 9%. However, the error is systematic. Therefore, the value of α [proportionality constant in Eq. (59)] was adjusted so that the predicted value agrees with the experimental value. The values of α have been given in the last column. It can be seen that the α value is less than 3 when $\varepsilon_{LC} > 60\%$. For such cases, the unbounded bed analysis is perhaps not sufficient and we need to consider the presence of the sparger and the side walls. These aspects are covered in Sections VI and VII. It may be pointed out that the values of transition hold-ups greater than 60% are observed in solid–liquid fluidized beds. In gas–solid fluidized beds, in most cases, the transition occurs at the condition of incipient fluidization. In some cases (fine particles or high-pressure fluidization), the transition may occur at hold-up values beyond minimum fluidization. In such cases, the bubble phase (which is formed at minimum fluidization) moves in the homogeneous regime up to the point of transition.

Model predictions and experimental observations are compared in Figs. 28 and 29. The agreement was found to be excellent with a standard deviation of 12%.

TABLE III

COMPARISON OF EXPERIMENTAL RESULTS OF GIBILARO *ET AL.* (1986) WITH UNBOUNDED ANALYSIS: SOLID–LIQUID FLUIDIZED BEDS

System	ρ_S (kg/m^3)	d_P (mm)	$\mu_L \times 10^3$ (Pas)	$V_{S\infty}$ (mm/s)	m	ε_{LC} experimental (%)	ε_{LC} predicted (%)	Proportionality constant for dispersion
Water–copper	8710	0.083	0.7	47.6	5.30	75	83	1.87
Water–copper	8710	0.083	0.6	50.9	5.11	72	80	1.82
Water–copper	8710	0.165	1.3	66.7	5.01	74	84	1.81
Water–copper	8710	0.165	1.0	82.9	4.91	71	75	2.30
Water–copper	8710	0.165	0.85	97.2	4.89	69	70	2.73
Water–copper	8710	0.165	0.7	105.9	4.71	66	68	2.71
Water–copper	8710	0.165	1.0	115.5	4.67	64	65	2.76
Water–copper	8710	0.275	0.85	110.3	3.62	66	70	2.57
Water–copper	8710	0.275	0.7	131.2	3.52	60	62	2.72
Water–copper	8710	0.275	0.6	152.2	3.42	56	56	3.01
Water–copper	8710	0.275	1.3	173.4	3.40	54	52	3.48
Water–copper	8710	0.275	1.0	190.0	3.30	51	48	3.64

TABLE IV
COMPARISON OF EXPERIMENTAL RESULTS WITH UNBOUNDED BED ANALYSIS: GAS–SOLID FLUIDIZED BEDS

Investigator	Gas phase	ρ_S (kg/m^3)	d_P (μm)	ε_{GC} experimental (%)	ε_{GC} predicted (%)
Rowe *et al.* (1982)	CO_2	819	70	57	56
	CO_2	819	70	59	59
	CO_2	819	70	61	63
	Air	819	70	61	63
	Ar	819	70	62	65
	Ar	819	70	63	67
	Ar	819	70	64	70
	CO_2	819	82	56	52
	CO_2	819	82	57	55
	CO_2	819	82	58	56
	Air	819	82	58	57
	Air	819	82	59	59
	Air	819	82	60	62
	Ar	819	82	60	61
	Ar	819	82	61	64
	Ar	819	82	62	66
Rietema (1973)	H_2	2400	70	38	42
	H_2	2400	70	43	42
	H_2	2400	70	48	46
	H_2	2400	70	55	52
	Air	2400	70	42	42
	Air	2400	70	45	43
	Air	2400	70	47	50
	Air	2400	70	57	62
	Air	2400	70	62	67
King and Harrison (1982)	N_2	2400	61	44	45
	N_2	2400	61	44.5	45.8
	N_2	2400	61	44.5	45.8
	N_2	2400	61	44.5	46.3
	N_2	2400	61	44	46.8
	N_2	2400	61	44	47.2
Jacob and Weimer (1987)	CO/H_2	850	44	76.5	79
	CO/H_2	850	44	76.7	80
	CO/H_2	850	44	77.8	81
	CO/H_2	850	112	57.8	64
	CO/H_2	850	112	60.4	62
	CO/H_2	850	112	63.3	60
Musters and Rietema (1977)	Air	920	39.7	77.6	76
	Air	920	78.0	74.2	68
	Air	920	103	70.1	65

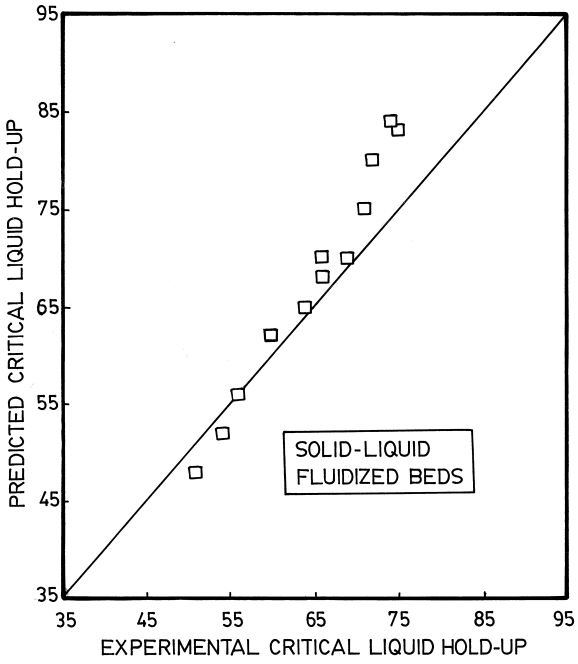

FIG. 28. Comparison of experimental and predicted critical hold-ups: solid–liquid fluidized beds.

2. *Bubble Columns*

The transition in bubble columns has been the subject of interest for the past 30 years. Table V summarizes the previous work. The value of $V_{B\infty}$ has been estimated from the corresponding V_{sup}–ε_G data on the basis of initial slope. Using this value of $V_{B\infty}$ and the physical properties, the bubble diameter was estimated using the correlation of Clift *et al.* (1978). The value of m was estimated using V_{sup}–ε_G data.

In the previous section, it was pointed out that the critical gas hold-up is very sensitive to the d_B–$v_{B\infty}$ relationship and the values of m, C_v, and α. It was thought desirable to calculate the value of α for all the experimental points shown in Table V. For each point, four values of m (1, 1.4, 1.9 and 2.4) and three levels of C_v were considered. The values of α are given in Table VI. The average value works out to be 3.14. Table V also gives the comparison between the experimental critical gas hold-up and the critical gas hold-up predicted using the transition criterion [Eq. (25)] with dispersion coefficient equal to 3. The comparison between predicted and experimental gas hold-up for bubble columns is shown in Fig. 30. It can be seen

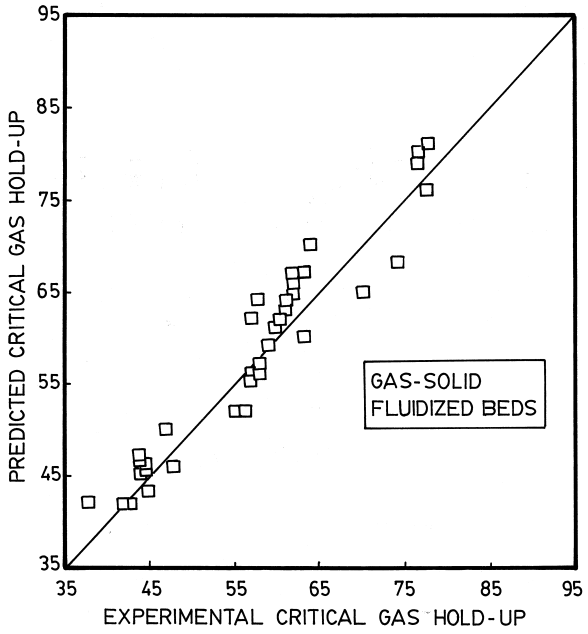

FIG. 29. Comparison of experimental and predicted critical hold-ups: gas–solid fluidized beds.

that the agreement is fairly good, but not as good as that obtained for gas–solid and solid–liquid fluidized beds. The reason for this is the higher sensitivity of the transition criterion in the case of bubble columns to the Richardson–Zaki index, the virtual mass coefficient, and the dispersion coefficient. Also, the predictions depend on the accuracy of prediction of d_B from the d_B–$V_{B\infty}$ relationship. Hence, a small variation in any of these parameters can change the predicted transition gas hold-up by a great magnitude. From the foregoing discussion, it can be seen that accuracy of estimation of $V_{B\infty}$, the Richardson–Zaki index m, α, and C_v is important for the prediction of ε_{GC}.

VI. Generalized Criteria for Bounded Dispersions

All the analysis in Section II focused on the unbounded case. The analysis of all investigators including the present authors concentrates on whether a periodic disturbance in the axial direction grows with respect to time, leading to instability or decays with time indicating a stable system. The

TABLE V
COMPARISON OF EXPERIMENTAL RESULTS WITH UNBOUNDED BED ANALYSIS: GAS–LIQUID BUBBLE COLUMNS

Investigator	System	$V_{B\infty}$	d_B	Proportionality constant for dispersion	V_{GC} experimental (mm/s)	ε_{GC} experimental (%)	ε_{GC} predicted (%)
Bach and Pilhofer (1978)	Tetrabromo ethane	267	3.76	3.15	37.8	14.2	8.0
	Butanediol	500	50.96	0.8	54.6	8.0	27.0
	Pure water	167	1.7	3.05	46.3	27.7	27.4
Maruyama *et al.* (1981)	Tap water	217	2.3	3.35	26.1	12.1	7.3
	10% glycerol	187	1.9	3.0	24.7	13.2	13.2
	0.075% acetic acid	250	1.8	5.65	30.4	12.1	22.5
Kelkar *et al.* (1983)	Na_2SO_4	243	3.8	2.55	33.9	13.9	22.3
	1% EtOH	224	2.3	4.1	67.0	29.9	22.6
	1% Propanol	238	2.4	3.9	36.3	15.3	19.0
	Na_2SO_3	253	3.4	3.45	69.5	27.6	16.6
Oels *et al.* (1978)	Dist. water	229	3.8	2.3	31.6	13.8	14.9
	Tap water	222	2.4	3.45	39.5	17.8	20.6
	Dist. water	242	2.7	3.55	30.5	12.6	14.9
	Dist. water	267	2.8	4.15	34.3	12.9	14.0
	1% ethanol	96.3	0.8	2.6	40.5	42.1	50.9
	1% *n*-propanol	85.1	0.7	3.25	50.0	58.7	56.1
	1% *n*-propanol	95.2	0.8	3.85	58.9	61.2	52.1
	1% *n*-butanol	87	0.7	3.3	50.0	57.5	54.2
	Water	250	3.8	2.85	51	20.4	28.0
	1% glucose	222	3.9	2.10	29.9	13.5	12.6
Kastanek *et al.* (1974)	Water	283	3.5	3.8	41.4	14.6	16.7
	Water	417	6.5	3.8	51.2	12.3	11.7

Tarmy *et al.* (1984)	Water–air 540 kPa	167	1.7	4.35	47.8	28.6	36.1
	Water–air 345 kPa	200	2.8	3.05	52.5	26.3	23.8
	Water–air 140 kPa	250	4.3	2.6	60.0	24.0	17.9
	Water–air 21 kPa	278	4.5	2.6	57.1	20.6	24.1
	1.56% CMC	375	5.9	2.95	16.4	4.37	3.2
	1% CMC	120	2.1	3.75	10.5	8.75	11.2
Buccholz *et al.* (1983)	Water–nitrogen	220	3.1	1.10	46.5	21.2	22.6
	Turpentine–nitrogen	250	3.2	2.70	58.2	23.2	9.222
Krishna *et al.* (1991)	NaCl–Ar/He	125	1.0	3.45	44.8	35.8	32.6
	Water	166	1.7	3.2	32.9	19.8	29.5
Koetsier *et al.* (1976)	Water–He	231	4.0	2.8	34.7	15.0	13.4
	Water	166	1.7	2.2	29.6	17.8	29.5
	Water	198	2.1	2.75	24.6	12.4	14.5
Yamashita and Inoue (1975)	Water	171	1.8	3.05	40.0	23.4	29.3
Wilkinson *et al.* (1992)	Deionized water	400	6.2	4.32.9	62.1	15.5	13.7
	Deionized water water–air (1 MPa)	300	5.4	2.9	61	20.3	26.9
Wilkinson *et al.* (1992)	Deionized water–air (1.5 MPa)	233	3.0	3.25	56.7	24.3	18.3
	Deionized water–air (0.1 MPa)	173	2.0	3.05	63.2	36.5	35.9

Note: Air at atmospheric pressure was used as gas phase unless stated otherwise.

TABLE VI
BACK CALCULATION OF PROPORTIONALITY CONSTANT FOR DISPERSION FROM EXPERIMENTAL DATA: GAS–LIQUID BUBBLE COLUMNS

C_v	$m = 1.0$	$m = 1.4$	$m = 1.9$	$m = 2.4$
0.5	2.41	2.07	1.75	1.50
$f(\varepsilon_L)$	3.56	2.86	2.21	1.91
1.0	3.65	3.11	2.61	2.22

treatment is strictly for axial direction and the axial nonuniformities are the source of transition. Analyses such as these have the limitation that the real fluidized beds are not of infinite extent and that some account must be taken of the boundaries at upper and lower surface of a bed of finite length, and also of the walls that bound the bed laterally. Therefore, an unbounded case is a simplification of the real systems and most of the criteria based on this approach have their limitations.

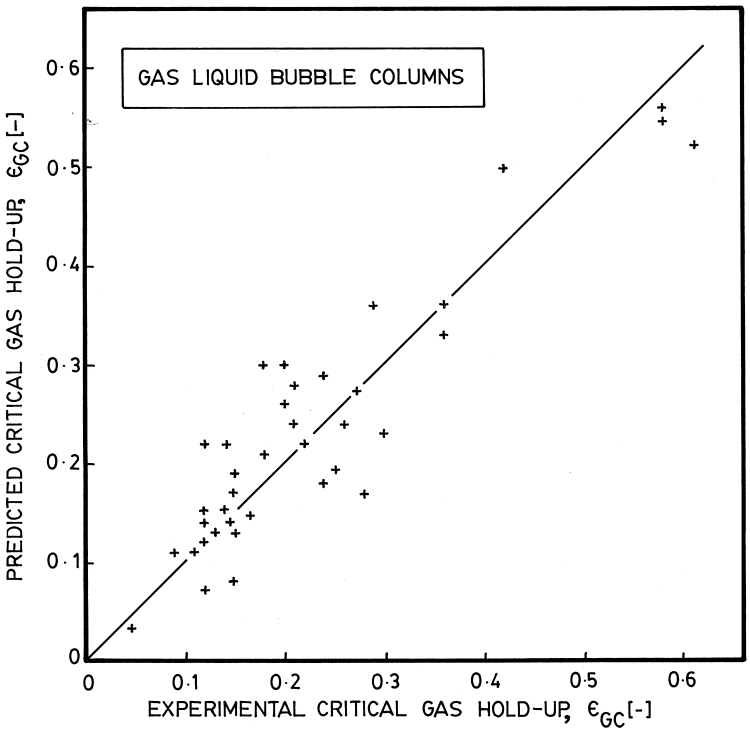

FIG. 30. Comparison of experimental and predicted critical hold-ups: bubble columns.

Therefore, a more elaborate model taking into account the presence of the lateral walls and the sparger design will now be presented.

A. Mathematical Model

In this section a criterion will be developed for the case of a two-dimensional bubble column. A schematic diagram of the column with the coordinate system is shown in Fig. 31. The criterion will be developed for the continuous mode of operation. The criterion for batch operation will be a special case of the criterion for the continuous mode of operation, in the limiting case of superficial liquid velocity becoming zero.

1. Basic Equations

The basic equations are similar to the equations for the unbounded case. However, for the bounded case, Z as well as X components of the equation are needed. The following additional assumptions are made:

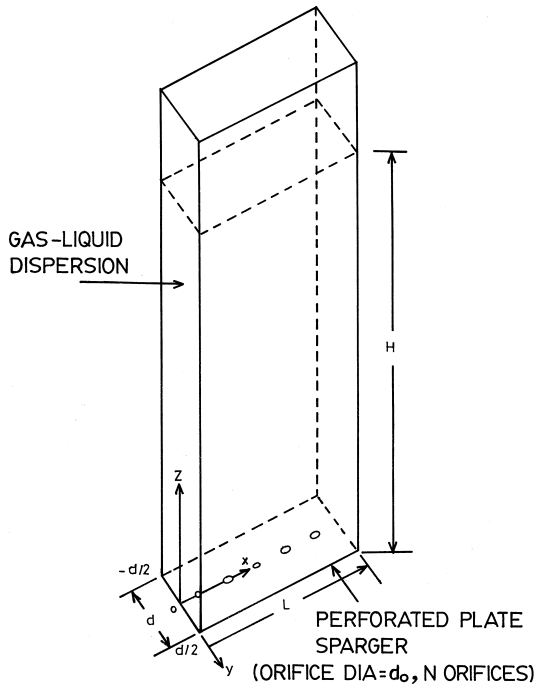

FIG. 31. Schematic diagram of a rectangular bubble column with coordinate system.

1. The gas phase convection terms and gravity forces are negligible.
2. The gas phase stress terms are negligible. (However, a more generalized criterion that includes the effect of gas phase stress terms will be presented later without the detailed derivation.)
3. There is no variation of gas hold-up in the smallest dimension (y). However, variation of the velocities in the y direction is considered.
4. The virtual mass terms are not considered. In bounded case, the disturbances (destabilizing effects) due to the sparger are present.

The equations of continuity and motion in their dimensionless form are as follows: Continuity equation for the liquid phase:

$$\frac{\partial \varepsilon_{\mathrm{L}}}{\partial \tau} + \frac{\partial}{\partial X}(\varepsilon_{\mathrm{L}} U_x) + \frac{\partial}{\partial Z}(\varepsilon_{\mathrm{L}} U_z) - \frac{\partial}{\partial X}\left(D_{\mathrm{L}} \frac{\partial \varepsilon_{\mathrm{L}}}{\partial X}\right) - \frac{\partial}{\partial Z}\left(D_{\mathrm{L}} \frac{\partial \varepsilon_{\mathrm{L}}}{\partial Z}\right) = 0. \quad (94)$$

Continuity equation for the gas phase:

$$\frac{\partial \varepsilon_{\mathrm{G}}}{\partial \tau} + \frac{\partial}{\partial X}(\varepsilon_{\mathrm{G}} V_x) + \frac{\partial}{\partial Z}(\varepsilon_{\mathrm{G}} V_z) - \frac{\partial}{\partial X}\left(D_{\mathrm{G}} \frac{\partial \varepsilon_{\mathrm{G}}}{\partial X}\right) - \frac{\partial}{\partial Z}\left(D_{\mathrm{G}} \frac{\partial \varepsilon_{\mathrm{G}}}{\partial Z}\right) = 0. \quad (95)$$

Equation of motion for the liquid phase, X component:

$$\begin{aligned}(1-\varepsilon_{\mathrm{G}})\left\{\frac{\partial U_x}{\partial \tau} + U_x \frac{\partial U_x}{\partial X} + U_z \frac{\partial U_x}{\partial Z}\right\} \\ = -(1-\varepsilon_{\mathrm{G}})\frac{\partial P}{\partial X} + B(V_x - U_X) + \frac{(1-\varepsilon_{\mathrm{G}})}{\mathrm{Re}_{\mathrm{L}}}\left\{\frac{\partial^2 U_x}{\partial X^2} + \frac{\partial^2 U_x}{\partial Y^2}\right. \\ \left. + \frac{\partial^2 U_x}{\partial Z^2}\right\} + \frac{2}{\mathrm{Re}_{\mathrm{L}}}\left\{\frac{\partial U_x}{\partial X}\frac{\partial \varepsilon_{\mathrm{L}}}{\partial X} + \frac{\partial U_x}{\partial Z}\frac{\partial \varepsilon_{\mathrm{L}}}{\partial Z}\right\}.\end{aligned} \quad (96)$$

Equation of motion for the liquid, Z component:

$$\begin{aligned}(1-\varepsilon_{\mathrm{G}})\left\{\frac{\partial U_z}{\partial \tau} + U_x \frac{\partial U_z}{\partial X} + U_z \frac{\partial U_z}{\partial Z}\right\} \\ = -(1-\varepsilon_{\mathrm{G}})\frac{\partial P}{\partial Z} + B(V_z - U_z) + \frac{(1-\varepsilon_{\mathrm{G}})}{\mathrm{Re}_{\mathrm{L}}}\left\{\frac{\partial^2 U_z}{\partial X^2} + \frac{\partial^2 U_z}{\partial Y^2}\right. \\ \left. + \frac{\partial^2 U_z}{\partial Z^2}\right\} + \frac{2}{\mathrm{Re}_{\mathrm{L}}}\left\{\frac{\partial U_z}{\partial X}\frac{\partial \varepsilon_{\mathrm{L}}}{\partial X} + \frac{\partial U_z}{\partial Z}\frac{\partial \varepsilon_{\mathrm{L}}}{\partial Z}\right\} - \hat{\mathrm{g}}(1-\varepsilon_{\mathrm{G}}).\end{aligned} \quad (97)$$

Equation of motion for the gas phase, X component:

$$0 = -\varepsilon_{\mathrm{G}} \frac{\partial P}{\partial X} - B(V_x - U_X). \quad (98)$$

Equation of motion for the gas phase, Z component:

$$0 = -\varepsilon_G \frac{\partial P}{\partial Z} - B(V_z - U_z), \tag{99}$$

The dimensionless variables are defined by

$$\begin{gathered}
U_x = \frac{u_x}{V_{B\infty}}; \quad U_z = \frac{u_z}{V_{B\infty}}; \quad V_s = \frac{v_s}{V_{B\infty}}; \quad V_x = \frac{v_x}{V_{B\infty}}; \\
V_z = \frac{v_z}{V_{B\infty}}; \quad Z = \frac{z}{L}; \quad X = \frac{x}{L}; \quad Y = \frac{y}{L}; \quad h = \frac{H}{L}; \\
\tau = \frac{tV_{B\infty}}{L}; \quad \mathrm{Re}_L = \frac{LV_{B\infty}\rho_L}{\mu_L}; \quad \mathrm{Re}_G = \frac{LV_{B\infty}\rho_L}{\mu_G}; \\
P = \frac{p}{\rho_L V_{B\infty}^2}; \quad \hat{g} = \frac{gL}{V_{B\infty}^2}\hat{D}_L = \frac{D_L}{LV_{B\infty}}; \\
\hat{D}_G = \frac{D_G}{LV_{B\infty}}; \quad B = \frac{\lambda L}{\rho_L V_{B\infty}}; \quad \rho = \frac{\rho_G}{\rho_L};
\end{gathered} \tag{100}$$

where μ_L, μ_G are the turbulent viscosities of the liquid phase and gas phase, respectively and $V_{B\infty} = v_s(\epsilon_G = 0)$.

Thus, Eqs. (94)–(99) describe the dynamics of gas–liquid dispersion in a two-dimensional bubble column.

2. *Boundary Conditions*

The pressure drop across the sparger for gas phase is due to viscous as well as turbulent resistance to the flow. It is expressed as

$$p_G - p(x, 0) = k_V v_{sup} + k_T v_{sup}^2, \tag{101}$$

where p_G is the pressure below the sparger plate and $p(x, 0)$ is the pressure just above the sparger plate, at the bottom of the column. k_v and k_T are the proportionality constants, and v_{sup} is the superficial gas velocity.

For a bubble column operated under net liquid flow conditions, both the gas and the liquid are introduced and removed continuously. The liquid flow may be cocurrent or countercurrent. The boundary condition at the bottom depends on the way in which the liquid is introduced or taken away. Consider the bottom design as shown in Fig. 32.

The liquid phase pressure drop consists of three parts, unlike that for gas, which consisted of only two parts. The liquid-phase pressure drop is due to the viscous and turbulent modes of friction across the sparger and

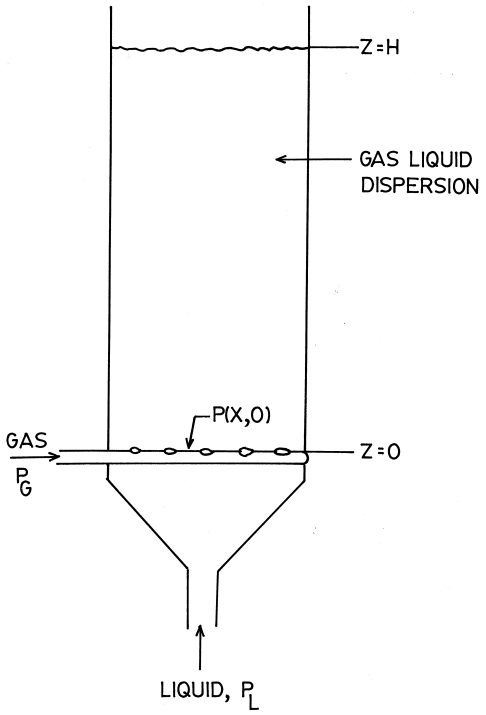

FIG. 32. Details of sparger.

due to the acceleration of the liquid as it passes through the sparger region. The liquid-phase pressure drop is given as

$$p_L - p(x,0) = k_{VL}u_{sup} + k_{TL}u_{sup}^2 + \frac{\rho_D u_z^2 - \rho_L u_{sup}^2}{2}, \tag{102}$$

where k_{VL} and k_{TL} are the proportionality constants, u_{sup} is the superficial liquid velocity, and $e_D = \rho_L\,(1 - \varepsilon_G)$ is the dispersion density.

Let us introduce the dimensionless variables as follows:

$$V_{sup} = \frac{v_{sup}}{V_{B\infty}}; \quad K_V = \frac{k_V}{\rho_L V_{B\infty}}; \quad K_T = \frac{k_T}{\rho_L}; \quad U_{sup} = \frac{u_{sup}}{V_{B\infty}}; \quad K_{VL} = \frac{k_{VL}}{\rho_L V_{B\infty}}$$
$$K_{TL} = \frac{k_{TL} - \dfrac{\rho_L}{2}}{\rho_L}; \quad P_G = \frac{p_G}{\rho_L V_{B\infty}^2}; \quad P(X,0) = \frac{p(x,0)}{\rho_L V_{B\infty}^2}; \quad P_L = \frac{p_L}{\rho_L V_{B\infty}^2}. \tag{103}$$

Thus, Eq. (101) and (102) in dimensionless form are, respectively,

$$P_G - P(X,0) = K_V V_{sup} + K_T V_{sup}^2 \tag{104}$$

$$P_L - P(X,0) = K_{VL} U_Z (1-\varepsilon_G) + U_Z^2 \left[K_{TL}(1-\varepsilon_G)^2 + \frac{1}{2}(1-\varepsilon_G) \right]. \tag{105}$$

The boundary conditions are

$$X = 0, \qquad U_x = 0 \tag{106a}$$

$$X = 1, \qquad U_x = 0 \tag{106b}$$

$$Z = 0, \qquad U_z = U_0 \tag{106c}$$

$$Z = \mathrm{h}, \qquad U_z = U_0 \tag{106d}$$

$$y = \pm d/2, \text{ all } x \text{ and } z,$$

$$U_x = 0, \qquad U_z = 0 \tag{106e}$$

$$V_x = 0, \qquad V_z = 0. \tag{106f}$$

The initial steady state of flow is the homogeneous flow regime (i.e., the uniform bubbly flow regime) and is represented by the following equations:

At time $t = 0$:

$$U_x = 0 \tag{107a}$$

$$U_z = U_0 = \text{constant} \tag{107b}$$

$$V_X = 0 \tag{107c}$$

$$V_z = V_0 = \text{constant} \tag{107d}$$

$$\varepsilon_G(X, Z) = \varepsilon_{G0} = \text{constant} \tag{107e}$$

$$P(X, Z) = \frac{p_{atm}}{\rho_L V_{B\infty}^2} + \hat{g}(h - Z)(1 - \varepsilon_{G0}) = P_0(X, Z). \tag{107f}$$

Substitution of the steady-state conditions in the equations of motion gives the following expression for the drag coefficient β:

$$\beta = \frac{\varepsilon_G(\rho_L - \rho_G)g}{(v_0 - u_0)}. \tag{108}$$

3. Linear Stability Analysis

According to the theory of hydrodynamic stability analysis, infinitesimally small perturbations are superimposed on the steady-state values of

variables and their transient behavior is studied. The variables in the perturbed state are represented by subscript 1 and steady-state values of the variables are represented by subscript 0. Using Eq. (107), we get the variables in their perturbed state as follows:

$$\varepsilon_G = \varepsilon_{G0} + \varepsilon_{G1} \tag{109a}$$

$$U_x = U_{x1} \tag{109b}$$

$$U_z = U_0 + U_{z1} \tag{109c}$$

$$V_x = V_{x1} \tag{109d}$$

$$V_z = V_0 + V_{z1} \tag{109e}$$

$$P = P_0 + P_1. \tag{109f}$$

The interaction term β or B is also linearized as follows:

$$B(\varepsilon_G) = B_0(\varepsilon_{G0}) + B_0'\varepsilon_{G1}, \tag{110}$$

where

$$B_0' = \left(\frac{\partial B}{\partial \varepsilon_G}\right)_{\varepsilon_G = \varepsilon_{G0}}. \tag{111}$$

Before introducing perturbations, some simplification of equations can be done by following an averaging procedure, given next.

a. Averaging in the Y Direction. Since $L \gg d$ and $H \gg d$, it is assumed that the velocity profiles in the Y direction can be represented as

$$U(X, Y, Z, \tau) = U_{\max}(X, Z, \tau)\left(1 - \frac{4Y^2L^2}{d^2}\right) \tag{112a}$$

$$V(X, Y, Z, \tau) = V_{\max}(X, Z, \tau)\left(1 - \frac{4Y^2L^2}{d^2}\right), \tag{112b}$$

where $U_{\max}$ and $v_{\max}$ are the velocities in the central plane, $Y = 0$. (U includes both the components U_x and U_z, and similarly for V.)

The average of these velocities in the Y direction can be obtained as

$$\bar{U}(X, Z, \tau) = \int_{-d/2L}^{d/2L} U(X, Y, Z, \tau)\, dY \tag{113a}$$

$$\bar{V}(X, Z, \tau) = \int_{-d/2L}^{d/2L} V(X, Y, Z, \tau)\, dY. \tag{113b}$$

Substituting Eq. (112) in Eq. (113),

$$U(X, Y, Z, \tau) = \frac{3L}{2d}\,\bar{U}(X, Z, \tau)\left(1 - \frac{4Y^2L^2}{d^2}\right) \tag{114a}$$

$$V(X, Y, Z, \tau) = \frac{3L}{2d}\,\bar{V}(X, Z, \tau)\left(1 - \frac{4Y^2L^2}{d^2}\right). \tag{114b}$$

It is assumed that the averaging holds for the perturbation variables as well, and that the hold-up and pressure are independent of Y.

With the preceding assumptions, substituting Eq. (114) in Eq. (96)–(99), integrating each term w.r.t. Y from $-d/2L$ to $+d/2L$, and dividing throughout by d/L, the Y-direction averaged equations can be obtained. After Y-direction averaging and substituting Eq. (109) in Eq. (95)–(99), and retaining only those terms that are linear in the perturbed variables, we can get the linearized continuity equations and equations of motion for both the phases. Proceeding in the usual manner, we assume perturbations of the form

$$\bar{U}_{x1}(X, Z, \tau) = \bar{U}_x(X, Z)e^{s\tau} \tag{115a}$$

$$\bar{U}_{z1}(X, Z, \tau) = \bar{U}_z(X, Z)e^{s\tau} \tag{115b}$$

$$\bar{V}_{x1}(X, Z, \tau) = \bar{V}_x(X, Z)e^{s\tau} \tag{115c}$$

$$\bar{V}_{z1}(X, Z, \tau) = \bar{V}_z(X, Z)e^{s\tau} \tag{115d}$$

$$\varepsilon_{G1}(X, Z, \tau) = \varepsilon_G(X, Z)e^{s\tau} \tag{115e}$$

$$P_1(X, Z, \tau) = P(X, Z)e^{s\tau}. \tag{115f}$$

The term's temporal growth rate in $e^{s\tau}$ is complex. When the real part of s equals zero, there can be two types of marginal states, depending on whether the imaginary part of s is also zero or nonzero. It is known that when the imaginary part of s is also equal to zero, the marginal state is charecterized by a stationary pattern of motion, in the form of cellular convection or secondary flow. If the imaginary part of s is nonzero in the marginal state, the instability sets in as oscillations of growing amplitude, also known overstability or oscillatory mode of instability. In the case of multiphase reactors, instability occurs in the form of cellular convection. In bubble columns, the transition from the homogeneous regime to the heterogeneous regime is marked by intense liquid recirculation in form of a single cell or multiple cells. This indicates that the imaginary part of s is equal to zero. In contrast, in the bounded bed analysis the imaginary part of s was not zero. Jackson and co-workers, Homsy and co-workers, and

Batchelor have assumed that the instability in unbounded beds sets in as oscillations of growing amplitude.

Using Eq. (115) and setting $s = 0$ gives the equations that determine the parameters at which the transition from homogeneous regime to the heterogeneous regime occurs. These neutral continuity equations and neutral equations of motion for both the phases after linearization and Y-direction averaging are as follows:

Linearized neutral continuity equation, liquid phase:

$$(1 - \varepsilon_{G0}) \left[\frac{\partial \bar{U}_x}{\partial X} + \frac{\partial \bar{U}_z}{\partial Z} \right] - U_0 \frac{\partial \varepsilon_G}{\partial Z} + D_L \frac{\partial^2 \varepsilon_G}{\partial X^2} + D_L \frac{\partial^2 \varepsilon_G}{\partial Z^2} = 0. \quad (116)$$

Linearized neutral continuity equation, gas phase:

$$\varepsilon_{G0} \left[\frac{\partial \bar{V}_x}{\partial X} + \frac{\partial \bar{V}_z}{\partial Z} \right] + V_0 \frac{\partial \varepsilon_G}{\partial Z} - D_G \frac{\partial^2 \varepsilon_G}{\partial X^2} - D_G \frac{\partial^2 \varepsilon_G}{\partial Z^2} = 0. \quad (117)$$

Linearized equation of motion for the liquid phase, X component:

$$(1 - \varepsilon_{G0}) U_0 \frac{\partial \bar{U}_x}{\partial Z} = -(1 - \varepsilon_{G0}) \frac{\partial P}{\partial X} + \frac{\eta}{Re_L} (1 - \varepsilon_{G0}) \bar{U}_x + B_0 (\bar{V}_x - \bar{U}_x). \quad (118)$$

Linearized equation of motion for the liquid phase, Z component:

$$(1 - \varepsilon_{G0}) U_0 \frac{\partial \bar{U}_Z}{\partial Z} = -(1 - \varepsilon_{G0}) \frac{\partial P}{\partial Z} + \hat{g} \varepsilon_G + \frac{\eta}{Re_L} (1 - \varepsilon_{G0}) \bar{U}_Z + B_0 (\bar{V}_z - \bar{U}_z) + B V_{s0} \varepsilon_G. \quad (119)$$

Linearized equation of motion for the gas phase, X component:

$$0 = -\varepsilon_{G0} \frac{\partial P}{\partial X} - B_0 (\bar{V}_X - \bar{U}_X). \quad (120)$$

Linearized equation of motion for the gas phase, Z component:

$$0 = -\varepsilon_{G0} \frac{\partial P}{\partial Z} - B_0 (\bar{V}_Z - \bar{U}_Z) - B_0^1 V_{s0} \bar{\varepsilon}_G \quad (121)$$

Here, $B_0^1 = (\partial B / \partial \varepsilon_G) \varepsilon_G = \varepsilon_{G0}$.

$$V_{s0} = V_0 - U_0. \quad (122)$$

The overbar indicates the velocities averaged in the Y direction, and η, the averaging parameter, is defined as

$$\eta = \frac{12L^3}{d^3}. \tag{123}$$

In writing equations (118) and (119), we have neglected the rate of momentum transferred in the X and Z directions as compared with that transferred in the smallest direction i.e., Y. As $L \gg d$, $H \gg d$, $\eta \gg 1$; therefore, we have

$$\eta \bar{U}_{x1} \geq \frac{\partial^2 \bar{U}_{x1}}{\partial X^2} + \frac{\partial^2 \bar{U}_{x1}}{\partial Z^2}. \tag{124}$$

b. Linearization of the Boundary Conditions. The linearized boundary conditions are as follows:

$$X = 0, \qquad \bar{U}_x = 0 \tag{125a}$$

$$X = 1, \qquad \bar{U}_x = 0 \tag{125b}$$

$$Z = h, \qquad P = 0. \tag{125c}$$

The gas sparger boundary condition is obtained by substituting Eq. (109) in Eq. (104) and linearizing.

At $Z = 0$,

$$\varepsilon_G = -E_1(P + F_1 U_z), \tag{126}$$

where

$$E_1 = [(U_0 + V_s + \varepsilon_{G0} V_s')(K_V + 2K_T \varepsilon_{G0}(U_0 + V_s))]^{-1} \tag{127}$$

$$V_s' = \left(\frac{\partial V_s}{\partial \varepsilon_G}\right)_{\varepsilon_G = \varepsilon_{G0}} \tag{128}$$

$$F_1 = K_V + 2\varepsilon_{G0} K_T (U_0 + V_s)\varepsilon_{G0}. \tag{129}$$

To linearize the liquid sparger boundary condition, substituting Eq. (109) in Eq. (104) and rearranging, we have

$$U_z = -A_1(P - C_5 \varepsilon_G), \tag{130}$$

where

$$A_1 = \left[(1 - \varepsilon_{G0}) \left(K_{VL} + 2U_0 \left\{ K_{TL}(1 - \varepsilon_{G0}) + \frac{1}{2} \right\} \right) \right]^{-1} \tag{131}$$

$$C_5 = U_0 \left[K_{VL} + U_0 \left(2K_{TL}(1 - \varepsilon_{G0}) + \frac{1}{2} \right) \right]. \tag{132}$$

From Eqs. (126) and (130), we get

$$\overline{U}_Z = -SP \tag{133a}$$

$$\varepsilon_G = -QP, \tag{133b}$$

where

$$S = \frac{A_1(1 + E_1C_5)}{(1 + A_1E_1C_5F_1)}, \qquad Q = \frac{E_1(1 - A_1F_1)}{(1 + A_1E_1C_5F_1)}. \tag{134}$$

c. Solution of Continuity Equations. Let us introduce stream functions ψ and ψ_G as follows:

$$\overline{U}_x = -\frac{\partial \psi}{\partial Z}, \overline{U}_z = \frac{\partial \psi}{\partial X} \tag{135}$$

$$\overline{V}_x = -\frac{\partial \psi_G}{\partial Z}, \overline{V}_z = \frac{\partial \psi_G}{\partial X}. \tag{136}$$

Adding Eq. (116) and (117) using Eq. (135) and (136) and rearranging gives

$$\frac{\partial^2 \varepsilon_G}{\partial Z^2} + \frac{V_s}{D_e} \frac{\partial \varepsilon_G}{\partial X} + \frac{\partial^2 \varepsilon_G}{\partial X^2} = 0, \tag{137}$$

where

$$D_e = D_L - D_G. \tag{138}$$

Let us use the method of separation of variables for solving Eq. (137).

$$\varepsilon_G = f(X)g(Z) \tag{139}$$

Using Eq. (139) and (137), we get

$$\frac{d^2g}{dZ^2} + \frac{V_s}{D_e}\frac{dg}{dZ} - \lambda^2 g = 0 \tag{140a}$$

$$\frac{d^2f}{dZ^2} + \lambda^2 f = 0, \tag{140b}$$

where λ is a separation constant.

The general solution of Eq. (140b) is

$$f(X) = C_1 \sin(\lambda X) + C_2 \cos(\lambda X). \tag{141}$$

At $X = 0$, $\varepsilon_G = 0$. This implies that $C_2 = 0$. Therefore,

$$f(X) = C_1 \sin(\lambda X). \tag{142}$$

This admits periodic solutions for each value of λ, and in general $\lambda = n\pi$. This indicates multiple cells in the horizontal direction. We restrict ourselves to just one horizontal cell, i.e., $n = 1$. The value of $n = 1$ corresponds to one horizontal cell, and all the values of n that are greater than 1 correspond to multiple cells in the horizontal direction. In bubble column transitions, the multiple cells in horizontal direction have been observed only in shallow bubble columns in which the height-to-diameter ratio is less than 1. In the present case, we have considered $H/D \gg 1$. Therefore, the transition to the heterogeneous regime is characterized by one cell in the horizontal direction. Thus, the first transition appears to correspond to a single cell in the horizontal direction:

$$\lambda_1 = \pi. \tag{143}$$

The solution to Eq. (140a) is

$$g(Z) = C_3 e^{aZ} + C_4 e^{bZ}, \tag{144}$$

where a and b are given by

$$a, b = 0.5\left[-\frac{V_s}{D_e} \pm \sqrt{\left(\frac{V_s}{D_e}\right)^2 + 4\pi}\right]. \tag{145}$$

Inspection of Eq. (145) reveals that the order of magnitude of v_s/D_e is 50–100 under normal operating conditions, indicating that a is a small positive number and b is a large negative number. The disturbance is induced in a stable bubble column because of the sparger. Therefore, any small disturbance in the free region below the sparger will manifest itself very close to the sparger (as Z tends to zero), and this disturbance will decay off rapidly as we move up the column, at a rate of e^{bz}, b being a

very large negative number. Thus, the term on the RHS of Eq. (144) represents the contribution of perturbations due to the sparger that die out within a very short distance from the sparger. These perturbations have little physical significance and hence can be neglected.

Equation (144) can thus be approximated to

$$g(Z) = C_3 e^{aZ}. \tag{146}$$

Combining Eqs. (139), (142), (143), and (146), we get

$$\varepsilon_G(X, Z) = C_1 C_3 \sin(\pi X) e^{aZ}. \tag{147}$$

At $Z = 0$,

$$\varepsilon_G(X, 0) = C_1 C_3 \sin(\pi X). \tag{148}$$

Combining Eqs. (147) and (148),

$$\varepsilon_G(X, Z) = \varepsilon_G(X, 0) e^{aZ}, \tag{149}$$

which then gives

$$\frac{\partial \varepsilon_G(X, Z)}{\partial X} = \frac{\partial \varepsilon_G(X, 0)}{\partial X} e^{aZ}. \tag{150}$$

d. Solution of the Momentum Equations. Adding Eqs. (118) and (120), we get the x direction linearized momentum equation for the gas–liquid dispersion as

$$M_4 \frac{\partial \bar{U}_x}{\partial Z} = -M_1 \frac{\partial P}{\partial X} + M_3 \bar{U}_x, \tag{151}$$

where

$$M_1 = 1 \tag{152}$$

$$M_3 = \frac{\eta}{\mathrm{Re}_L} (1 - \varepsilon_{G0}) \tag{153}$$

$$M_4 = (1 - \varepsilon_{G0}) U_0. \tag{154}$$

Similarly, adding Eqs. (119) and (121) gives the combined z direction momentum equation for gas–liquid dispersion as

$$M_4 \frac{\partial \bar{U}_z}{\partial Z} = -M_1 \frac{\partial P}{\partial Z} + M_3 \bar{U}_z + M_2 \hat{g}, \tag{155}$$

where

$$M_2 = 1. \tag{156}$$

Eliminating P from Eqs. (151) and (155), and introducing stream functions from Eq. (135), we get

$$M_4 \frac{\partial}{\partial Z}\left(\frac{\partial^2 \psi}{\partial X^2} + \frac{\partial^2 \psi}{\partial Z^2}\right) = M_3 \left(\frac{\partial^2 \psi}{\partial X^2} + \frac{\partial^2 \psi}{\partial Z^2}\right) + M_2 \hat{g} \frac{\partial \varepsilon_G}{\partial X} = 0. \tag{157}$$

Substitution of boundary condition (133b) in equation (150) gives

$$\frac{\partial \varepsilon_G(X, Z)}{\partial X} = -Q \frac{\partial P(X, 0)}{\partial X} e^{aZ}. \tag{158}$$

Equation (151) at the boundary (X, 0) takes the form

$$M_1 \frac{\partial \psi(X, 0)}{\partial X} = M_4 \frac{\partial^2 \psi(X, 0)}{\partial Z^2} - M_3 \frac{\partial \psi(X, 0)}{\partial Z}. \tag{159}$$

From Eqs. (158) and (159), we get

$$\frac{\partial \varepsilon_G(X, Z)}{\partial X} = \frac{Q}{M_1}\left(-M_4 \frac{\partial^2 \psi}{\partial Z^2} + M_3 \frac{\partial \psi}{\partial Z}\right)_{Z=0} e^{aZ}. \tag{160}$$

Substitution of Eq. (160) in (157) gives

$$\begin{aligned} M_4 \left[\frac{\partial}{\partial Z}\left(\frac{\partial^2 \psi}{\partial X^2}\right)\right] + \left(\frac{\partial^2 \psi}{\partial Z^2}\right) - M_3 \left(\frac{\partial^2 \psi}{\partial X^2} + \frac{\partial^2 \psi}{\partial Z^2}\right) \\ + \sigma \left(M_4 \frac{\partial^2 \psi}{\partial Z^2} - M_3 \frac{\partial \psi}{\partial Z}\right)_{Z=0} e^{aZ} = 0, \end{aligned} \tag{161}$$

where

$$\sigma = \frac{M_2 \hat{g} Q}{M_1}. \tag{162}$$

The boundary conditions for ψ are

$$X = 0, \qquad \frac{\partial \psi}{\partial Z} = 0 \tag{162a}$$

$$X = 1, \qquad \frac{\partial \psi}{\partial Z} = 0 \tag{162b}$$

$$Z = h, \qquad M_4 \frac{\partial^2 \psi}{\partial Z^2} - M_3 \frac{\partial \psi}{\partial Z} = 0 \tag{162c}$$

$$Z = 0, \qquad \frac{\partial^2 \psi}{\partial X^2} = -S M_4 \frac{\partial^2 \psi}{\partial Z^2} - M_3 \frac{\partial \psi}{\partial Z} \tag{162d}$$

$$Z = 0, \qquad \frac{\partial \psi}{\partial Z} = 0. \tag{162e}$$

Let us define

$$\phi = M_4 \frac{\partial^2 \psi}{\partial Z^2} - M_3 \frac{\partial \psi}{\partial Z}. \tag{163}$$

Equation (162) suggests the following form for ψ:

$$\psi = \exp\left(\frac{M_3 Z}{M_4}\right)\left[\int_0^Z \frac{1}{M_4} \exp\left(-\frac{M_3 Z}{M_4}\right) \phi dZ + C\right]. \tag{164}$$

Equation (161) along with its boundary conditions represents an eigenvalue problem. The lowest eigenvalue is the value at which the transition from the homogeneous to the heterogeneous regime occurs. Using the method of separation for solving Eq. (164),

$$\psi(X, Z) = \mathbf{X}(X) \cdot \mathbf{Z}(Z). \tag{165}$$

Substitution of (165) in Eq. (161) gives

$$\frac{d^2\mathbf{X}}{dX^2} = -k^2\mathbf{X} \tag{166a}$$

$$\frac{d^2\phi}{dZ^2} - k^2\mathbf{Z} = -M_5 e^{a\mathbf{Z}}, \tag{166b}$$

where k is a separation constant and

$$M_5 = \sigma \frac{d\mathbf{Z}(0)}{dZ}. \tag{167}$$

The boundary conditions for Eqs. (166) are

$$X = 0, \quad \mathbf{X} = 0 \tag{168a}$$

$$X = 0, \quad \mathbf{X} = 1 \tag{168b}$$

$$Z = 0, \quad \phi = 0 \tag{168c}$$

$$Z = h, \quad \phi = 0. \tag{168d}$$

The general solution of Eq. (166a) is

$$\mathbf{X} = A_1 \sin(kX) + A_2 \cos(kX). \tag{169}$$

To satisfy the boundary condition (168a),

$$A_2 = 0.$$

Further, to satisfy boundary condition (168b),

$$k = n\pi (n = 1, 2, 3, 4, \ldots). \tag{170}$$

The general solution of Eq. (166b) is

$$\phi(Z) = A_3 \sinh(kZ) + A_4 \cosh(kZ) + \frac{M_5}{k^2 - a^2} e^{aZ}. \tag{171}$$

Using the boundary conditions (168c) and (168d), we get the transition criterion at the lowest value of k, (i.e., $n = 1$):

$$\frac{((M_2\hat{g}Q/M_1) - M_3\mathrm{S})}{1 - ((M_2\hat{g}Q/M_1) - M_3S)(a/(\pi^2 - a^2))} = \frac{\pi^2 - a^2}{\pi} \coth(\pi h). \tag{172}$$

The homogeneous regime will prevail as long as the LHS of this equation is less than the RHS, and the transition to the heterogeneous regime will occur as the LHS becomes greater than the RHS.

This criterion involves the assumption that the gas phase stress terms are negligible. This assumption may not be valid in case of solid–liquid fluidized beds or liquid–liquid dispersions. In this case, the criterion is of the same form as Eq. (172), with different definitions of the parameters M_1, M_2, and M_3, which are given in Table VII. Table VII also gives the parameters of the criterion when the dispersion terms are not included in the continuity equations of both the phases.

Two special cases can be considered here.

Case 1. The pressure drop across the liquid sparger is very much less than that caused by its acceleration over the gas sparger region. This case

TABLE VII
PARAMETERS APPEARING ON THE STABILITY CRITERION (BOUNDED ANALYSIS) FOR RECTANGULAR BUBBLE COLUMNS: CARTESIAN COORDINATES

Parameter	Generalized criterion	$\hat{D}_G = 0$
M_1	$1 - \frac{\eta\varepsilon_{G0}(1 - \varepsilon_{G0})}{\mathrm{Re}_G B_0}$	1
M_2	$1 - \rho + \frac{\eta\varepsilon_{G0}}{\mathrm{Re}_G B_0} \frac{(\hat{g} + B_0' V_{S0})}{\hat{g}}$	$1 - \rho$
M_3	$\frac{\eta(1 - \varepsilon_{G0})}{\mathrm{Re}_L} + \frac{\eta\varepsilon_{G0}}{\mathrm{Re}_G}\left(1 - \frac{\eta(1 - \varepsilon_{G0})}{\mathrm{Re}_L B_0}\right)$	$\frac{\eta(1 - \varepsilon_{G0})}{\mathrm{Re}_L}$
M_4	$U_0(1 - \varepsilon_{G0})\left(1 - \frac{\eta\varepsilon_{G0}}{\mathrm{Re}_G B_0}\right)$	$U_0(1 - \varepsilon_{G0})$

Note: These parameter definitions hold for the semibatch operations with $U_0 = 0$ and $V_s = V_0$.

corresponds to a situation when the column is connected at its bottom to a huge reservoir of liquid. Mathematically, this can be written as

$$k_{VL}v_{sup} + k_{TL}v_{sup}^2 \ll \frac{\rho u_z}{2} - \frac{\rho_L v_{sup}}{2}. \tag{173}$$

Under limiting conditions this means that $k_{VL} \to 0$, and $k_{TL} \to 0$ parameters A_1 and C_5 are defined as

$$A_1 = \frac{1}{U_0(1-\varepsilon_{G0})}, \quad C_5 = \frac{U_0^2}{2}. \tag{174}$$

Parameters E_1 and F_1 are defined as in Eqs. (127) and (129). The stability criterion is given by Eq. (172).

Case 2. Pressure drop across the liquid sparger is sufficiently large to ensure uniform liquid flow into the column irrespective of the pressure perturbations in the column. Mathematically this means that

$$k_{VL}v_{sup} + k_{TL}v_L^2 \gg \frac{\rho u_z}{2} - \frac{\rho_L v_{sup}}{2}. \tag{175}$$

Under these limiting conditions, we have

$$k_{VL} \to \infty \text{ and } k_{TL} \to \infty. \tag{176a}$$

Also,

$$U_{z1}(X, 0) = 0; \quad \text{hence,} \quad S = 0. \tag{176b}$$

Using these conditions in (131), (132), and (134), we get

$$A_1 \to 0,\ C_5 \to \infty; \quad \text{therefore,} \quad Q = E_1. \tag{177}$$

Under these conditions, the stability criterion becomes

$$\frac{(M_2/M_1)(\hat{g}\beta_1'/\alpha')}{1-(M_2/M_1)(\hat{g}\beta_1'/\alpha')(a/\pi^2 - a^2)} = \frac{\pi^2 - a^2}{\pi}\coth(\pi h), \tag{178}$$

where α' and β'_1 are the modified parameters corresponding to the continuous mode of operation defined as follows:

$$\alpha' = (U_0 + V_s + \varepsilon_{G0}V_s') \tag{179}$$

$$\beta_1' = [K_v + 2K_T\varepsilon_{G0}(U_0 + V_s)]^{-1}. \tag{180}$$

e. Criterion for Batch Operation. The criterion for batch operation is a special case of the criterion for continuous mode of operation, when $U_0 = 0$.

4. Criterion for Cylindrical Bubble Columns

Following a procedure analogous to that used in derivation of the stability criterion for two-dimensional bubble columns, the stability criterion for cylindrical bubble columns is given as

$$\frac{N_2 Q}{1 - N_2 Q(a/(\lambda_2^2 - a^2))} = \frac{\lambda_2^2 - a^2}{\lambda_2} \frac{\sinh(\lambda_2 h)}{\cosh(\lambda_2 h) - e^{ah}}, \tag{181}$$

where λ_2 is the first nonzero root of the equation:

$$J_1\left(\lambda_2 \sqrt{\frac{N_1}{N_3 G h}}\right) = 0, \text{ i.e., } \lambda_2 = 3.8693 \sqrt{\frac{N_1}{N_3 G h}}. \tag{182}$$

The parameters appearing in Eqs. (181) and (182) are defined in Table VIII. The assumption of negligible gas phase stresses leads to some simplifications. The modified definitions of the parameters for these special cases are also listed in Table VIII. Other special cases depending upon the limiting values of pressure drop across the sparger are similar to those given for a rectangular column. The criteria for the special cases are given next.

Case 1. $k_{VL} = 0$ and $k_{TL} = 0$, A_1 and C_5 are defined by Eq. (174), and the criterion is given by Eq. (181).

TABLE VIII
PARAMETERS APPEARING IN THE STABILITY CRITERION (BOUNDED ANALYSIS) FOR CYLINDRICAL BUBBLE COLUMNS: CYLINDRICAL COORDINATES

Parameter	Generalized criterion	$\gamma_G = 0$
N_1	$\frac{Y_1 - Y_3(B_0 - 2Y_1)/B_0}{1 - 2Y_3(1 - \varepsilon_{G0})/B_0}$	$\frac{Y_1 + V_0\varepsilon_{G0}(B_0 - 2Y_1)/2B_0 h}{1 + V_0\varepsilon_{G0}(1 - \varepsilon_{G0})/B_0 h}$
N_2	$\frac{1 - Y_4(\hat{g} - B_0' V_{S0})/B_0}{1 - Y_4(1 - \varepsilon_{G0})/B_0}$	$\frac{1 + V_0(\hat{g} - B_0' V_{S0})/B_0\varepsilon_{G0}}{1 + V_0(1 - \varepsilon_{G0})/B_0\varepsilon_{G0}}$
N_3	$\frac{Y_2 - Y_4(B_0 h - Y_2)/B_0 h}{h\hat{g}(1 - Y_4(1 - \varepsilon_{G0})/B_0 h)}$	$\frac{Y_2 + V_0(B_0 h - Y_2)/\varepsilon_{G0} B_0 h}{\hat{g}h(1 + V_0(1 - \varepsilon_{G0})/\varepsilon_{G0} B_0 h)}$
Y_1	$(1 - \varepsilon_{G0})\left(\frac{8 + 0.5(1/h)^2}{Re_L} - \frac{U_0}{2h}\right)$	Remains same
Y_2	$h(1 - \varepsilon_{G0})\left(\frac{8 + 2.5(1/h)^2}{Re_L} - \frac{U_0}{h}\right)$	Remains same
Y_3	$\varepsilon_{G0}(1 - \varepsilon_{G0})\left(\frac{8 + 0.5(1/h)^2}{Re_G} - \frac{V_0}{2h}\right) - \frac{V_0\varepsilon_{G0}}{2h}$	
Y_4	$h\varepsilon_{G0}(1 - \varepsilon_{G0})\left(\frac{8 + 2.5(1/h)^2}{Re_G} - \frac{V_0}{h}\right) - \frac{V_0}{\varepsilon_{G0}}$	

Case 2. $k_{VL} = \infty$ and $k_{TL} = \infty$, and the criterion becomes

$$\frac{N_2(\beta_1'/\alpha)}{1 - N_2(\beta_1'/\alpha')(a/(\lambda_2^2 - a^2))} = \frac{\lambda_2^2 - a^2}{\lambda_2} \frac{\sinh(\lambda_2 h)}{\cosh(\lambda_2 h) - e^{ah}}, \tag{183}$$

where β'_1 and α' are given by Eqs. (180) and (179).

B. Estimation of Model Parameters

In order to predict fractional gas hold-up and superficial gas velocity at the point of transition using the stability criteria developed, it is necessary to estimate the following parameters:

1. Slip velocity: $v_s(V_{B\infty}, \varepsilon_G)$
2. Dispersion coefficients
3. Pressure drop across the gas sparger: $\Delta p(k_V, k_T, v_{sup})$

The estimation procedure for slip velocity and dispersion coefficient was given earlier in Section V. For the bounded bed analysis, the pressure boundary condition at the sparger becomes important. The procedure for predicting pressure drop at the sparger is given next.

1. Estimation of Sparger Pressure Drop

Pressure drop across the gas sparger is expressed as follows:

$$\Delta P = k_V v_{sup} + k_T v_{sup}^2 = k_V V_G + k_T V_G^2. \tag{184a}$$

The two terms on the right-hand side represent the contributions due to viscous and turbulent flow resistances. It was assumed that the pressure drop due to viscous resistance is negligible ($k_v = 0$). However, the parametric sensitivity of k_v on the critical superficial gas velocity was also studied. The turbulent pressure drop was estimated using the orifice equation

$$\Delta P = k_T V_G^2, \tag{184b}$$

where

$$k_T = \frac{\rho_G}{2} \left(\frac{R}{C_{hole}} \right)^2. \tag{184c}$$

R is the ratio of column cross-sectional area to orifice area, and C_{hole} is the orifice coefficient and was taken as 0.61.

In the case of fluidized beds, since all reported data on transition are

for very small particles of the order of a few hundred micrometers, the sparger resistance calculated by Eq. (184) is very high, and therefore, in the further analysis, it was assumed to be a very high quantity tending to infinity.

C. Results and Discussion

1. Fluidized Beds

The stability criterion is given by Eq. (183). The homogeneous flow regime can be maintained as long as the left-hand side of this equation is less than the right-hand side. For the aspect ratio ($h = H/D$) > 1, the right-hand side is a constant quantity. The left-hand side depends on the design of the sparger and the physical properties of the fluid. As mentioned earlier, data on the design of a sparger for fluidized beds has not been reported. Therefore, the role of sparger design in transition cannot be studied. However, under the limiting case of infinite sparger resistance, the criterion can be simplified. Under these conditions k_v and $k_T \to \infty$ and hence $\beta'_1 \to 0$. In order to keep the RHS of Eq. (183) finite, α' should tend to zero. With this condition, we get

$$\varepsilon_{SC} = \frac{1}{m}, \tag{185}$$

where m is the Richardson–Zaki index and is a function of the particle Reynolds number.

2. Bubble Columns

The superficial gas velocity (v_{sup}, V_G), at which the transition from the homogeneous to the heterogeneous flow regime occurs depends mainly on the design of the gas sparger and the physical properties of the system. In order to understand the effect of these parameters on v_{sup}, plots were constructed on the basis of the stability criterion [Eq. (183)]. The effects of the number of orifices, orifice diameter, bubble rise velocity, and gas hold-up index on V_{GC} were studied. In the case of continuous operation, the effect of superficial liquid velocity on ε_{GC} and v_{sup} was studied. While studying the effect of orifice diameter and the contribution of viscous flow resistance on ε_{GC} and v_{sup}, the value of m was taken as 2.4 in the following equation:

$$\frac{v_{sup}}{\varepsilon_G} = V_{B\infty}\varepsilon_L^{m-1}. \tag{186}$$

The homogeneous flow regime can be maintained as long as the LHS of Eq. (183) is less than the RHS. For the aspect ratio ($h = H/D$) > 1 the RHS is a constant quantity. The LHS depends on the design of the gas sparger and the physical properties of the liquid. The role of these parameters will now be discussed systematically.

a. Semibatch Operation

(i) *Effect of Sparger Resistance.* The sparger resistance is represented by Eq. (184). The sparger resistance increases with an increase in the area ratio (R). The effect of area ratio on ε_{GC} is shown in Fig. 33. It can be seen that the value of ε_{GC} increases with an increase in R up to about 800, and then ε_{GC} levels off. The limiting value of ε_{gc} can be obtained as R tends to infinity. Under these conditions $k_T \to \infty$ and hence $\beta'_1 \to 0$. In order to keep the RHS of Eq. (183) finite, α' should tend to zero. With this condition, we get

$$\varepsilon_{GC} = \frac{1}{m}. \tag{187}$$

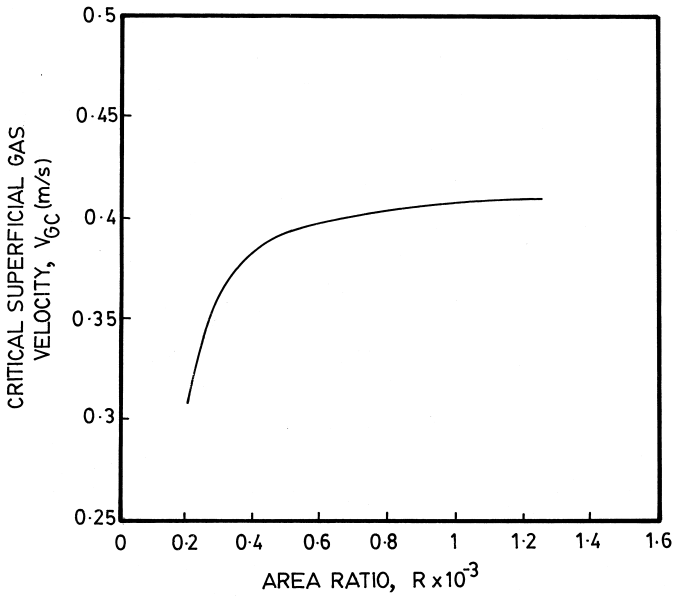

FIG. 33. Effect of area ratio on critical gas hold-up.

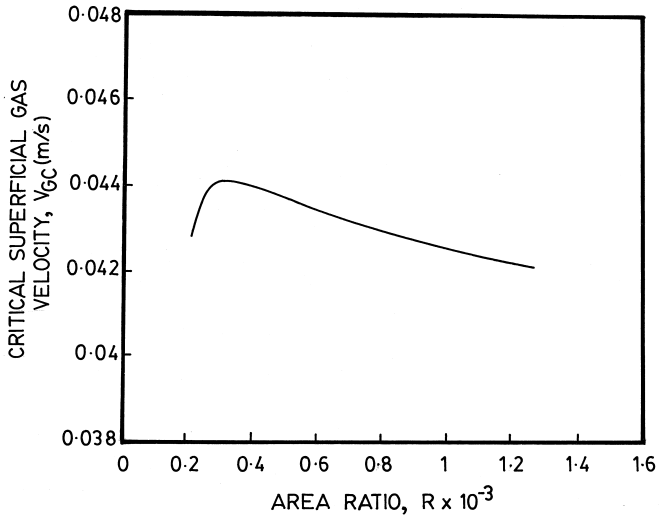

FIG. 34. Effect of area ratio on superficial gas velocity.

For a typical value of m equal to 1.42 (Richardson and Zaki, 1954), the value of ε_{GC} works out to be 0.42. In the published literature, the maximum value of hold-up ($u_{sup} = 0$) has been reported by Oels *et al.* (1978) and is in the range of 0.42 to 0.48. The experimental value agrees with the limiting value predicted by Eq. (186).

The effect of area ratio on the transition gas velocity, V_{GC}, is shown in Fig. 34. Figure 35 shows the parametric sensitivity of V_{GC} on k_v. The effect

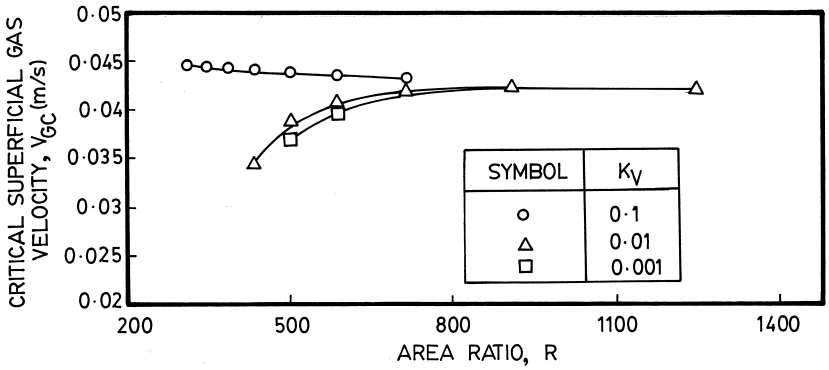

FIG. 35. Parametric sensitivity of k_V on critical superficial gas velocity.

of hole size d_0 on ε_{GC} and V_{GC} is shown in Figs. 36 and 37, respectively. It can be seen that the values of ε_{GC} and V_{GC} decrease with an increase in d_0.

(ii) *Effect of Bubble Rise Velocity.* Liquid viscosity, surface tension, and liquid density govern the bubble rise velocity. It was thought desirable to study the effect of physical properties through the value of $V_{B\infty}$. The relationship between physical properties and bubble size has been given by Kumar and Kuloor (1972) and the relationship between physical properties and the bubble rise velocity (for a given size) has been given by Clift *et al.* (1978). The effect of bubble rise velocity on V_{GC} is shown in Fig. 38. It can be seen that the value of V_{GC} increases with an increase in $V_{B\infty}$.

(iii) *Effect of Gas Density.* Effect of gas density was studied over a wide range of gas density. The turbulent contribution of sparger resistance, k_T, depends proportionally on the gas density as given by Eq. (184c). An increase in the gas density therefore stabilizes the bed, as shown in Fig. 39.

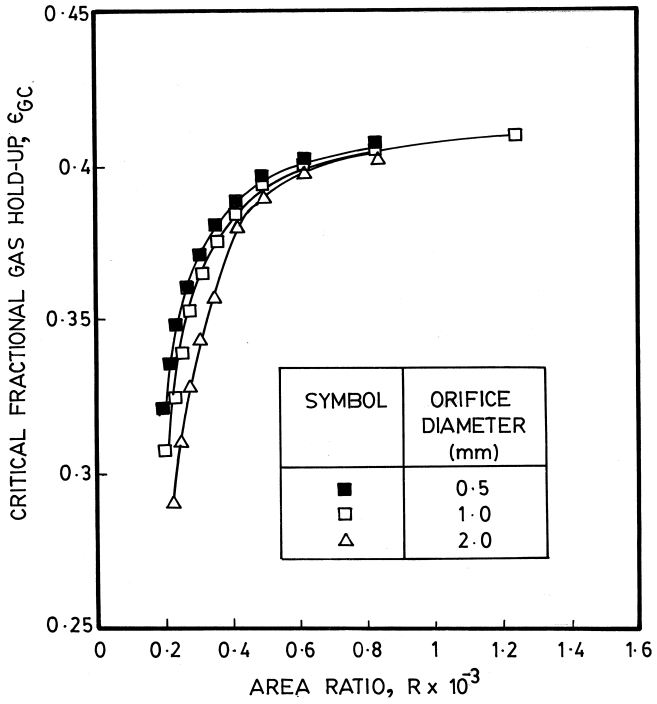

FIG. 36. Effect of hole size of the sparger on critical gas hold-up.

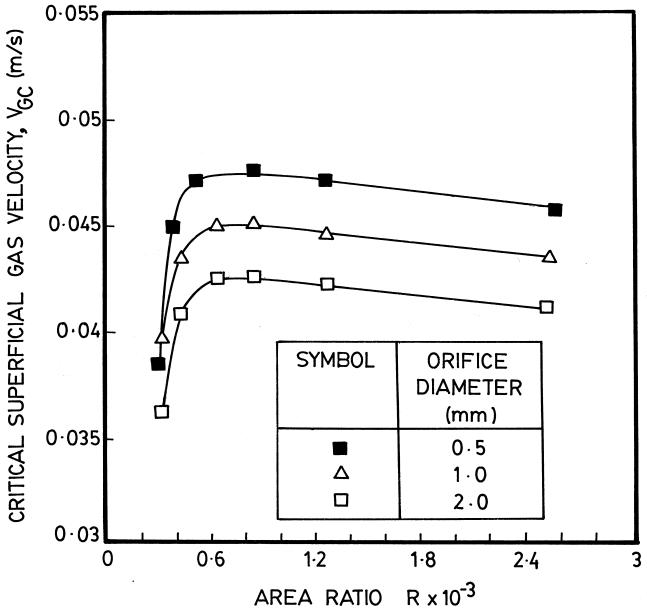

FIG. 37. Effect of hole size of the sparger on critical superficial gas velocity.

(iv) *Effect of Hold-up Parameter.* In a bubble column the bubble rises in the presence of many bubbles. Because of the presence of other bubbles, the actual bubble rise velocity is lower than the terminal value, and this hindrance effect increases with an increase in the gas hold-up. With the hindrance effect, the relationship between superficial gas velocity and fractional gas hold-up is given by Eq. (186).

The hold-up parameter n depends upon the bubble Reynolds number. The effect of m on V_{GC} and ε_{GC} is shown in Fig. 40 and 41 for hole diameters of 0.5 mm. It can be seen that at a constant R the value of V_{GC} increases with a decrease in m. The asymptotic value of ε_{GC} given by Eq. (186) is shown in Fig. 41.

(v) *Effect of Dispersion.* The dispersion coefficient has a stabilizing effect on the performance of bubble columns. This implies that the transition is delayed with the inclusion of dispersion. Figures 42 and 43 show the effect of dispersion on the superficial gas velocity and gas hold-up for a fixed column geometry over a wide range of dispersion coefficient. It can be seen that the effect of dispersion on V_{GC} and ε_{GC} is nominal over a 100-fold variation of the dispersion coefficient. Figure 44 shows the effect of relaxing most of the assumptions made by Shnip *et al.* (1992).

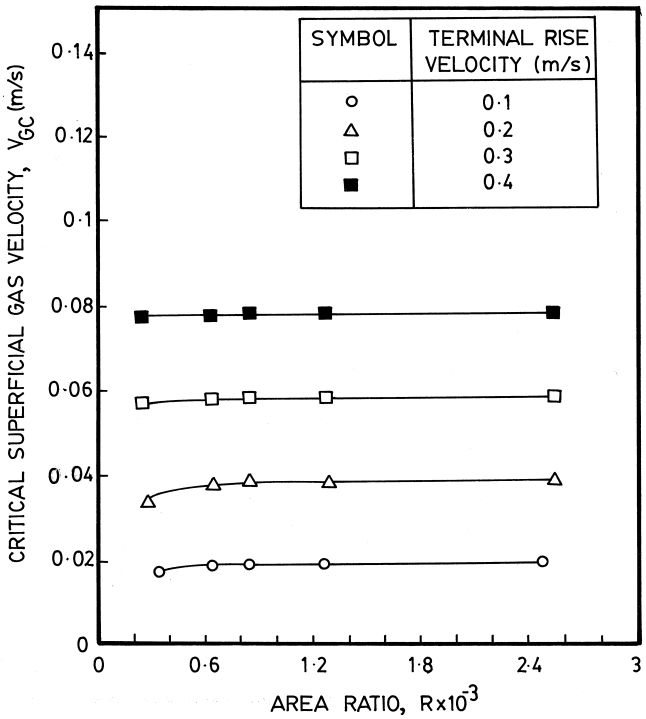

FIG. 38. Effect of terminal bubble rise velocity on critical superficial gas velocity.

(vi) *Effect of Column Diameter.* Figure 45 shows the effect of column diameter for a fixed sparger design and dispersion height. As seen from the plots, a decrease in the column diameter has a stabilizing effect and the critical superficial gas velocity increases with a decrease in D, the column diameter.

(vii) *Effect of Dispersion Height.* As noted earlier, once the aspect ratio h becomes equal to 1, the RHS of Eq. (183) becomes more or less a constant. Figure 46 shows the effect of dispersion height for a fixed diameter and sparger design. The curves are seen to become almost insensitive to h, above a value of h =1–1.5.

The liquid flow is either cocurrent or countercurrent to the gas flow. Liquid is introduced with the help of a distributor. Two limiting cases of the distributor resistance (k_{VL}) are considered: $k_{VL} = \infty$ and $k_{VL} = 0$. For the first case, the stability criterion was given by Eq. (183). The results

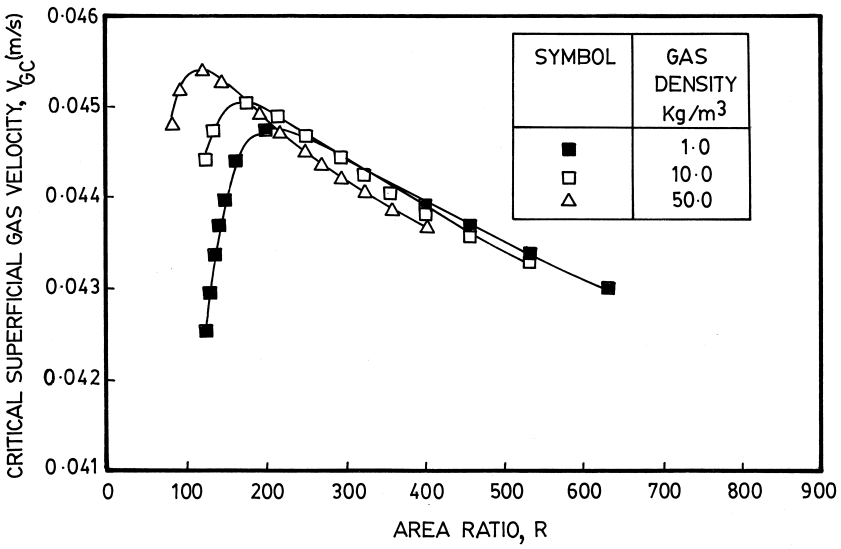

FIG. 39. Effect of gas density on critical superficial gas velocity.

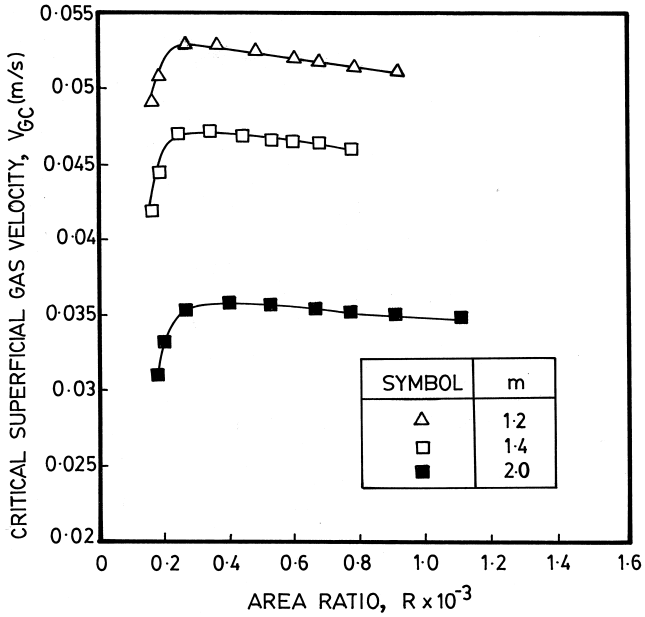

FIG. 40. Effect of m on critical superficial gas velocity for orifice diameter of the sparger = 0.5 mm.

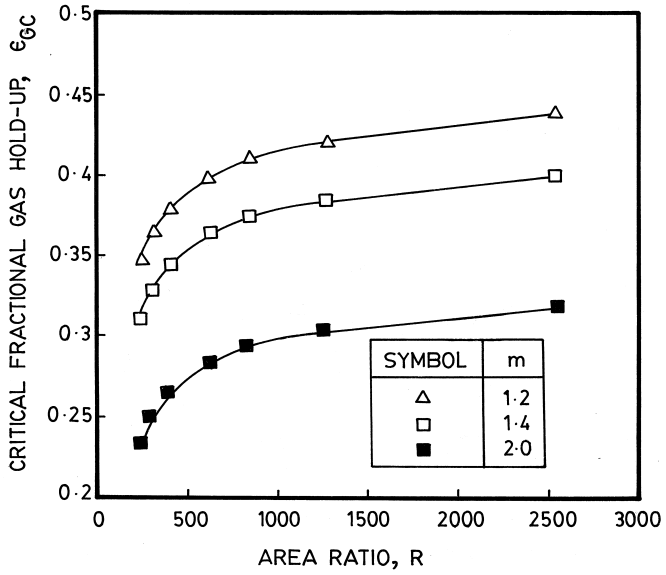

FIG. 41. Effect of m on critical gas hold-up for orifice diameter of the sparger = 0.5 mm.

are shown in Fig. 47 for cocurrent ($u_L = +10$ and $+20$ mm/s) and countercurrent (-10 and -20 mm/s) flows. It can be seen that the value of V_{GC} increases with an increase in the cocurrent liquid velocity, whereas it decreases with an increase in the countercurrent liquid velocity. These predictions agree with the experimental observations of Oels *et al.* (1978).

The effect of liquid velocity can be qualitatively explained as follows. In the heterogeneous regime, liquid circulation is developed that is upward in the central region and downward in the annular region. With cocurrent liquid upflow, the downward annular flow is restricted, resulting into a reduction in the liquid circulation. Therefore, the cocurrent liquid flow delays the transition. The countercurrent liquid flow has the opposite effect.

When the liquid distributor resistance is zero ($k_{VL} = 0$), the results are shown in Fig. 48. In this case also, the transition delays with an increase in the cocurrent v_{sup}. However, the increase in V_{GC} is less for the case of $k_{VL} = 0$ as compared to the case of $k_{VL} = \infty$. When $k_{VL} = 0$, the disturbances at the bottom grow because of the absence of the possible dampening effect of the liquid distributor. For this case, the homogeneous regime is not possible when the liquid flow is countercurrent.

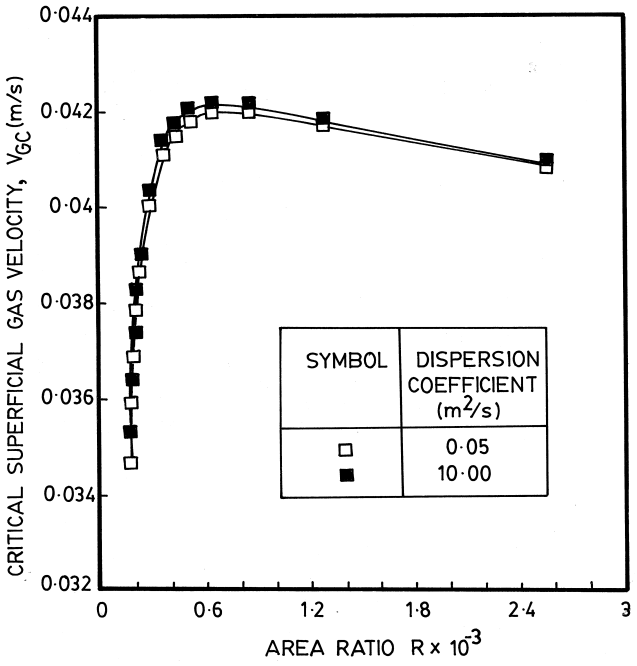

FIG. 42. Effect of dispersion coefficient on critical superficial gas velocity.

D. COMPARISON WITH EXPERIMENTAL DATA

1. Fluidized Beds

Table IX comparies model predictions with experimental values for solid–liquid fluidized beds. As mentioned earlier, in fluidized beds of very fine heavy particles, transition occurs because of radial nonuniformity. Further, almost all reported data on fluidized beds have mentioned that the sparger resistance was very large. Therefore, the comparison is made for the limiting case of the model, i.e., Eq. (183). Also, to bring out the limitation of the unbounded analysis, the same system data are compared. The comparison is favorable using the model of the present work. Table X shows the comparison for gas–solid fluidized beds. Again, fairly good agreement can be seen between the model predictions and the experimental observations.

2. Bubble Columns

Yamashita and Inoue (1975), Maruyama *et al.* (1981), and Chisti (1989) have measured the values of critical superficial gas velocity for transition.

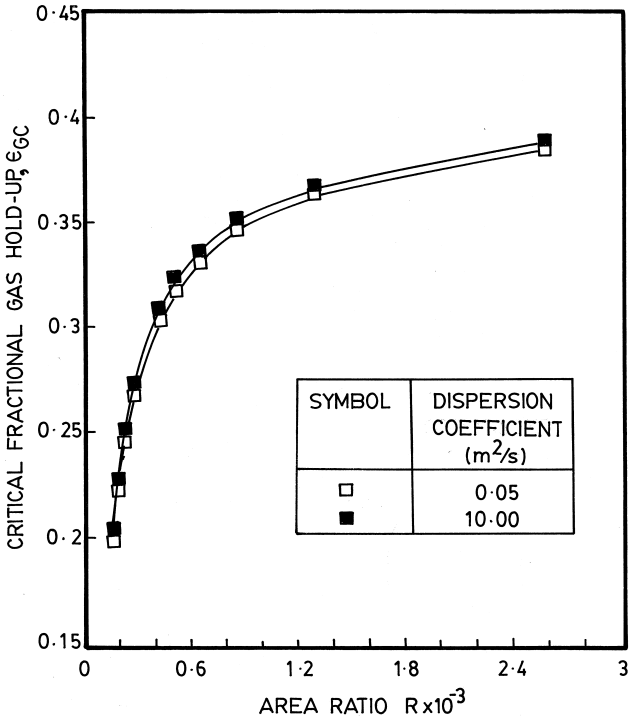

FIG. 43. Effect of dispersion coefficient on critical gas hold-up.

The details pertaining to the experiments along with the comparison between model predictions and experimental observations is shown in Table XI. It can be seen that the agreement is favorable over a wide range of column widths, hole diameters, and numbers of holes.

It has been pointed out earlier that the maximum possible hold-up in the homogeneous regime is 42%. This prediction compares favorably with the experimental observations of Maruyama *et al.* (1981) and Koetsier *et al.* (1976).

VII. Comparison of Bounded and Unbounded Analysis

In Sections II and VI, the stability of multiphase systems was analyzed for unbounded and bounded beds, respectively. In the unbounded case, it was dispersion that was the most important parameter in deciding the stability of the system. An increase in the dispersion coefficient led to a

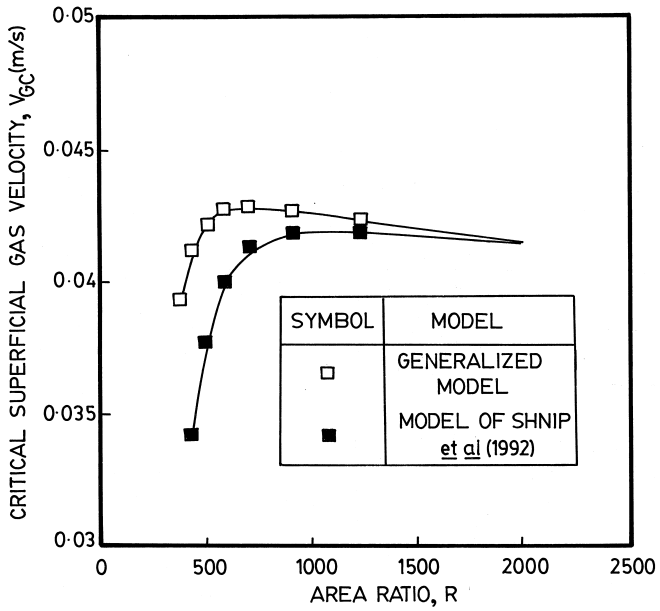

FIG. 44. Comparison with the predictions of Shnip *et al.* (1992).

more stable system. This has been depicted in Fig. 17, 18, 19, and 20 for gas–solid and solid–liquid fluidized beds. In the bounded case as well, the dispersion figures in the final criterion. However, the dependence of stability on the dispersion is very weak. Figure 42 shows, the dependence of critical superficial gas velocity, V_{GC}, on the dispersion coefficient. The plot is almost insensitive to the value of the dispersion coefficient over a wide range. This apparent discrepancy which arises because of the fundamental difference between the bounded and unbounded analysis, is explained next.

We define more clearly what is meant by an unbounded bed. In an unbounded bed, the bed dimensions are infinite, there are no lateral walls, and the presence of a sparger is not considered. Thus, unbounded analysis is valid in a situation when the sparger resistance is relatively small and the column dimensions are large. Once any perturbation or disturbance starts, dispersion is quick (or large) enough to nullify the gradients and make the bed stable. Thus, the dispersion always levels off all the gradients and is always a stabilizing mechanism. At this point, the question arises: If dispersion is always stabilizing, what is its upper limit? Unbounded bed analysis predicts that a sufficiently high value of dispersion coefficient can make the bed totally stable for a given particle diameter and physical properties. However, in reality, the destabilizing mechanisms associated

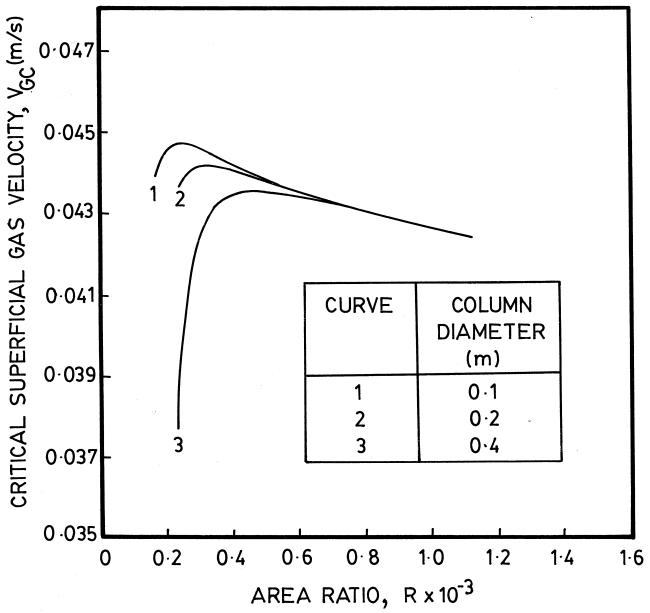

FIG. 45. Effect of column diameter on critical superficial gas velocity.

with the sparger and/or lateral walls may become important. When this happens; the stabilizing effect of dispersion is no longer unlimited, the unbounded analysis breaks down, and we have to resort to the bounded bed analysis. Thus, the comparison of experimental transition hold-up using the unbounded bed criterion in Eq. (25), and the values of proportionality constant for dispersion equal to 3, shows that the unbounded analysis cannot predict the transitions where $\varepsilon_L > 60\%$, i.e., the unbounded bed analysis predicts the fully particulate regime when the experimental transitions are occuring above the hold-up value of 60%. As the sparger resistance increases, the transition occurs at higher values of hold-up. However, the increase in sparger resistance also reduces the applicability of unbounded analysis. It must be emphasized that the applicability of unbounded analysis is limited to low values of sparger resistance. In the case of high sparger resistance, bounded bed analysis should be used to get realistic predictions.

From this discussion, we propose the following procedure to predict transitions in two-phase systems in a quantitative manner:

1. Check the stability using the unbounded bed criterion, neglecting the sparger and column dimensions. If the bed is unstable, then the bed will be unstable throughout, no matter how well the sparger is de-

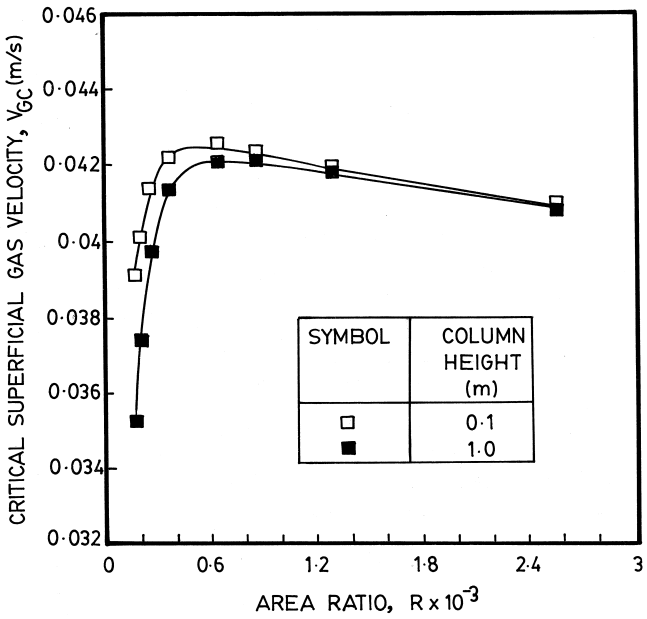

FIG. 46. Effect of dispersion height on superficial gas velocity.

signed or how the column dimensions are altered. However, if the unbounded criterion predicts a stable bed, it just means that the bed is stable against the axial disturbances. It may or may not be stable against the radial disturbances due to sparger or wall. Therefore:

2. Check the stability using the bounded bed criterion. If the bounded criterion also predicts a stable bed, the bed is fully stable and will exhibit all the characteristics of the homogeneous regime. However, if the bounded criterion predicts an unstable bed, then the bed will exhibit all the characteristics of the heterogeneous regime even though the unbounded criterion predicted a stable bed. Stability can, however, be achieved in this case by increasing the sparger resistance or by reducing the column dimensions.

VIII. Three-Phase Fluidization

A. INTRODUCTION

Three-phase fluidization refers to operation in which an upward flow of gas and cocurrent or countercurrent flow of liquid supports a bed of

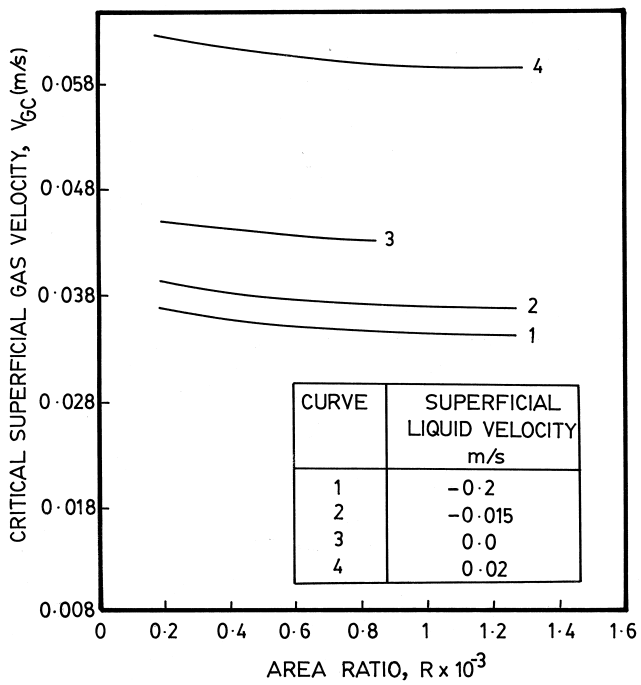

FIG. 47. Effect of liquid superficial velocity for cocurrent and countercurrent operation [$k_{VL} = \infty$].

solid particles. The gas flows as bubbles. The three-phase fluidization is characterized by the unique phenomenon that an increase in the gas velocity may cause an increase in the height (expansion) or a decrease in the bed height (contraction), whereas an increase in the liquid velocity always causes an increase in the bed height. This phenomenon was first observed by Turner (1964) and subsequently by Stewart and Davidson (1964), Ostergaard (1965), Ostergaard and Thiesen (1966), Adlington and Thompson (1965), and Epstein and co-workers. All these investigators agree that (a) the bed expansion occurs with an increase in the liquid velocity, and (b) an increase in the gas velocity can cause either contraction or expansion.

Bed expansion and contraction are important phenomena in three-phase fluidization, since these affect the bed volume and the residence time(s) of all the phase(s). The phenomenon of bed contraction/expansion is also very closely linked to the problem of transition. The relationship between the expansion/contraction behavior and the transition will be clearly brought out later.

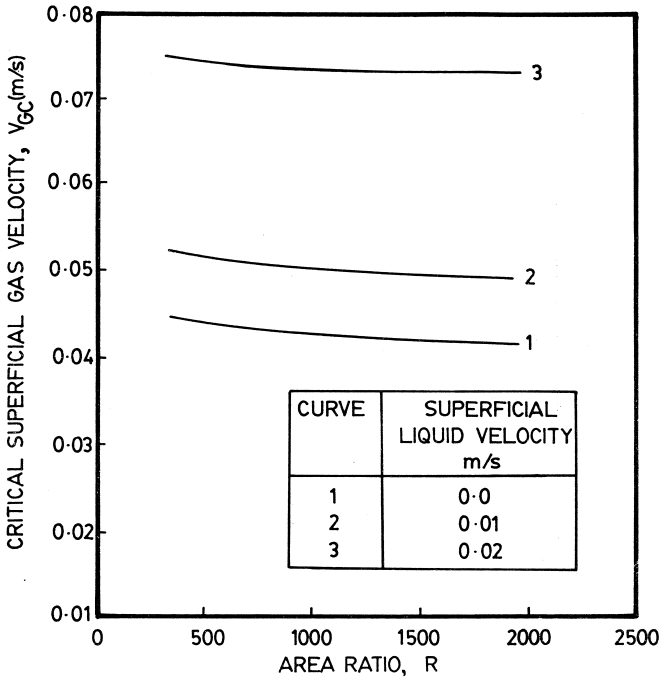

FIG. 48. Effect of liquid superficial velocity for cocurrent and countercurrent operation [$k_{VL} = 0$].

B. HEURISTIC MODELS

Stewart and Davidson (1964) and Ostergaard (1965) proposed similar mechanisms to explain the contraction phenomenon. They offered qualitative and semiquantitative explanations based on the assumption that gas bubbles in the bed are followed by wakes. The wakes travel at velocities equal to the bubble velocities and thus considerably higher than the average superficial liquid velocity in the bed. Therefore, it follows from the continuity equation that the velocity in the bed outside the bubble wakes is lower than the average superficial velocity, and thus the expansion of this part of the bed must be correspondingly reduced.

Epstein and co-workers (Bhatia and Epstein, 1974; Epstein, 1976; Epstein and Nicks, 1976; El-Temtamy and Epstein, 1978, 1979) have made very valuable contributions to the understanding of expansion/contraction characteristics of three-phase fluidized beds. Bhatia and Epstein (1974) proposed a wake model in which the solid contents of the liquid wakes behind the gas bubbles is negligible compared to the solid contents of the remaining

TABLE IX

COMPARISON OF EXPERIMENTAL DATA WITH BOUNDED BED ANALYSIS PREDICTIONS FOR SOLID–LIQUID FLUIDIZED BEDS

Investigator	d_P (mm)	ρ_S (kg/m^3)	ρ_L (kg/m^3)	$\mu_L \times 10^3$ Pas	ε_{LC} experimental (%)	ε_{LC} predicted[a] (%)	ε_{LC} predicted[b] (%)
Gibilaro *et al.* (1986)	655	8710	1000	1.25	0.48	0.55	0.478
	655	8710	1000	0.60	0.45	0.49	0.452
	275	8710	1000	1.05	0.60	0.67	0.595
	275	8710	1000	0.60	0.51	0.59	0.520
	165	8710	1000	1.25	0.74	0.81	0.726
	165	8710	1000	0.75	0.66	0.73	0.676
	82.5	8710	1000	1.25	0.75	0.91	0.742
	82.5	8710	1000	0.75	0.72	0.86	0.7345

[a] Unbounded bed analysis.

[b] Bounded bed analysis.

TABLE X
COMPARISON OF EXPERIMENTAL DATA WITH PREDICTIONS OF BOUNDED-BED ANALYSIS: GAS–SOLID FLUIDIZED BEDS

Investigator	d_P (mm)	ρ_S (kg/m^3)	ε_{GC} experimental (%)	ε_{GC} predicted[a] (%)	ε_{GC} predicted[b] (%)
Jacob and Weimer (1987)	0.044	850	76.5	79.0	75.2
	0.044	850	76.7	80.0	76.1
	0.044	850	79.8	81.0	78.2
	0.112	850	79.8	64.0	77.1
	0.112	850	79.8	62.0	78.3
	0.112	850	79.8	60.0	79.3
Musters and Rietema (1977)	0.0397	920	77.6	76.0	78.2
	0.078	920	74.2	68.0	76.5
	0.103	920	70.1	65.0	76.5

[a] Unbounded bed analysis.
[b] Bounded bed analysis.

liquid. More direct experimental evidence for wakes that are nearly solids-free was cited in the published discussion of this paper.

The equations governing the solids-free wake model, assuming steady state, are as follows:

$$\varepsilon_L + \varepsilon_G + \varepsilon_S = 1. \tag{188}$$

Since the liquid divides itself between the solids-free wake and the particulate region of the liquid-fluidized solids,

$$\varepsilon_L = \varepsilon_k + (1 - \varepsilon_G - \varepsilon_k)\varepsilon_{lf}. \tag{189}$$

TABLE XI
COMPARISON OF EXPERIMENTAL DATA WITH PREDICTIONS OF BOUNDED-BED ANALYSIS: TWO-DIMENSIONAL GAS–LIQUID BUBBLE COLUMNS

Investigator	Column length (mm)	Column width (mm)	Orifice diameter (mm)	Area ratio	Sparger thickness (mm)	V_{GC} experimental (mm/s)	V_{GC} predicted (mm/s)
Chisti (1989)	460	155	1.0	50	2.0	63.41	42.45
Maruyama *et al.* (1981)	300	10	0.2	29	20.0	39.13	46.05
Yamashita and Inoue (1975)	300	10	0.3	29	0.7	50.00	46.08
	300	10	0.5	29	0.7	44.10	43.40

Note: Air–water system was used by all investigators.

The ratio of wake volume to gas bubble volume is given by

$$\frac{\varepsilon_k}{\varepsilon_G} = k_A(\varepsilon_G, \varepsilon_S). \tag{190}$$

A gas balance yields

$$v_{sup} = v\varepsilon_G, \tag{191}$$

and a liquid balance gives

$$u_{sup} = \varepsilon_k v + (1 - \varepsilon_G - \varepsilon_k)\varepsilon_{lf} v_{lf}. \tag{192}$$

The velocity of the gas bubbles relative to the velocity of liquid in the particulate region is given by

$$v_s = v - v_{lf}. \tag{193}$$

The interstitial velocity of the liquid in particulate region can be represented by a Richardson–Zaki type equation, assuming uniform-sized solids:

$$v_{lf}\varepsilon_{lf} = aV_{S\infty}\varepsilon_{lf}^m. \tag{194}$$

Combining Eqs. (188)–(193), we get the bed voidage, ϵ,

$$\varepsilon = 1 - \varepsilon_S = \frac{u_{sup} - v_{sup}k_A}{v_{lf}} + \frac{v_{sup}(1 + k_A)}{v_{lf} + v_s}. \tag{195}$$

Combining equations (190)–(194), we get

$$(u_{sup} - v_{sup}k_A)\left(\frac{aV_{S\infty}}{v_{lf}}\right)^{\frac{1}{m-1}} = v_{lf} - \frac{V_G v_{lf}(k_A + 1)}{v_{lf} + v_s} \tag{196}$$

Equation (196) can be arranged to give v_{sup} explicitly:

$$v_{sup} = v_{sup}(v_{lf}, v_s, k_A, aV_{S\infty}, m, u_{sup}). \tag{197}$$

Substitution of Eq. (197) in Eq. (195) yields

$$\varepsilon = \varepsilon(v_{lf}, v_s, k_A, aV_{S\infty}, m, u_{sup}). \tag{198}$$

It was assumed that the wake volume to bubble volume ratio, k_A, is a known constant and v_s can be determined if the bubble size is specified. It was further assumed that v_{sup}, *a, m,* and $v_{s\infty}$ are fixed. (This assumption is tantamount to the assumption of starting with liquid-fluidized bed at t = 0, or with a bed of specified properties and degree of expansion.) With these assumptions, Eqs. (197) and (198) were simplified to

$$v_{sup} = f(v_{lf}) \tag{199}$$

and

$$\varepsilon = h(v_{\mathrm{lf}}). \tag{200}$$

Bhatia and Epstein (1974) proposed that bed contraction/expansion behavior can be predicted by evaluating $\partial\epsilon/\partial v_{\mathrm{sup}}$ at $v_{\mathrm{sup}} = 0$. This derivative was obtained by

$$\left.\frac{\partial \varepsilon}{\partial v_{\mathrm{sup}}}\right|_{v_{\mathrm{sup}}=0} = \left.\frac{\partial \varepsilon/\partial v_{\mathrm{lf}}}{\partial v_{\mathrm{sup}}/\partial v_{\mathrm{lf}}}\right|_{v_{\mathrm{sup}}=0}, \tag{201}$$

which gave

$$\left.\frac{\partial \varepsilon}{\partial v_{\mathrm{sup}}}\right|_{v_{\mathrm{sup}}=0} = \frac{(m/(m-1)+k_{\mathrm{A}})u - (1+k_{\mathrm{A}})u_{\mathrm{sup}} - (k_{\mathrm{A}}v_{\mathrm{s}}/(m-1))}{(m/(m-1))u(u-v_{\mathrm{s}})}, \tag{202}$$

where, for zero gas flow (i.e., $\varepsilon_{\mathrm{lf}} = \varepsilon_{\mathrm{L}}$ and $v_{\mathrm{lf}} = u_{\mathrm{sup}}$), Eq. (194) gives

$$u = \frac{u_{\mathrm{sup}}}{\varepsilon_{\mathrm{L}}} = (aV_{\mathrm{s}\infty})^{1/m} u_{\mathrm{sup}}^{(m-1)/m}. \tag{203}$$

The magnitude and the sign of the bed expansion on first introducing gas can be predicted by using LHS of Eq. (202), with the negative sign indicating contraction. If it is desired to predict qualitatively whether the expansion or contraction will occur, only the numerator in the RHS of Eq. (202), ϕA, needs to be considered, as the denominator is always positive:

$$\phi_{\mathrm{A}} = \left[\left(\frac{m}{m-1} + k_{\mathrm{A}}\right)\frac{1}{\varepsilon_{\mathrm{L}}} - (1+k_{\mathrm{A}})\right] u_{\mathrm{sup}} - \frac{k_{\mathrm{A}}v_{\mathrm{s}}}{m-1}. \tag{204}$$

The criterion of Eq. (202) is a simplified fluid dynamic description of three-phase fluidized beds capable of application over a wide range of conditions. They have also compared the predictions of Eq. (202) with their experimental data, showing a good agreement.

In Eq. (202) a value of $k_{\mathrm{A}} = 1$ was assumed as a first approximation. However, a better estimate of k_{A} for the case of negligible gas hold-up was obtained from

$$k_{\mathrm{A}} = 3.5(1 - \varepsilon_{\mathrm{s}})^3. \tag{205}$$

For the case of $k_{\mathrm{A}} = 0$, the numerator of Eq. (204) becomes

$$\phi_{\mathrm{A}} = \frac{m}{m-1}\frac{1}{\varepsilon_{\mathrm{L}}} - 1, \tag{206}$$

which is always positive for $m > 1$. In other words, Eq. (202) correctly predicts that, in the absence of bubble wakes, bed expansion will always occur when gas is introduced to a liquid fluidized bed.

1. Effect of Various Parameters.

It is instructive to analyze the qualitative criterion in terms of the numerator in Eq. (202), ϕ_A, to understand the effect of various parameters. Rearranging Eq. (204), we get,

$$\phi_A = k_A \left[u_{sup} \frac{1 - \varepsilon_L}{\varepsilon_L} - \frac{v_s}{m - 1} \right] + u_{sup} \left[\frac{m}{(m-1)\varepsilon_L} - 1 \right]. \qquad (207)$$

1. Equation (207) reveals that a high ratio of wake volume to bubble volume favors bed contraction.
2. Increase in the bubble velocity v_s favors bed contraction. At $v_{sup} = 0 = \varepsilon_G$, v_s represents the rise velocity of bubble in a stagnant liquid. Since the rise velocity of a single bubble increases with gas–liquid interfacial tension, it follows that any decrease in surface tension favors expansion. This effect of surface tension has been observed by, among others, Dakshinamurty *et al.* (1971) and Kim *et al.* (1975).
3. Increasing the liquid viscosity favors contraction. This follows from the fact that in Eq. (204), the coefficient of u_{sup} is always positive, and since the value of u_{sup} required to produce a fixed value of ϵ_L decreases with an increase in liquid viscosity, the value of ϕ_A decreases as the viscosity is increased. The contraction favoring behaviour of liquid viscosity has been observed by Bhatia and Epstein (1974) and Kim *et al.* (1975).
4. Increasing the solid particle size or density favors bed expansion. This effect was observed by Bhatia and Epstein (1974), Kim *et al.* (1975), and Nicklin (1962).

Darton and Harrison (1975) derived a criterion for the point of transition to predict whether a solid–liquid fluidized bed will expand or contract when the gas is first introduced. The definition of k_A used by Darton and Harrison was the ratio of upper clear (particle-free) wake volume to the bubble volume. But since they did not consider the circulation of solids associated with the lower nonclear portion of the wake, their k_A was effectively the same as that of Bhatia and Epstein (1974). The use of the Wallis drift flux approach by Darton and Harrison (1975) also represents no real difference from the relative velocity approach taken by Bhatia and Epstein (1974), since the two methods are rigorously interrelated. It is therefore not surprising that the final criteria of Bhatia and Epstein (1974) and Darton and Harrison (1975) are identical.

El-Temtamy and Epstein (1979) later found that the assumption of solids-free liquid wake behind the bubbles is tenable only for relatively coarse and/or heavy particles and becomes increasingly untenable for solids smaller than 1–2 mm, especially if the particle densities do not exceed 3000

kg/m_3. They rederived the criterion without the assumption of a solids-free wake. The rederived expression for ϕ_A together with the correction suggested by Jean and Fan (1987) is given as

$$\phi_A = \left[\frac{m}{m-1} + k_A\right] u - \left[(1+k_A)u_{sup} + \frac{k_A v_s}{m-1}\right] + \frac{\chi k_A (u+v_s)}{m-1} + \frac{m\chi(u_{sup}-u)k_A}{m-1} \tag{208}$$

where, χ denotes the ratio of solid hold-up in bubble wakes to the solid hold-up in the liquid fluidized region.

C. New Criterion for the Prediction of Contraction/Expansion

It was thought desirable to develop an alternative model for the prediction of contraction/expansion. The proposed model is based on the behavior of the particle settling velocity in solid–liquid and three-phase fluidization.

In the case of solid–liquid fluidized beds, the settling velocity of the particle is less than the terminal settling velocity. The hindered settling velocity is given by the well-known Richardson–Zaki equation,

$$u_{sup} = V_{S\infty}\varepsilon_L^m, \tag{209}$$

where m is a parameter that depends on the particle Reynolds number.

When the gas is introduced in the solid–liquid fluidized bed, the situation becomes more complex. The settling velocity in the presence of gas can either be higher or lower than the terminal settling velocity.

Imafuku *et al.* (1968) estimated the effective settling velocity of a particle in the presence of gas. They found that the settling velocity of the particles in the presence of gas was always larger than the hindered settling velocity. They attributed the increase in settling velocity in the presence of gas to the formation of aggregates. They proposed the correlation (for $1.3 < V_{S\infty} < 27.2$mm/s)

$$\frac{V_{GLS}}{V_{SL}} = 1.45 V_{S\infty}^{-0.35}, \tag{210}$$

where V_{SL} represents the settling velocity in the absence of a gas phase and V_{GLS} represents the settling velocity in the presence of gas.

Kato *et al.* (1972) have reported the following correlation:

$$V_{GLS} = 1.33 V_{S\infty}^{0.75} V_G^{0.25} \varepsilon_L^{2.5}. \tag{211}$$

Smith and Reuther (1985) also have given a correlation with a form similar to the correlation of Kato *et al.* (1972). However, the values of

exponents and constants are different. A careful analysis of the settling data reported by Kato *et al.* (1972) and Smith and Reuther (1985) indicates that V_{GLS} may be higher or lower than the terminal settling velocity. However, it was always higher than that in the absence of gas (only solid–liquid fluidized bed). We will try to use this information for prediction of contraction/expansion behavior.

Consider a solid–liquid fluidized bed in which the gas phase is introduced. From a stability viewpoint, there are three distinct possibilities regarding the stability of the bed before and after introducing the gas phase.

1. Homogeneous–heterogeneous. If the solid–liquid fluidized bed becomes heterogeneous after the introduction of gas, the settling velocity of the solids increases, and the bed tends to contract. The contracting tendency due to an increase in the settling velocity of solids is higher than the expanding tendency due to the additional gas hold-up, and contraction is observed. We have tested data of Epstein (1976) on three-phase fluidization, and the results are given in Table XII. In all the cases when the bed contraction was experimentally observed, the stability criterion for the solid–liquid fluidized beds given by Eq. (224) predicts that the initial solid–liquid bed was indeed in the homogeneous regime.

2. Heterogeneous–heterogeneous. On the other hand, if the bed is heterogeneous before as well as after the introduction of the gas phase, the settling velocity of solids does not change much and the additional hold-up of the gas phase causes bed expansion. This inference was also tested using the data of Epstein (1976). The stability criterion for the solid–liquid fluidized bed given by Eq. (20) does predict the initial heterogeneous regime, when the bed expansion was observed experimentally as shown in Table XII.

TABLE XII
PREDICTION OF CONTRACTION/EXPANSION BEHAVIOR IN THREE-PHASE FLUIDIZED BEDS

No.	System	d_P (mm)	ρ_S (kg/m^3)	$\mu_L \times 10^5$ (Pas)	Observed behavior	Predicted behavior
1	Water–glass beads	1.08	2824	80	Contraction	Contraction
2	Aqueous glycerol–glass beads	1.08	2824	210	Contraction	Contraction
3	Water–sieved sand	0.458	2578	80	Contraction	Contraction
4	Water–glass beads	0.273	2938	80	Contraction	Contraction
5	Water–glass beads	0.456	2935	80	Contraction	Contraction
6	Water–glass beads	1.08	2824	80	Contraction	Contraction
7	Water–glass beads	1.08	2949	80	Contraction	Contraction
8	Water–lead shots	2.18	11030	80	Expansion	Expansion
9	Aqueous PEG–glass balls	3.18	7756	6300	Contraction	Contraction
10	Water–glass beads	1.08	2824	6300	Expansion	Expansion

3. Homogeneous–homogeneous. If the solid–liquid bed remains homogeneous after introduction of the gas phase, the settling velocity of the solids does not change much. However, the additional gas phase hold-up should cause the expansion of the bed. This case can be observed if the experiments are performed with sufficiently high sparger resistance that the sparger-related disturbances themselves do not induce heterogeneity. In order to check the validity of this case, experimental data are needed.

Joshi (1983) used a simpler form of this model for the prediction of contraction/expansion in three-phase fluidized beds.

IX. Conclusions

1. Jackson and co-workers, Wallis, Homsy, and co-workers, Gibilaro, Foscolo and co-workers, Rietema and co-workers, and Batchelor have made pioneering contributions to the analysis of transition in fluidized beds.
2. A unified approach has been developed for the prediction of transition in multiphase reactors such as gas–liquid bubble columns, liquid–liquid spray columns, solid–liquid fluidized beds, gas–solid fluidized beds, and three-phase fluidized beds.
3. The role of sparger (distributor) design on the transition has been brought out. When the sparger resistance is small, the bed can be considered as unbounded. The bed is considered bounded at high sparger resistance. For both these cases, transition criteria have been developed using the theory of linear stability. Clear physical significance has been attributed to all the terms in the transition criteria. A comparison between the predictions for unbounded and bounded beds has been presented.
4. All the published literature has been critically reviewed. The reported criteria have been classified into (a) fundamental and (b) heuristic approaches. An attempt has been made to establish a relationship between the fundamental approach and the heuristic approach. It has been shown that the criterion based on the heuristic approach can be considered as a special case of the generalized criterion based on the fundamental approach.
5. Parametric sensitivity of the criteria has been presented in the form of stability maps. The particle phase dispersion coefficient has been shown to be the most important parameter governing the stability. It has also been shown that the stability maps can be conveniently and advantageously drawn in terms of particle Reynolds number.
6. All the published data on transition for solid–liquid fluidized beds, gas–solid fluidized beds, three-phase fluidized beds, and gas–liquid

bubble columns have been compared with the predictions of the criteria. Reasonably good agreement has been shown in all the cases. A stepwise procedure has been presented for the use of criteria based on unbounded and bounded beds.

7. The phenomenon of expansion/contraction in three-phase fluidized beds was analyzed. A brief review of literature has been presented. Epstein and co-workers have made outstanding contributions in this area. An alternative method has been presented. A favorable comparison between the model predictions and the experimental observations was observed.

X. Suggestions for Future Work

1. The most important parameter governing stability is the dispersion coefficient of the dispersed phase such as bubbles, drops, and particles. The published information is not sufficient. A comprehensive research program is needed for the measurement of dispersion in all multiphase reactors over a wide range of terminal velocities, column diameters, column heights, sparger designs, phase velocities, and continuous-phase physical properties.
2. It will be useful to develop an understanding of the relationship between turbulent flow field and dispersion. Measurement techniques need to be developed for the measurement of turbulent flows in multiphase systems. The relationship between eddy diffusion and the dispersion coefficient needs to be brought out over a wide range of particle sizes, settling velocities, column diameters, column heights, phase velocities, and physical properties.
3. The debate pertaining to the definition of buoyancy force is given in Appendix B. A systematic experimental program is still needed in this area.
4. Homsy and co-workers and Gibilaro, Foscolo, and co-workers have proposed neat methods for the experimental measurement of transition. The techniques of measurement of dynamic pressure and dynamic measurement of bed heights will prove to be extremely useful in understanding the hydrodynamics of multiphase systems. The measurements will also be useful for understanding other transport phenomena.
5. Additional experimental information is needed from liquid–liquid spray columns, liquid–gas spray columns, solid–gas transport reactors, and three-phase fluidized beds.

APPENDIX A: MODELING OF CORRELATION OF FLUCTUATING PRESSURE AND HOLD-UP

The equation of motion for a single phase is written as

$$\frac{\partial u_i}{\partial t} + u_j \frac{\partial u_i}{\partial x_j} = -\frac{1}{\rho}\frac{\partial p}{\partial x_i} + \frac{\mu}{\rho}\nabla^2 u + gh. \tag{212}$$

To derive the pressure interaction correlation, we neglect viscous effects and write the time-averaged momentum equation as

$$\frac{\partial \bar{u}_i}{\partial t} + \bar{u}_j \frac{\partial \bar{u}_i}{\partial x_j} = -\frac{1}{\rho}\frac{\partial \bar{p}}{\partial x_i} + gh - \frac{\partial \overline{u_i' u_j'}}{\partial x_j}. \tag{213}$$

Now subtracting Eq. (212) from Eq. (213) we get the equation of motion in terms of fluctuating components:

$$u_j' \frac{\partial \bar{u}_i}{\partial x_j} + \bar{u}_j \frac{\partial u_i'}{\partial x_j} - \frac{\partial}{\partial x_j}(u_i' u_j' - \overline{u_i' u_j'}) = -\frac{1}{\rho}\frac{\partial p'}{\partial x_i}. \tag{214}$$

We can get the correlation of fluctuating pressure and hold-up by taking the product of Eq. (214) with ε' and then time averaging the equation so obtained:

$$\overline{\varepsilon' u_j'} \frac{\partial \bar{u}_i}{\partial x_j} + \bar{u}_j \frac{\partial \overline{\varepsilon' u_i'}}{\partial x_j} - \frac{\partial \overline{\varepsilon' u_i' u_j'}}{\partial x_j} = -\frac{1}{\rho}\frac{\partial \overline{\varepsilon' p'}}{\partial x_i}. \tag{215}$$

Therefore, the pressure correlation term can be obtained by neglecting the triple product of the fluctuations:

$$\frac{\partial \overline{\varepsilon' p'}}{\partial x_i} = -\rho\left[\overline{\varepsilon' u_j'} \frac{\partial \bar{u}_i}{\partial x_j} + \bar{u}_j \frac{\partial \overline{\varepsilon' u_i'}}{\partial x_j}\right]. \tag{216}$$

Using this equation, we can write

$$\frac{\partial \overline{\varepsilon_S' p'}}{\partial z} = -\rho\left[\overline{\varepsilon_S' v_z'} \frac{\partial \bar{v}_z}{\partial z} + \overline{\varepsilon_S' v_x'} \frac{\partial \bar{v}_z}{\partial x} + \bar{v}_z \frac{\partial \overline{\varepsilon_S' v_z'}}{\partial z} + \bar{v}_x \frac{\partial \overline{\varepsilon_S' v_z'}}{\partial x}\right]. \tag{217}$$

APPENDIX B: FORCES ACTING ON A PARTICLE IN A FLUIDIZED BED

For a single particle in an infinite fluid medium, the buoyancy force was defined by Archimedes and is given by

$$F_B = v_P \rho g, \tag{218}$$

where v_p is the particle volume and ρ is the fluid density. This definition of buoyancy force for a single particle is well established. However, for multiparticle systems (such as fluidized beds), there has been a vigorous debate regarding the formulation of buoyancy force. Epstein (1984), Joshi (1983, 1984), Clift *et al.* (1987), Fan *et al.* (1987), Grbavcic *et al.* (1992), and Clift (1993) have defined the buoyancy force similarly to Eq. (218). It is given by

$$F_B = v_P \rho g. \tag{219}$$

In contrast, Richardson and Meikle (1961), Barnea and Mizrahi (1973), Rietema (1982), Rowe (1984), Foscolo *et al.* (1984), and Gibilaro *et al.* (1987a, 1987b) have defined the buoyancy force on the basis of average suspension density ($\bar{\rho}$) and

$$F_B = v_P \bar{\rho} g, \tag{220}$$

where

$$\bar{\rho} = \varepsilon\rho + (1 - \varepsilon)\rho_S. \tag{221}$$

$\bar{\rho}$ is the average density of the suspension and ε is the volume fraction of the continuous phase fluid in the bed.

Though there has been a difference of opinion regarding the definition of buoyancy force, there is no disagreement on the definition of gravitational force on a bed particle in a fluidized bed, which is given as $v_p \rho_s g$, where ρ_s is the particle density. However, when this force is equated with the sum of the buoyancy force and fluid dynamic drag force, the buoyancy question affects the magnitude of the drag portion of the gravitational force, since

$$v_P \rho_S g = v_P \rho g + (\rho_S - \rho) v_P g, \tag{222}$$

or

$$v_P \rho_S g = v_P \bar{\rho} g + (\rho_S - \bar{\rho}) v_P g. \tag{223}$$

For an isolated particle i.e., $\varepsilon \to 1$, Eq. (223) reduces to Eq. (222). The buoyancy term represents the net force arising from the pressure distribution over the surface of the particle with the fluid at rest. The drag term represents the additional force exerted on the particle by a flowing fluid. Drag gives rise to mechanical energy dissipation.

Energy Dissipation

Consider the case of a particle settling in an infinite liquid medium with a terminal velocity $v_{S\infty}$. The rate of decrease of potential energy is given by

$$e_t = (\rho_S - \rho_L) v_P g \frac{dh}{dt} \tag{224}$$

$$= (\rho_S - \rho_L) v_P g V_{S\infty}. \tag{225}$$

The rate of energy dissipation at the solid–liquid interface is also given by this equation. As the particle settles, the equivalent volume of the liquid rises so that the potential energy of the particle at any height h is equal to $(\rho_s - \rho_L) v_p gh$. Since the medium is infinite, the rising superficial liquid velocity is negligible as compared with $v_{S\infty}$.

Now consider the case of particulate fluidized bed. Though the particles in the bed are moving randomly, there is no net displacement and the particles can be considered stationary with respect to the column wall. The superficial velocity is u_{sup} and the interstitial velocity is

$$v_s = u_{sup}/\varepsilon. \tag{226}$$

It is important to know whether the energy dissipation at the solid–liquid interface is $F_D u_{sup}$ or $F_D v_s$.

Let us write the energy balance for the two situations of a falling bed and a stationary bed, respectively. These are shown in Fig. 49A and 49B, respectively. In the first case, the liquid phase is stationary, the support plate is absent, and the bed falls. The second case is the usual solid–liquid fluidized bed where the particle phase is stationary and the liquid moves upward and supports the solid phase. In the case of stationary fluid (Fig. 49A), let the bed level be at an elevation h from a certain reference level. At time t, let the falling bed reach the reference level. The change in potential energy of the bed is

$$E_P = V_P \rho_S g h, \tag{227}$$

where V_p is the total volume of solid phase.

As the bed falls, the equivalent volume of the liquid rises and the gain in potential energy of liquid is

$$E_L = V_P \rho_L g h. \tag{228}$$

The net energy dissipated during the fall of the bed is

$$E_P - E_L = V_P (\rho_S - \rho_L) g h, \tag{229}$$

and the energy dissipation rate is

$$E_D = V_P (\rho_S - \rho_L) g \frac{dh}{dt}. \tag{230}$$

The bed falls at the rate dh/dt.

Now, consider the usual case of Fig. 49B. The energy input rate to the fluidized bed is given by

$$E_i = \frac{\pi}{4} D^2 u_{sup} H (\varepsilon_S \rho_S + \varepsilon_L \rho_L) g, \tag{231}$$

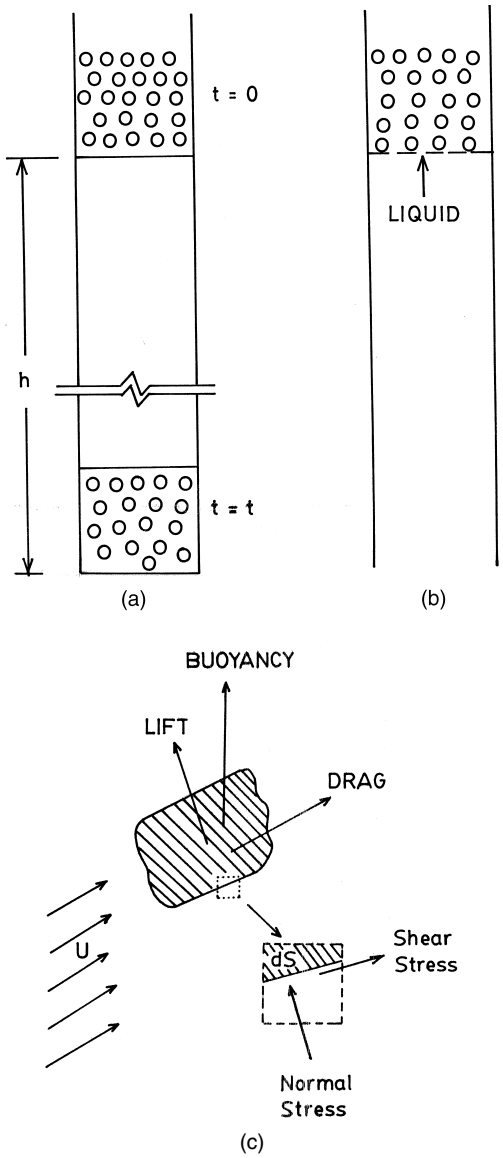

FIG. 49. (a) Falling bed (liquid phase is stationary). (b) Stationary bed (solid–liquid fluidized bed). (c) Particle in a flowing fluid.

where D and H are the diameter and height of the fluidized bed, respectively. At height H, the liquid phase gains potential energy at a rate given by

$$E_L = \frac{\pi}{4} D^2 u_{sup} H \rho_L g. \tag{232}$$

The net energy dissipation rate is

$$\begin{aligned} E_D &= \frac{\pi}{4} D^2 u_{sup} H \varepsilon_S (\rho_S - \rho_L) g \\ &= V_P u_{sup} (\rho_S - \rho_L) g. \end{aligned} \tag{233}$$

If the two situations of stationary fluid and rising fluid are to be equivalent, dh/dt must equal the superficial liquid velocity. Therefore, if F_D is the drag force on the solid phase, the energy dissipation rate is given by

$$E_D = F_D u_{sup}. \tag{234}$$

Substitution of Eqs. (234) in (233) gives

$$F_D = V_P (\rho_S - \rho_L) g. \tag{235}$$

For a single particle,

$$e = v_P (\rho_S - \rho_L) g u_{sup} \tag{236}$$

$$= F_d u_{sup}. \tag{237}$$

From Eqs. (236) and (237),

$$F_d = v_P (\rho_S - \rho_L) g. \tag{238}$$

Equations (236) and (238) represent the energy and the force balance for a single particle. The following additional discussion may be useful.

Consider the case of Fig. 49A. The bed descends with a velocity dh/dt equal to u_{sup}. Because of the fall of the bed, the equivalent amount of liquid rises and the generated liquid velocity on the superficial basis is given by

$$\begin{aligned} U^* &= \frac{\pi}{4} D^2 (1 - \varepsilon_L) u_{sup} \Big/ \frac{\pi}{4} D^2 \varepsilon_L \\ &= \frac{1 - \varepsilon_L}{\varepsilon_L} u_{sup}. \end{aligned} \tag{239}$$

The relative velocity between the particle and fluid is

$$\begin{aligned} u_{sup} + U^* &= u_{sup} + \frac{1 - \varepsilon_L}{\varepsilon_L} u_{sup} \\ &= \frac{u_{sup}}{\varepsilon_L}. \end{aligned} \tag{240}$$

It may be pointed out that the rising fluid gains potential energy at a rate given by

$$\frac{\pi}{4} D^2 U^* g h \rho_L, \tag{241}$$

where h is the position of the bed at any time. Thus, the velocity U^* is responsible for increasing the potential energy of liquid phase and is not available for doing work on the solid particles, and the energy dissipation rate is governed by u_{sup} and not v_s.

However, Gibilaro *et al.* (1987) defined the energy balance on the basis of v_s:

$$E_D = V_P(\rho_S - \rho_L) g v_s. \tag{242}$$

Therefore,

$$\begin{aligned} F_D &= V_P[(\rho_S - (\varepsilon_S \rho_S + \varepsilon_L \rho_L)] g \\ &= V_P(\rho_S - \bar{\rho}) g. \end{aligned} \tag{243}$$

From the foregoing discussion, it can be said that the buoyancy force is decided by the fluid density and not the suspension density.

In order to understand the formulation of buoyancy force and hence the drag force, Grbavcic *et al.* (1992) did ingenious experiments. They started with the following formulation:

$$\rho_s = \rho^* + \frac{3}{4} \frac{\rho_L C_D(\varepsilon_L)}{d_S g} v_s^2. \tag{244}$$

Grbavcic *et al.* (1992) used equation (244) for finding the value of ρ^*. The experimental plan consisted of the measurement of slip velocity (v_s) over a wide range of ρ_s. A plot of ρ_s vs v_s^2 gave the value of ρ^*. For this purpose, ε_L, $C_D(\varepsilon_L)$, and d_S were held constant. In a typical experiment (say, particle size 1.2 mm), the desired value of ε_L was obtained by adjusting the superficial liquid velocity. In such a bed, the slip velocities of 10- and 19.5- mm particles were measured over a wide range of solid phase density (324–8320 kg/m^3), and a plot of ρ_s vs. v_s^2 was constructed. Several such plots were obtained by varying ε_L. They found that ρ^* equals ρ_L when the diameter of sedimenting (or rising) particle was less than 3.36 times the particle diameter in a fluidized bed. Above this particle size, ρ^* was found to be equal to $\bar{\rho}$. Therefore, it may be concluded that the buoyancy force for any particle in the bed (the sizes of all the particles are within a range) is decided by the fluid density and not the suspension density.

Pressure Gradients

Gibilaro *et al.* (1987a, 1987b) proposed that the buoyancy force can be obtained by integrating the pressure gradients, irrespective of the source

and direction of pressure gradient. Thus,

$$F_B = v_P \frac{\partial p}{\partial z} \tag{245}$$

and

$$F_d = v_P \left(\rho_S g - \frac{\partial p}{\partial z} \right). \tag{246}$$

Joshi (1987) and Clift (1993) have addressed this point in detail. Clift (1993) has provided the following systematic derivation. Consider a particle of arbitrary shape that is stationary in a fluid approaching with velocity u_{sup}, where the fluid velocity need not be in the vertical direction (Fig. 49C). At any point on the surface of the particle, the fluid exerts a normal stress σ and shear stress τ_s. The force obtained by integrating τ over the surface of the particle is the skin friction, and the component of this force parallel to u_{sup} is the skin friction drag. There is no argument over the formulation of τ and hence skin friction.

The buoyancy argument centers on σ. Integrating σ over the surface gives another force including both buoyancy and form drag, and the argument concerns the division between these two.

Taking the simple case of an incompressible Newtonian fluid, the fluid motion is described by the Navier–Stokes equation:

$$\rho \frac{Du}{Dt} = \rho g - \nabla p + \mu \nabla^2 u. \tag{247}$$

Equation (247) has a directionality introduced by the body force. To remove this directionality, it is common to introduce the modified or reduced pressure, p, where

$$p = p_o + \rho g \mathbf{x} + P_r \tag{248}$$

where $\mathbf{x}$ is the position vector and p_o a reference pressure. The difference between P_r and p is the hydrostatic pressure. Integrating the hydrostatic component of σ over the surface of the particle always gives the simple Archimedean buoyancy, which always acts in the vertical direction.

In terms of the reduced pressure, Eq. (248) becomes

$$\rho \frac{Du}{Dt} = -\nabla P_r + \mu \nabla^2 u. \tag{249}$$

Integrating the component of σ arising from the modified pressure, p, gives a force, additional to skin friction, arising from the fluid motion. The component of this force parallel to u is called the form drag.

From the foregoing discussion, it can be seen that, for a fluidized bed, some part of $\partial p/\partial z$ or $\bar{\rho} g$ contributes to form drag. When the form drag is subtracted from $\bar{\rho} g$, we get $\rho_L g$ and the buoyancy force is given by $v_p \rho_L g$.

Nomenclature

a	Wall effect factor (194)
A	Constant defined by (22a)
A_1	Parameter defined by (131)
A_S	Area, m^2
B	Parameter of the stability criterion
B_0	Dimensionless interaction parameter at steady state [Eq. (110)]
B_0'	Parameter defined in (111)
C	Parameter of the stability criterion
C_1	Constant defined in Eq. (141)
C_2	Constant defined in Eq. (141)
C_3	Constant defined in Eq. (144)
C_4	Constant defined in Eq. (144)
C_5	Parameter defined by (132)
C_{hole}	Orifice coefficient
$C_{D\infty}$	Drag coefficient under terminal rise conditions
C_D	Drag coefficient in presence of other bubbles
C_D'	Dimensional drag coefficient, $kg/m^3 s$ or $N \cdot s/m^4$
C_V	Virtual mass coefficient
d	Width of two dimensional column, m
d_B	Dimensionless bubble diameter defined by (70)
$\hat{d}_B$	Bubble diameter, m
d_0	Orifice diameter
d_P	Particle diameter, m
d_{PL}	Lower limit of critical particle diameter, m
d_{PU}	Upper limit of critical particle diameter, m
D	Coefficient of dispersion, m^2/s
$\hat{D}$	Dimensionless coefficient of dispersion
D_e	Difference in dimensionless dispersion coefficients of the gas and liquid phases
e	Energy dissipation rate for a single particle
e_t	Rate of decrease of potential energy of a single particle, J/s
E	Parameter of the stability criterion
E_1	Parameter defined by (127)
E^*	Mean elasticity modulus of the bed
E_D	Energy dissipation rate, J/s
E_i	Energy input rate, J/s
E_L	Potential energy for the liquid, J
E_o	Energy output rate, J/s
E_P	Potential energy for a swarm of particles, J
E_s	Elasticity modulus of the bed material
f_1	Interaction force per unit volume term defined by (10), N/m^3

f_x	x component of interaction force per unit volume, N/m^3 function defined by equation (25) which determines stability
f_z	z component of interaction force per unit volume, N/m^3
$f_{z\mathrm{d}}$	Drag part of interaction force per unit volume, N/m^3
f_{zv}	Virtual mass part of interaction force per unit volume, N/m^3
F	Parameter of the stability criterion
F_1	Parameter defined by equation (129)
F_B	Buoyancy force, N/m^2
F_d	Drag force on a particle in fluidized bed, N/m^2
$F_{\mathrm{d}\infty}$	Drag force on a particle in an infinite medium, N/m^2
F_D	Drag force on the solid phase (all the particles put together)
Fr	Froude number
g	Acceleration due to gravity, m/s^2
$\hat{g}$	Dimensionless acceleration due to gravity [equation (100)]
G	Parameter of the stability criterion
Ga	Galileo number defined in Eq. (82)
h	Height of the column, m
H	Dimensionless height of bubble column
I	Parameter of the stability criterion
J	The drift velocity, m/s
k	Separation constant in (166)
k_A	Ratio of wake volume to bubble volume
k_T	Constant in pressure drop–velocity relationship, Eq. (101)
k_TL	Constant in pressure drop–velocity relationship, Eq. (102)
k_V	Constant in pressure drop–velocity relationship, Eq. (101)
k_VL	Constant in pressure drop–velocity relationship, Eq. (102)
K_0	Proportionality constant in Eq. (31)
K_T	Dimensionless constant defined in Eq. (103)
K_V	Dimensionless constant defined in Eq. (103)
K_TL	Dimensionless constant defined in Eq. (103)
K_VL	Dimensionless constant defined in Eq. (103)
l	Length scale of turbulence, m
L	Width of two-dimensional bubble column, m
m	Richardson–Zaki index
m_P	Poisson ratio of the bed material
M_1	Parameter defined in (152)
M_2	Parameter defined in (156)
M_3	Parameter defined in (153)
M_4	Parameter defined in (154)
N_1	Parameter defined in Table VIII
N_2	Parameter defined in Table VIII
N_3	Parameter defined in Table VIII
N_m	LHS of the stability criterion
N_s	Number of particles

p	Instantaneous pressure, N/m^2
$\bar{p}$	Time-averaged pressure, N/m^2
p'	Fluctuating pressure, N/m^2
p'_s	Particle phase pressure in (26), N/m^2
P_{atm}	Atmospheric pressure, N/m^2
P	Dimensionless pressure
P_0	Dimensionless pressure at steady state
P_r	Reduced pressure, Pa
Q	Term defined in (134)
r_0	Characteristic dimension of bubble or particle, m
r_c	Radius of curvature, m
R	Ratio of the orifice area to the column area
Re	Reynolds number
Re_B	Reynolds number of a bubble
Re_p	Particle Reynolds number
s	Growth rate constant in time, s
S	Term defined in (134)
t	Time, s
$\hat{t}$	Dimensionless time
u	Liquid phase (or continuous phase) velocity, m/s
u_0	Steady-state continuous phase velocity, m/s
u_1	Perturbation in steady-state continuous phase velocity, m/s
u_e	Elastic wave velocity, m/s
u_ε	Voidage propagation velocity, m/s
u_{sup}	Superficial velocity of the continuous phase, m/s
u_x	Instantaneous value of X component of the continuous phase velocity, m/s
$\bar{u}_x$	Time-averaged value of X component of the velocity of the continuous phase, m/s
u'_x	Fluctuating value of X component of the continuous phase velocity, m/s
u_z	Instantaneous value of Z component of the continuous phase velocity, m/s
$\bar{u}_z$	Time-averaged value of Z component of the velocity of the continuous phase, m/s
u'_z	Fluctuating value of Z component of the continuous phase velocity, m/s
U	Dimensionless liquid phase (or continuous phase) velocity
$\bar{U}$	Dimensionless liquid phase velocity averaged in y-direction
U_D	Downward liquid velocity, m/s
U_x	Dimensionless liquid phase velocity in x-direction
U_z	Dimensionless liquid phase velocity in z-direction
v	Gas (dispersed phase) velocity, m/s

v_0 Steady-state dispersed phase velocity, m/s
v_1 Perturbation in steady-state dispersed phase velocity, m/s
v_P Particle volume, m^3
v_s Slip velocity, m/s
v_{lf} Velocity in the wake region, m/s
v_{sup} Superficial velocity of the dispersed phase, m/s
v_x Instantaneous value of X component of the dispersed phase velocity, m/s
$\bar{v}_x$ Time-averaged value of X component of the velocity of the dispersed phase, m/s
v'_x Fluctuating value of X component of the dispersed phase velocity, m/s
v_z Instantaneous value of Z component of the dispersed phase velocity, m/s
$\bar{v}_z$ Time-averaged value of Z component of the velocity of the dispersed phase, m/s
v'_z Fluctuating value of Z component of the dispersed phase velocity, m/s
V Dimensionless velocity
$\bar{V}$ Dimensionless gas phase velocity averaged in y-direction
$V_{B\infty}$ Terminal bubble rise velocity, m/s
V_G Superficial gas velocity, m/s
V_{GC} Critical superficial gas velocity at transition
V_{GLS} Settling velocity in presence of the gas phase, m/s
V_{mf} Minimum fluidization velocity, m/s
V_p Volume of the solid phase, m^3
V_S Dimensionless slip velocity, v_s/V_{B00} or v_s/V_{S00}
V_{S0} Value of V_S at steady state
V'_S $\partial V_S/\partial \varepsilon_G$
$V_{S\infty}$ Terminal settling velocity, m/s
V_{SL} Settling velocity in absence of the gas phase, m/s
V_x Dimensionless gas phase velocity in x-direction
V_z Dimensionless gas phase velocity in z-direction
W_e Effective weight, kg
W Dimensionless component of axial liquid velocity, w/V_{B00}
w Component of true axial liquid velocity, m/s
w_G Average linear velocity of the gas phase, m/s
w_L Average linear velocity of the liquid phase, m/s
x Coordinate
X Dimensionless x coordinate
y Coordinate
Y Dimensionless y coordinate
z Axial coordinate
Z Parameter of the stability criterion

Greek Symbols

α	Proportionality constant for dispersion
α'	A parameter defined in (179)
β	Two-phase interaction term, kg/m$^3\cdot$s
β_1'	A parameter defined in (180)
δ	Characteristic dimension of pore space, m
δ_τ	Ratio of distance between particles to particle diameter
Δh	Change in the height
Δt	Change in the time
Δu_{sup}	Change in superficial velocity of continuous phase
σ	Surface tension
σ_0	Defined in Eq. (72)
γ	Dimensionless gas throughput
γ_{G}	Dimensionless gas throughput
Γ	Interfacial energy
ε	Phase hold-up, dimensionless
ε_{c}	Continuous phase hold-up, dimensionless
ε_{G}	Instantaneous gas phase hold-up
$\bar{\varepsilon}_{\text{G}}$	Time-averaged gas phase hold-up
ε_{G}'	Fluctuating gas phase hold-up
ε_{GA}	Gas hold-up after suddenly reducing the gas flowrate
ε_{GB}	Gas hold-up before suddenly reducing the gas flowrate
ε_{GC}	Critical gas hold-up at which transition occurs
ε_K	Hold-up in the wake region
ε_{L}	Instanataneous liquid phase hold-up
$\bar{\varepsilon}_{\text{L}}$	Time-averaged liquid phase hold-up
ε_{L}'	Fluctuating liquid phase hold-up
ε_{lf}	Average liquid hold-up in the wake region
ε_{L0}	Steady-state liquid hold-up
ε_{L1}	Perturbation in steady-state liquid hold-up
ε_{LC}	Critical liquid hold-up at which transition occurs
ε_{S}	Instantaneous solid phase hold-up
$\bar{\varepsilon}_{\text{S}}$	Time-averaged solid phase hold-up
ε_{S}'	Fluctuating solid phase hold-up
ε_{SC}	Critical solid hold-up
ϕ	Defined in Eq (163)
ϕ_{A}	Defined in Eq. (204)
η	Averaging parameter defined in Eq. (123)
ψ	Stream function
λ	Separation constant, Eq. (140)
μ	Viscosity, kg/m s
μ_C	Viscosity of the continuous phase, kg/m s
ν_L	Molecular kinematic viscosity of the liquid, m^2/s
ν_t	Turbulent kinematic viscosity, m^2/s

ν_0 Mobility in Eq. (31)
ρ Density, kg/m^3
$\bar{\rho}$ Average density of two-phase dispersion, kg/m^3
ρ_C Density of continuous phase,kg/m^3
ρ_D Density of dispersed phase, kg/m^3
ρ_f Density of the fluid, kg/m^3
τ Dimensionless time
τ_S Shear stress
$\tau_{S,xx}$ Normal stress in solid phase, N/m^2
$\tau_{S,zz}$ Shear stress in solid phase, N/m^2
χ Ratio of solid hold-up in bubble wakes to that in liquid fluidization, in equation (208)
ζ Parameter defined in Eq. (68)
ξ Proportionality constant in Eq. (12)

Subscripts

0 Initial steady state
1 Perturbation
G Gas phase
L Liquid phase
max Maximum
sup Superficial
S Solid phase

ACKNOWLEDGMENT

The research work was supported by a grant under the Indo-U.S. Collaborative Research Program (DST/INT/USHRF/336/92). Authors express sincere thanks to Professor M. C. Jones for several valuable suggestions.

REFERENCES

Abdel-Ghani, M., Petrie, J. G., Seville, J. P. K., Clift, R., and Adams, J. *Powder Tech.* **65,** 113 (1991).
Adlington, D., and Thompson, E. *in* "Proc. Third European Symp. Chem. React. Eng.," 203 (1965).
Agarwal, G. P., Hudson, J. L., and Jackson, R. *Ind. Eng. Chem. Fundamentals* **19,** 59 (1980).
Anderson, T. B., and Jackson, R. *Ind. Eng. Chem. Fundamentals* **6,** 478 (1967a).
Anderson, T. B., and Jackson, R. *Ind. Eng. Chem. Fundamentals* **6,** 527 (1967b).
Anderson, T. B., and Jackson, R. *Ind. Eng. Chem. Fundamentals* **7,** 12 (1968).
Anderson, T. B., and Jackson, R. *Ind. Eng. Chem. Fundamentals* **8,** 137 (1969).
Astarita, G. *Chem. Eng. Sci.* **48,** 3438 (1993).
Bach, H. F., and Pilhofer, T. *Ger. Chem. Eng.* **1,** 278 (1978).

Barnea, E., and Mizrahi, J. *Chem. Eng. J.* **5,** 171 (1973).
Batchelor, G. K. *J. Fluid Mech.* **193,** 75 (1988).
Bhatia, V. K., and Epstein, N. *in* "Proc. Int. Conf. on Fluidization and Its Applications," 380, Toulouse (1974).
Biesheuvel, A., and Gorrisen, W. C. M. *Int. J. Multiphase Flow* **16,** 211 (1990).
Buchholz, R., Tsepetonides, J., Steinmann J., and Onken, U. *Ger. Chem. Eng.* **6,** 105 (1983).
Chisti, M. Y. "Airlift Bioreactors." Elsevier, New York, 1989.
Clift, R. *A. I. Ch. E. Symp. Ser.* **89,** 1 (1993).
Clift, R., Grace, J. R., and Weber, M. E. "Bubbles, Drops, and Particles." Academic Press, New York, 1978.
Clift, R., Seville, J. P. K., Moore, S. C., and Chavarie, C. *Chem. Eng. Sci.* **42,** 191 (1987).
Cook, T. L., and Harlow, F. H., *Int. J. Multiphase Flow,* **12,** 35 (1986).
Dakshinamurty, P., Subramhanyam, V., and Rao, J. N. *Ind. Eng. Chem. Proc. Des. Dev.* **11,** 151 (1971).
Darton, R. C., and Harrison, D. *Chem. Eng. Sci.* **30,** 581 (1975).
Davidson, J. F., and Harrison, D. *Chem. Eng. Sci.* **21,** 731 (1966).
Davies, R. M., and Taylor, Sir G. I. *Proc. Roy. Soc.* **A200,** 375 (1950).
Deckwer, W. D., Allenbach, U., and Bretschneider, H. *Chem. Eng. Sci.* **32,** 43 (1977).
Didwania, A. K., and Homsy, G. M. *Int. J. Multiphase Flow* **7,** 563 (1981a).
Didwania, A. K., and Homsy, G. M. *Ind. Eng. Chem. Fundamentals* **20,** 318 (1981b).
Didwania, A. K., and Homsy, G. M. *J. Fluid Mech.* **122,** 433 (1982).
Dorgelo, E. A. H., Van Der Meer, A. P., and Wesseslingh, J. A. *Chem. Eng. Sci.* **40,** 2150 (1985).
Drew, D., Cheng, L., and Lahey, R. T. *Int. J. Multiphase Flow* **5,** 233 (1979).
Elgobashi, S. E., and Abou-Arab, T. W. *Phys. Fluids* **26,** 931 (1983).
El-Kaissy, M. M., and Homsy, G. M. *Int. J. Multiphase Flow* **2,** 379 (1976).
El-Temtamy S. A., and Epstein, N. *Int. J. Multiphase Flow* **4,** 19 (1978).
El-Temtamy, S. A., and Epstein, N. *Can. J. Chem. Eng.* **57,** 520 (1979).
Epstein, N. *Can. J. Chem. Eng.* **54,** 259 (1976).
Epstein, N. *Chem. Eng. Sci.* **39,** 1533 (1984).
Epstein, N. and Nicks, D. *in* "Fluidization Technology," Vol. I (D. L. Keairns, Ed.). Hemisphere, Washington, D. C., 1976.
Ergun, S. *Chem. Eng. Progr.* **48,** 89 (1952).
Fan, L. S., Han, L. S. and Brodkey, R. S. *Chem. Eng. Sci.* **42,** 1269 (1987).
Foscolo, P. U., and Gibilaro, L. G. *Chem. Eng. Sci.* **39,** 1667 (1984).
Gaudin, A. M. *in* "Flotation," 2nd ed. McGraw-Hill, New York, 1977.
Gibilaro, L. G., Waldram, S. P., and Foscolo, P. U. *Chem. Eng. Sci.* **39,** 607 (1984).
Gibilaro, L. G., Hossain, I., and Foscolo, P. U. *Can J. Chem. Eng.* **64,** 93 (1986).
Gibilaro, L. G., Di Felice, R., Waldram, S. P., and Foscolo, P. U. *Chem. Eng. Sci.* **42,** 194 (1987a).
Gibilaro, L. G., Di Felice, R., Foscolo, P. U., and Waldram, S. P. *Chem. Eng. Sci.* **42,** 1272 (1987b).
Gibilaro, L. G., Di Felice, R., Hossain, I., and Foscolo, P. U. *Chem. Eng. Sci.* **44,** 101 (1989).
Gibilaro, L. G., Di Felice, R., and Foscolo, P. U. *Chem. Eng. Sci.* **45,** 1561 (1990).
Grbavcic, Z. B., Vukovic, D. V., Jovanovic, S. D. J., and Littman, H. *Chem. Eng. Sci.* **47,** 2120 (1992).
Green, D., and Homsy, G. M. *Int. J. Multiphase Flow* **13,** 447 (1987a).
Green, D., and Homsy, G. M. *Int. J. Multiphase Flow* **13,** 459 (1987b).
Ham, J. M., Thomas, S., Guazzelli, E., Homsy, G. M., and Anselmet, M. C. *Int. J. Multiphase Flow* **16,** 171 (1990).
Handley, D., Doraiswami, A., Butcher, K. L., and Franklin, N. L. *Trans. Inst. Chem. Engr.* **44,** T266 (1966).
Homsy, G. M., and El-Kaissy, M. M. *Int. J. Multiphase Flow* **6,** 305 (1980).

Imafuku, K., Wang, T. Y., Koide, K., and Kuboto, H. *J. Chem. Eng. Japan* **1,** 153 (1968).
Jackson, R. *Trans. Inst. Chem. Engr.* **41,** 13 (1963a).
Jackson, R. *Trans. Inst. Chem. Engr.* **41,** 21 (1963b).
Jackson, R. *Chem. Eng. Sci.* **19,** 509 (1964).
Jackson, R. *in* ''Fluidization'' (Davidson, J. F., Clift, R., and Harrison, D., Eds.). Academic Press, London, 1985.
Jacob, K. V., and Weimer, A. W. *A.I.Ch.E.J.* **33,** 1698 (1987).
Jean, R. H., and Fan, L. S. *Can. J. Chem. Eng.* **65,** 351 (1987).
Joshi, J. B. *Trans. Instn. Chem. Engr.* **58,** 155 (1981).
Joshi, J. B. *Chem. Eng. Res. Des.* **61,** 143 (1983).
Joshi, J. B. *Chem. Eng. Res. Des.* **62,** 271 (1984).
Joshi, J. B. *unpublished* (1987).
Joshi, J. B., and Lali, A. M. *in* ''Frontiers in Chemical Reaction Engineering'' (L. K. Doraiswamy and R. A. Mashelkar, Eds.). Wiley Eastern Ltd., 1984, p. 314.
Kastanek, F., Nyvlt, V., and Rylek, M. *Collect. Czech. Chem. Commun.* **39,** 3246 (1974).
Kataoka, I. *Int. J. Multiphase Flow* **12,** 745 (1986).
Kataoka, I., and Serizawa, A. *Int. J. Multiphase Flow* **15,** 843 (1989).
Kato, Y., Nishiwaki, A., Fukuda, T., and Tanaka, S. *J. Chem. Eng. Japan* **5,** 112 (1972).
Kelkar, B. G., Phulgaonkar S. P., and Shah, Y. T. *Chem. Eng. J.* **27,** 125 (1983).
Khare, A. S., and Joshi, J. B. *Chem. Eng. J.* **44,** 11 (1990).
Kim, S. D., Baker, C. G .J., and Bergougnou, M.A. *Can. J. Chem. Eng.* **53,** 134 (1975).
King, D. F., and Harrison, D. *Trans. Instn. Chem. Engrs.* **60,** 26 (1982).
Koetsier, W. T., Van Swaij, W. P. M., and Van der Most, M. J. *J. Chem. Eng. Japan* **9,** 332 (1976).
Krishna, R., Wilkinson, P. M., and Van Dierendonck, L. L. *Chem. Eng. Sci.* **46,** 2491 (1991).
Kumar, R., and Kuloor, N. R. *Adv. Chem. Eng.* **8,** 55 (1972).
Lali, A. M., Khare, A. S., Joshi, J. B., and Nigam, K. D. P. *Powder Technol.* **57,** 39 (1989).
Lisseter, P. E., and Fowler, A. C. *Int. J. Multiphase Flow* **18,** 195 (1992).
Liu, J. T. C. *Proc. Royal Soc. London* **A380,** 228 (1982).
Lockett, M. J., and Kirkpatrick, R. D. *Trans. Instn. Chem. Engrs.* **53,** 267 (1975).
Marucci, G. *Ind. Eng. Chem. Fundamentals* **4,** 224 (1965).
Maruyama, T., Yoshida, S., and Mizushina, T. *J. Chem. Eng. Japan* **14,** 352 (1981).
Medlin, J., and Jackson, R. *Ind. Eng. Chem. Fundamentals* **14,** 315 (1975).
Medlin, J., Wang, H. W., and Jackson, R. *Ind. Eng. Chem. Fundamentals* **13,** 247 (1974).
Mendelsen, H. D. *A.I.Ch.E.J.* **13,** 250 (1967).
Mersmann, A. *Ger. Chem. Eng.* **1,** 1 (1978).
Molerus, O. *in* ''Principles of Flow in Disperse Systems.'' Chapman and Hall, London, 1993.
Musters, S. M. P., and Rietema, K. *Powder Technol.* **18,** 239 (1977).
Nicklin, D. J. *Chem. Eng. Sci.* **17,** 693 (1962).
Oels, U., Lucke, J., Buchholz, R., and Schugerl, K. *Ger. Chem. Eng.* **1,** 115 (1978).
Ostergaard, K. *Chem. Eng. Sci.* **20,** 165 (1965).
Ostergaard, K., and Thiesen, P.I. *Chem. Eng. Sci.* **21,** 413 (1966).
Pal, R., and Masliyah, J. *Can J. Chem. Eng.* **67,** 916 (1989).
Pandit, A. B., and Joshi, J. B. *Reviews in Chem. Eng.* **2,** 1 (1984).
Pandit, A. B., and Joshi, J. B. *Chem. Eng. Res. Des.* **64,** 125 (1986).
Pauchon, C., and Banerjee, S. *Int. J. Multiphase Flow* **14,** 253 (1988).
Ranade, V. V., and Joshi, J. B. *in* ''Proceedings of International Symposium on Transfer Processes in Multiphase Systems'' (Upadhyay, S. N., Ed.). Banaras Hindu University Press, Varanasi (India), 1987, p. 113.
Richardson, J. F. *in* ''Fluidization'' (Davidson, J.F., and Harrison, D., Eds.). Academic Press, New York, 1971, p. 25.
Richardson, J. F., and Meikle, R. A. *Trans. Instn. Chem. Engrs.* **39,** 348 (1961).

Richardson, J. F., and Zaki, W. N. *Trans. Inst. Chem. Engr.* **32,** 35 (1954).
Rietema, K. *Chem. Eng. Sci.* **28,** 1493 (1973).
Rietema, K. *Chem. Eng. Sci.* **37,** 1125 (1982).
Rowe, P. N. *Chem. Eng. Res. Des.* **62,** 190 (1984).
Rowe, P. N., Foscolo, P. U., Hoffman, A. C., and Yayes, J. G. *Chem. Eng. Sci.* **37,** 355 (1982).
Sangani, A. S., and Didwania, A. K. *J. Fluid Mech.* **248,** 27 (1993).
Schugerl, K., Lucke, J., and Oels, U. *Adv. Biochem. Eng.* **7,** 1 (1977).
Shnip, A. I., Kolhatkar, R. V., Dinakar, S., and Joshi, J. B. *Int. J. Multiphase Flow* **18,** 705 (1992).
Slis, P. L., Willemse, Th. W., and Kramers, H. *Appl. Sci. Research* **A8,** 209 (1959).
Smith, D. N., and Reuther, J. A. *Chem. Eng. Sci.* **40,** 741 (1985).
Stewart, P. S. B., and Davidson, J. F. *Chem. Eng. Sci.* **21,** 165 (1964).
Taitel, Y., Barnea, D., and Dukler, A. E. *A.I.Ch.E.J.* **26,** 345 (1980).
Tarmy, B. L., Chang, M., Coulaloglou, C. A. and Ponzi, P. R., *Inst. Chem. Eng. Symp. Ser.* **87,** 303 (1984).
Tsinontides, S. C., and Jackson, R. *J. Fluid Mech.* **255,** 237 (1993).
Turner, R. *in* "Fluidization." Soc. Chem. Eng., London, 1964, p. 42.
Turner, R. *Chem. Eng. Sci.* **21,** 971 (1966).
Verloop, J., and Heertjes, P. M. *Chem. Eng. Sci.* **25,** 825 (1970).
Wallis, G. B. *in* "One-Dimensional Two-Phase Flow." McGraw-Hill, New York, 1969.
Whithman, G. B., "Linear and Nonlinear Waves." Wiley, New York, 1974.
Wilkinson, P. M., Spek A. P., and Van Dierendonck, L. L. *A.I.Ch.E.J.* **38,** 544 (1992).
Willhelm, R. H., and Kwauk, M. *Chem. Eng. Prog.* **44,** 201 (1948).
Yamashita, F., and Inoue, H. *J. Chem. Eng. Japan* **8,** 334 (1975).
Zhou, Z.A., and Egiebor, N.O. *Minerals Eng.* **6,** 199 (1993).
Zuber, N., and Hench, J., Rept. No. 62GL100, General Electric Company, Schenectady, NY (1962).